AUTOMATED FIVE-AXIS TOOL PATH GENERATION BASED ON DYNAMIC ANALYSIS

WANG SIBAO

(M. Eng., B. Eng.)

A THESIS SUBMITTED

FOR THE DEGREE OF DOCTOR OF PHILOSOPHY

DEPARTMENT OF MECHANICAL ENGINEERING

NATIONAL UNIVERSITY OF SINGAPORE

2015

DECLARATION

I hereby declare that this thesis is my original work and it has been written by me in its entirety. I have duly acknowledged all the sources of information which have been used in the thesis.

This thesis has also not been submitted for any degree in any university previously.

Wang Sibao

Wang Sibao

11 August 2015

ACKNOWLEDGEMENT

First and foremost, I would like to express my sincere gratitude and appreciation to my supervisor, A/Prof. ZHANG Yunfeng, from the Department of Mechanical engineering in National University of Singapore, for his invaluable guidance, advice and discussion throughout the entire duration of this project. It has been a rewarding research experience under his supervision.

I would also like to show my appreciation for the financial support in the form of research scholarship from the CSC (China Scholarship Council).

Special thanks are given to Dr. LI Lingling, Dr. LI Haiyan and Dr. GENG Lin for their excellent work which laid down the foundation of the research and whose suggestions help me very much. I also wish to thank all my other fellow students for their support and providing a pleasant research environment. In addition, thanks to the Dr. LIU Kui, Dr. GENG Lin and MR. NG Thai Ee from SIMTech (Singapore Institute of Manufacturing Technology), without them, my experiments may not have been implemented. In addition, I wish to give my thanks to all my other friends, MR. SHI Kaining, DR. YAN Shijun, etc. for their continuous encouragement.

Finally, I would thank my family for their kindness and love. Without their deep love and constant support, I would not have completed the study.

TABLE OF CONTENTS

SUMMARY

In this thesis, automated 5-axis tool path generation considering true dynamic factors (cutting force and chatter) is studied. The research objectives are to develop models for predicting cutting forces and chatter in 5-axis milling and algorithm for optimizing the cutter posture at each cutter contact (CC) point in tool path generation.

Firstly, an accurate force prediction algorithm in 5-axis milling is proposed by considering the influence of cutter vibrations and cutter run-out. The effect of cutter run-out is modelled as an extra feed on the designed feed-per-tooth, which produces a cyclic change on the uncut chip thickness (UCT). Meanwhile, for cutter vibrations, by solving the differential motion equation of the machining system with the measured modal parameters, real-time vibrations of the cutter during machining are obtained, which are taken as a feedback of the machining system on the designed feed-per-tooth. Integrating the effect of cutter run-out and vibrations on the designed feed-per-tooth, prediction accuracy is improved.

Secondly, chatter prediction in 5-axis milling is studied and a new tool called posture stability graph (PSG) is proposed for guiding the user to select chatter-free cutter posture. The stability of 5-axis milling is affected by not only the depth-of-cut and spindle speed, but also the cutter posture (lead angle and tilt angle). The dynamic cutting force caused by dynamic displacement of the cutter can be predicted using the proposed cutting force prediction model. Subsequently, the dynamic equation of the machining system can be constructed using the measured modal parameters. Using the full-discretization (FD) method, the transition matrix of the dynamic equation is constructed. Modulus of the eigenvalues of the transition matrix will indicate the stability of the machining system, i.e., the stability of the cutter posture. By

identifying the cutter postures that make the system borderline stable under the given machining conditions, the allowable range of cutter postures can be divided into stable/chatter zones, which forms the PSG.

Thirdly, an algorithm for chatter-free and interference-free cutter posture selection in 5-axis milling is proposed. For a given CC point, the chatter- and interference-free (CIF) cutter posture range can be constructed by intersecting the posture accessible graph (PAG), which was developed in our previous work, and the PSG. In this way, the optimal cutter posture can be selected from the CIF-map at each CC point. For demonstration, an algorithm for optimal tool path generation in 5-axis milling is proposed, aiming at minimal maximum deflection cutting force (MDC-F) at each CC point.

The proposed cutting force prediction and chatter prediction methods in 5-axis milling have been implemented and validated by experiments. The CIF-map construction and its application in optimal cutter posture determination have also been implemented. It represents a significant step in 5-axis tool path generation from static model to dynamic mode.

LIST OF FIGURES

LIST OF TABLES

LIST OF GLOSSARY

Symbols:

K_{te}, K_{re}, K_{ae} : Edge force coefficients

K_{tc}, K_{rc}, K_{ac} : Shear specific coefficients

dF_t, dF_r, dF_a : cutting force of elemental cutting edge in local frame

dF_x, dF_y, dF_z : cutting force of elemental cutting edge in cutter coordinate system

F_x, F_y, F_z : Total cutting force generated by the cutter in cutter coordinate system

N_{fc}: Number of flute of cutter

N_e: Number of elemental cutting edge

N_s: Number of swarm size

$\boldsymbol{n}_{nv}$: Normal vector of elemental cutting edge

$\boldsymbol{f}_{fv}$: Feed vector during machining

dS: Differential element length of the cutting edge

t_{uct}: uncut chip thickness caused by dynamic displacement

uct_0: Uncut chip thickness under ideal conditions

uct_{ro}: Uncut chip thickness caused by cutter run-out

uct_{v}: Uncut chip thickness caused by cutter vibration

db: Uncut chip width

κ : Axial immersion angle of elemental cutting edge

ϕ_z : Lag angle

ψ: Angular position of elemental cutting edge

θ: Angular position of the first flute measured at the tool tip

R_z: Circle radius of elemental cutting edge

R: Cutter radius

r_f: Corner radius of cutter

z_e: z coordinate of the cutting edge in CCS

i_0: Helix angle of cutter

φ_p: Pitch angle of cutter

θ_{ra}: Rotation angle for a-map generation

λ_{ia}: Inclination angle for a-map generation

$|\lambda_\Phi|$: Modulus of eigenvalue of transition matrix

$F_{\text{x-y}}$: Deflection cutting force

$J_{\max}$: Maximum joint movements

d: Dynamic displacement of cutter

ρ: Cutter axis offset caused by cutter run-out

ϕ_{ro}: Locating angle for offset caused by cutter run-out

T: Tooth-passing period of cutter

$\mathbf{T}_l$: Transformation matrix from local frame to CCS

$\mathbf{T}_{cTm}$: Transformation matrix from CCS to modal frame

$\mathbf{T}_{mTf}$: Transformation matrix from modal frame into feed frame

Abbreviations:

3D: Three-dimensional

A-map: Accessibility map

CCS: Cutter coordinate system

WCS: Workpiece coordinate system

MTCS: Machine tool coordinate system

CAD: Computer-aided design

CAM: Computer-aided manufacture

NC: Numerical control

CNC: Computer numerical control

CC point: Cutter contact point

CL data: Cutter location data

GSS: Golden section search

PSO: Particle swarm optimization

GA: Generic algorithms

IDI: Interference during interpolation

CCW: Count clockwise

DOF: Degree of freedom

UCT: Uncut chip thickness

CSW: Cutting strip width

B-CSW: Backward-CSW

F-CSW: Forward-CSW

MDC-F: Maximum deflection cutting force

PAG: Posture accessible graph

PSG: Posture stability graph

CIF: Chatter- and interference-free

FD: Full-discretization method

SD: Semi-discretization method

ZOA: Zeroth order approximation method

CHAPTER 1

INTRODUCTION

Three-dimensional (3D) parts with sculptured surfaces play a more and more important role in automotive, aerospace and shipbuilding industries. These surfaces are widely used in modelling free form shapes as they have high level of continuity and flexibility. However, as they have irregular curvature distribution and lack of explicit mathematical description, it is difficult to finish these surfaces using traditional machining methods. Computer numerical controlled (CNC) machines have been introduced to make this process easier because of their high accuracy, efficiency and repeatability. In CNC machining, with the help of advanced Computer-aided Manufacture (CAM) packages, tool paths, including cutter contact (CC) points and cutter postures (lead angle and tilt angle), can be generated for each given Computer-aided Design (CAD) model of the workpiece. Subsequently, corresponding Numerical Control (NC) commands are obtained by converting the tool path by post processer and used to drive the movements of CNC machines.

There are two main machine tool styles among commercially available CNC machines, i.e., 3-axis and 5-axis machines. In 3-axis machines, the cutter can only translate in three orthogonal directions simultaneously; while in 5-axis machines, the cutter not only can translate in three orthogonal directions but also can rotate with two rotational joints, simultaneously. Compared to 3-axis machining, 5-axis machining has more flexibility in machining of sculptured surface because of the two rotational joints. However, tool path generation in 5-axis machining is also more difficult than that in 3-axis machining because the cutter posture needs to be carefully assigned at each CC point to avoid any interference for 5-axis machining. Although the function of tool path generation for 5-axis machining is available in most of current commercially available CAM packages, there are some common shortcomings, e.g., insufficient level of tool path optimization, lack of machining dynamics consideration.

This chapter introduces the technology of 5-axis machining of sculptured surfaces, followed by an introduction to process planning for 5-axis sculptured surface machining in our previous study, including constraints, requirements and tasks. Further to that, by discussing the-state-of-art in the published works related to tool path optimization, the motivation of this thesis is presented, followed by the detailed description of the research objectives and scope.

1.1. Five-axis Machining of Sculptured Surface

Although tool path generation for 5-axis machining is more difficult than that for 3-axis machining, 5-axis machining is widely employed for sculptured surface machining because of its numerous advantages compared to 3-axis machining, such as setups reduction, possibility of tool path optimization, stable machining process and improved surface quality.

Firstly, 5-axis machining needs fewer setups as it provides better accessibility. As shown in Figure 1.1, for 3-axis machining, only those visible regions on the part along the cutter axis direction can be machined. For 5-axis machining, however, machining area is not limited to those visible in the setup direction. Therefore, with 5-axis machining, more area can be machined in a single setup. This feature can reduce the number of setups, thus saving processing time and improving productivity.

Secondly, 5-axis machining provides more flexibility in tool path optimization. In tool path generation for 3-aixs machining, since the cutter cannot rotate, cutter posture remains the same. In tool path generation for 5-axis machining, however, due to the two extra rotary degrees of freedom (DOF) of the machine tool, there may be many choices of cutter posture combination, which provides the possibility for tool path optimization.

Thirdly, machining process will be more stable and good surface quality can be assured. Due to better accessibility of cutter in 5-axis machining, shorter cutter can be selected to machine given workpiece surface. Intuitively, shorter cutter is more rigid and provides more machining stability. Therefore, good machined surface quality is assured.

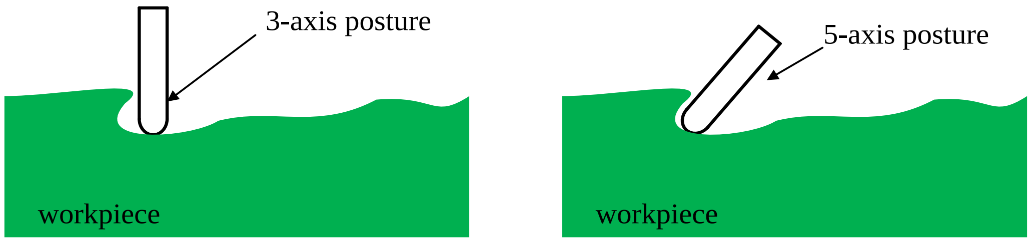

Figure 1.1 Accessibility comparisons between 3-axis and 5-axis milling

To make good use of these advantages of 5-axis milling, effective process planning is needed. The most important yet most difficult task of process planning in 5-axis milling is tool path planning, which includes the generation of CC points and cutter location (CL) data. The CC point can be generated by ensuring the deviation between the cutter trajectories and design surface below the given surface tolerance. This is followed by cutter posture assignment at each CC point. The cutter posture must not cause interference. In addition, due to the influence of cutter posture on cutter-workpiece engagement distribution on the cutter, the cutting force will be affected by the cutter posture as well. Vibrations caused by cutting force are therefore inevitable due to lack of stiffness of the machining system which includes cutter, holder and machine tool. Chatter may emerge when the vibration frequency approaches the chatter frequency. Therefore, cutter posture at a CC point needs to be carefully selected to achieve *dynamically smooth* machining process by avoiding chatter. Finally, the cutting force should also be controlled to minimize the amplitude of cutter deflection. As shown in Figure 1.2, the cutting force exerted on the cutter will cause cutter deflection and subsequently dimensional error. To obtain the desirable surface accuracy, the dimensional error should be minimized. In summary, cutter posture selection can be considered as an optimization problem (minimizing deflection cutting force) with various constraints, i.e., interference-free and chatter-free. While interference-free tool path generation is considered under *static mode*, chatter-free tool path generation is considered under *dynamic mode*.

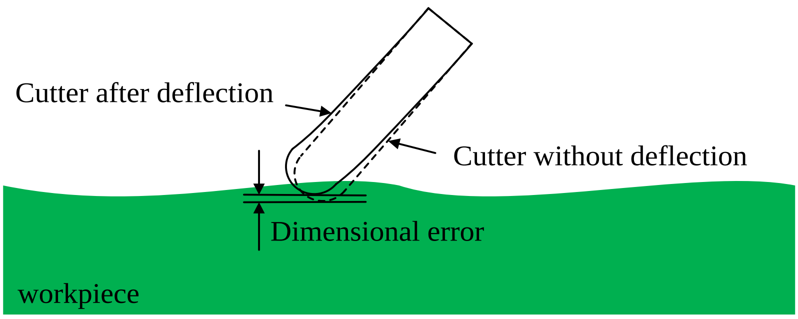

Figure 1.2 Dimensional error caused by cutting force

1.2. Process Planning for Sculptured Surface Machining

At the National University of Singapore, the process planning problem for 5-axis milling of sculptured surfaces has been studied extensively (Li and Zhang 2004; Li and Zhang 2006; Li and Zhang 2009; Li *et al.* 2011). The overall framework for automated process planning of 5-axis milling of sculptured surfaces (finish cut) is shown in Figure 1.3.

The inputs to the planning system include the 5-axis machine specification, list of available cutters, and the workpiece’s geometry (machining surface and non-machining surface). In the first stage, the machining surface is firstly sampled and accessibility evaluation for every cutter is then carried out at every sampled point. The cutter's accessibility information at a sampled point is stored in the form of accessibility map, called A-map. Based on the A-map at every sampled point, the best cutter or cutter-set for finishing the whole machining surface is selected. The output from this stage is one or several sets of machining-region/cutter (one: if a single cutter is selected for the whole machining-region; several: if a cutter-set (with several cutters) is selected to share the whole machining-region.

In the second stage, a tool path pattern is firstly selected. At the moment, only iso-planar tool path has been implemented. Tool path generation is then carried out for every machining-region/cutter, one at a time. For a given machining-region/cutter, the cutting direction for the iso-planar tool path is firstly determined based on heuristics aiming at minimizing posture change rate. Subsequently, the position of the first tool path is then determined and its CC points are generated. Following that, the cutter posture at every CC point is determined based on the A-map of the cutter at the CC point. If the current machining region is not fully covered, the position of the next tool path is determined based on a heuristics for maximum cutting efficiency (largest material remove rate). This procedure is repeated until the whole region is finished.

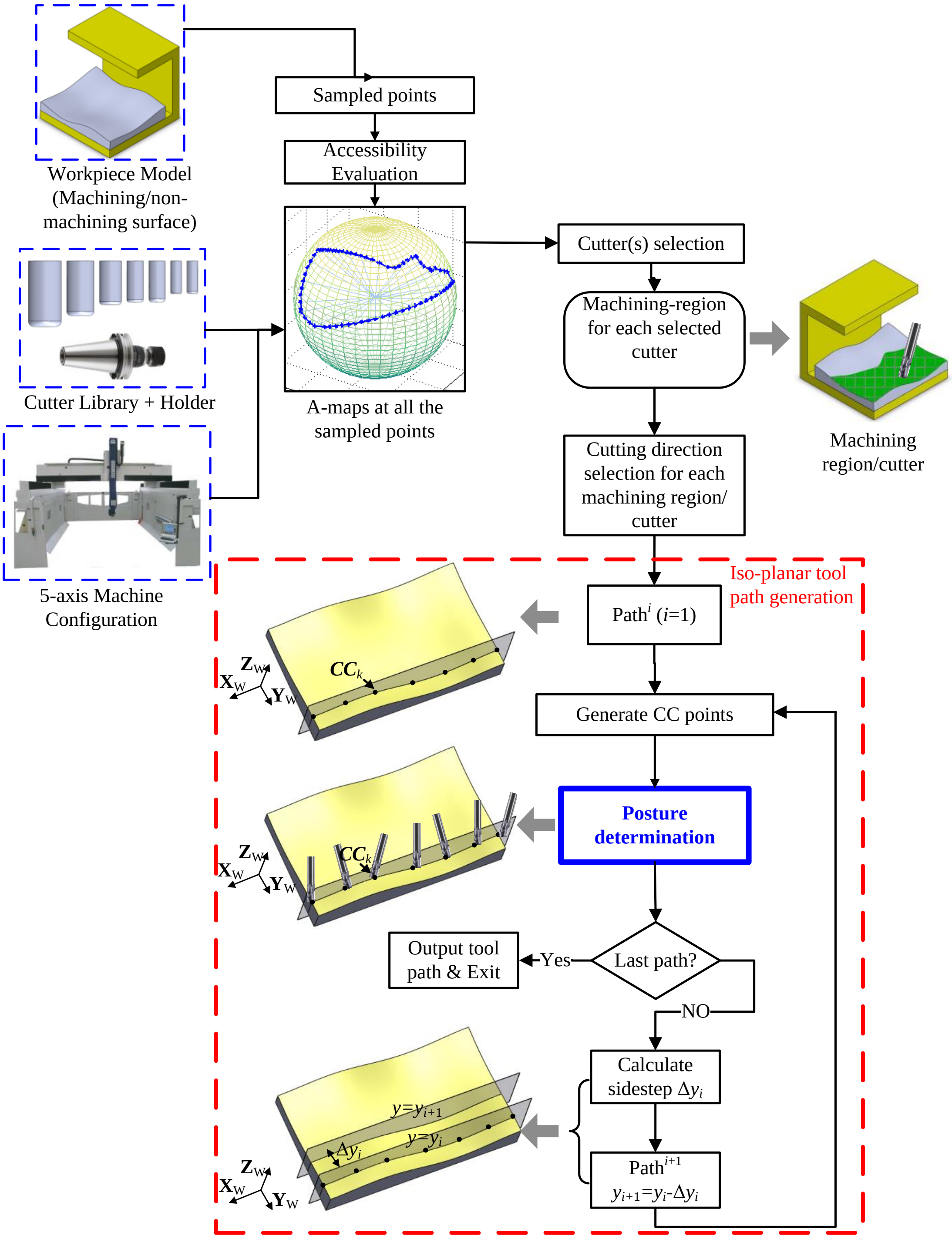

Figure 1.3 The process planning framework for 5-axis milling of sculptured surfaces

The core of the whole process planning system is posture determination for the CC points on a single path (see Figure 1.3). In our recent study (Geng 2013), an optimal cutter posture is assigned to a CC point (from its A-map) using a proposed genetic algorithm (GA) aiming at two objectives: minimizing the machine joint movement between neighbouring CC points and maximizing the cutting efficiency. Although tool path smoothness is considered by minimizing joint movement between consecutive CC points, it is still limited to geometric view point. To generate dynamically smooth tool paths, real machining dynamics, i.e., cutting force, cutter deflection and chatter, must be considered in cutter posture assignment. This forms the main motivation for the research in this thesis.

1.3. State-of-the-art in Tool Path Planning for Sculptured Surface Machining

Tool path planning for 5-axis machining of sculptured surface has been studied extensively by many researchers since late 1980s. A number of reviews and surveys are available that effectively summarizes the proposed solutions to various issues of 5-axis machining. (Choi and Jerard 1998) gave an extensive introduction of 5-axis sculptured surface machining from several aspects, such as fundamental mathematics, avoidance of machining interference, and principles of CNC machining. (Lasemi *et al.* 2010) provided a detailed review of those more recently proposed methods for 5-axis machining. The methods are grouped into several categories to cover different stages of process planning, such as tool-path topology, tool orientation identification and tool geometry selection. As for tool path generation and optimization, some focused on cutting efficiency based on geometrical analysis (Tournier and Duc 2005; Can and Unuvar 2010; Gong 2010), while others considered dynamical constraints heuristically (Wang and Tang 2007; Li *et al.* 2011). However, cutting dynamics was never considered analytically in these algorithms, leading to uncertainty when machining is carried out, e.g., cutter deflection causing dimensional error and cutting force fluctuation causing chatter (Hyun-Chul 2011). Ideally, in an ideal tool path, deflection cutting force is minimized and chatter is avoided at every CC point. To achieve this, methods for cutting force prediction and chatter prediction in 5-axis milling must be developed first. A posture can then be evaluated in terms of cutting force and chatter. In the following sections, a brief review of recent research efforts on cutting force prediction, chatter prediction and tool path optimization considering dynamics in 5-axis machining will be presented.

1.3.1. Cutting force prediction

Cutting force is one of the most important factors that influence machined surface quality, part accuracy, tool wear, and tool life. It can also be used to predict chatter which is adverse for machined surface quality and machine tool (Lacerda and Lima 2004). Therefore, to optimize the tool path considering dynamic factors, cutting force during the machining process must be obtained first. However, cutting force prediction is a complicated task as it is influenced by many parameters, such as feed-per-tooth, uncut chip geometry, cutter postures, machining parameters and combination of cutter and workpiece materials. Here, we assume the material combination of cutter and workpiece and machining parameters, such as depth-of-cut and spindle speed, are given. Based on the assumption, cutting force can be predicted analytically.

Much research has been conducted for the prediction of the cutting force, mainly on 3-axis machining (Feng and Menq 1994; Kim *et al.* 2000; Dang *et al.* 2010; Zeroudi *et al.* 2012). One notable work is (Lee and Altintas 1996) in which a 3-step approach was proposed to calculate milling force. Firstly, the helical flute of the cutter is divided into small layer oblique cutting edge segments, then corresponding cutting edge length and uncut chip thickness can be obtained for each segments. Secondly, the cutting coefficients are obtained from the orthogonal cutting data which are only related to material property of the cutter and workpiece combination by repeated experiments. Finally, the total cutting force for the cutter is calculated by integrating the effective cutting edge segments. This approach is also adopted in this study and will be extended to predict the cutting force for 5-axis milling.

Recently, cutting force prediction in 5-axis machining has caught the attention of some researchers. (Ozturk *et al.* 2009) investigated the effect of lead and tilt angle on the cutting force in 5-axis ball-end milling. (Lazoglu 2003) proposed a new model to calculate the cutting force for a given CL by meshing the cutter and workpiece into small square elements in 5-axis ball-end milling. (Ozturk and Budak 2007) and (Lamikiz *et al.* 2004) extended the model presented by (Lee and Altintas 1996) to predict the cutting force by considering the influence of tilt and lead angle in 5-axis ball-end milling. In current research, however, the cutter vibration, which is inevitable during machining, is not included. As the cutter vibration will change the designed feed-per-tooth, it is believed that the influence of cutter vibration should be considered to improve the prediction accuracy. On the other hand, in the cutter setup stage, the axis misalignment may cause cutter run-out which again influences the cutting force (Kline and DeVor 1983; Li and Li 2005). Therefore, it is believed that to develop a more accurate cutting force prediction model in 5-axis milling, the influence of cutter vibration and cutter run-out must be considered.

1.3.2. Chatter prediction

Chatter is a kind of self-excited and regenerative vibration, usually caused by inadequate stiffness of the machining system, made of the cutter, holder, workpiece, and the machine tool itself (Altintas 2000; Quintana and Ciurana 2011; Siddhpura and

Paurobally 2012). Many modelling and solution methods (Merritt 1965; Sridhar *et al.* 1968; Minis *et al.* 1990; Budak and Altintas 1998; Altintas 2001; Bediaga *et al.* 2005; Eynian and Altintas 2010; Peng *et al.* 2014) have been proposed to study the mechanism of chatter and predict chatter under given machining conditions. Generally, chatter during machining process can be predicted in two steps. In the first step, the dynamic equation of the machining system is established based on the dynamic cutting force prediction and measured or predicted modal parameters. In the second step, the dynamic equation of the machining system is solved using numerical or analytical method and the stability of the machining system (machining with or without chatter) is determined according to the obtained solution.

In the dynamic equation construction stage, the main focus is to obtain the dynamic cutting force under different conditions. For example, the inclined angle is included during chatter prediction (Shamoto and Akazawa 2009). The effect of cutter run-out on chatter prediction in 3-axis milling is studied (Insperger *et al.* 2006; Schmitz *et al.* 2007). Chatter prediction in 5-axis machining is also studied considering the effect of lead angle and tilt angle on cutting force prediction (Ozturk *et al.* 2007). When the dynamic cutting force is predicted under given machining conditions, the dynamic equation of the machining system can be constructed using measured or predicted modal parameters under the assumption that the machining system is a spring-mass-damper vibrational system. Although there are two kinds of assumptions for the vibrational system, i.e., 2D (Li and Li 2000) and 3D (Altintas 2001), most of the current research on chatter prediction is based on the assumption that the machining system is a 2D spring-mass-damper vibration system as the stiffness in the tool axis is high enough to be neglected.

In the second stage, the constructed dynamic equation of the machining system will be solved and corresponding stability of the machining system will be determined according to the obtained solution. Several solution methods have been presented in the published work (Altintaş and Budak 1995; Insperger and Stépán 2004; Insperger 2010; Ahmadi and Ismail 2012; Peng *et al.* 2014). Among these methods, the *time domain* method (Peng *et al.* 2014) is the most accurate but most time-consuming method. On the other hand, the *zeroth order approximation* (ZOA) method (Altintaş and Budak 1995; Altintas 2001; Ahmadi and Ismail 2011) is probably the most widely used method for chatter prediction due to its simplicity. However, In the situation when low radial depth-of-cut and low spindle speed are used, the accuracy of the chatter prediction using ZOA will be reduced (Ahmadi and Ismail 2012). Therefore, the *multiple frequency* method was proposed by extending the ZOA method (Budak and Altintas 1998). In recent years, the *time discretization* (*full-discretization* (FD) and *semi-discretization* (SD)) method has attracted much attention due to its simplicity, high prediction accuracy and wide application in the chatter prediction (Insperger and Stépán 2002; Insperger and Stépán 2004; Ding *et al.* 2010; Ding *et al.* 2010). Although the computational efficiency of the FD method is higher than the SD method (Ding *et al.* 2010), they have the same mechanism to solve the time delayed differential dynamic equation (Insperger 2010).

By solving the dynamic equation, a given combination of spindle speed and depth-of-cut can be evaluated to determine whether chatter will occur. Following this approach, all the sampled combination of spindle speed and depth-of-cut (when other machining conditions are kept constant) can be accessed. The result can be represented in a graph, called *stability diagram* (SLD), which can be used to guide users to select chatter-free machining parameters. For 3-axis milling, SLD is very useful for the selection of chatter-free depth-of-cut under given machining conditions, in which the cutter posture is fixed. For 5-axis milling, however, as the cutter posture also influences the stability of machining system (Ozturk *et al.* 2009), the SLD with depth-of-cut and spindle speed is apparently not sufficient. Instead, a diagram specifying chatter-free cutter posture combination (lead angle and tilt angle) under a given machining condition is considered to be more effective. Since the process planning studied in this thesis aims at finish-cut stage, the depth-of-cut and spindle speed can be treated as approximately constant. In this thesis, a new tool called *posture stability graph* (PSG) will be constructed to represent the chatter-free cutter posture range.

1.3.3. Tool path optimization considering machining dynamics

Tool path optimization in 5-axis milling refers to the optimization of cutter posture assignment at each CC point. Previously reported work on 5-axis toolpath optimization mainly focused on maximizing machining efficiency by minimizing total tool path length. Typically, the cutter and workpiece are treated as rigid bodies and tool path optimization is achieved mainly from geometric analysis (Geng 2013). In reality, however, due to the existence of cutting force (causing cutter deflection) and chatter, there is always deviation between the simulated machined surface and the actual one. To resolve this problem, the toolpath optimization must take into account the dynamic factors (cutting force and chatter).

Previously reported research works on tool path optimization considering machining dynamics are quite limited. An example in 3-axis machining is (de Lacalle *et al.* 2007) in which the cutting force is calculated in every 15° on the surface tangent plane and the direction with the minimal cutting force is chosen. For 5-axis milling, as the effect of lead and tilt angles on cutting force and chatter varies significantly for different cutter posture assignments, optimization strategy can be very different. To reduce cutter deflection, (Lopez de Lacalle *et al.* 2005) optimized the tool path to minimize the cutting forces in every CC point. Later, (Lazoglu *et al.* 2009) presented a method to generate the globally minimal-cutting-force tool path for the zigzag pattern. To optimize multiple objectives including dynamical and geometric factors, (Manav *et al.* 2011) optimized the mean resultant force, cycle time, and scallop height using varying objective weighting approach. (Geng 2013) presented a new method to optimize tool path towards maximizing cutting strip width and minimizing maximum joint movement. (Shamoto *et al.* 2012) presented a method to optimize the cutter postures to avoid chatter in turning operation. In 3-axis milling, chatter-free radial width-of-cut and axial depth-of-cut are selected to achieve maximum chatter-free machining efficiency from the SLD generated by time domain simulation method (Weck *et al.* 1994), analytical chatter prediction method (Budak and Tekeli 2005) and experimental method (Quintana *et al.* 2011). However, chatter-free tool path optimization for 5-axis milling has not been studied so far. Therefore, further research is necessary for generating truly dynamically smooth tool path in 5-axis milling.

1.4. Research Motivation

Up to now, process planning still remains as the bottleneck limiting the wider application of 5-axis machining, especially for the machining of sculptured surfaces. Commercially available CAM packages still lack of capability of automated tool path generation and optimization. In fact, most of them rely on the user for cutter selection, machining region allocation, and even for providing key parameters for tool-path generation, such as path intervals and cutting direction. Assignment of tool postures usually follows a simple heuristic while a trial-and-error approach is adopted to deal with possible machining interferences.

Meanwhile, in our previous research, an automated process planning system for 5-axis machining of sculptured surfaces has been developed (Li, 2007; Geng 2013). At the core of the system is an effective interference checking algorithm, which is able to compute the accessible posture range (A-map) of a given fillet-end cylindrical cutter at any point on the machining surface. With this algorithm, selection of single and/or multiple cutter(s) can be carried out based on the cutters' accessibility information over the whole machining surface. For tool path generation, various optimization objectives are provided to cater for the user's specific requirements, such as machining efficiency (total tool path length), tool path smoothness and computational efficiency. The process planning system was extensively tested with case studies and proved to have high level of robustness and efficiency.

However, the state-of-the-art advances in 5-axis tool path generation still have great potential for improvement. The generated tool paths only guarantee interference-free as only geometric factors are considered during generation process. The critical gap is that, in the current systems, machining dynamic factors, including cutting force and chatter, are not considered during tool path generation. This gap will directly affect the generated tool paths and eventually the quality of the machined surface. First of all, chatter may exist in the generated tool path and it would cause chatter marks on the machined surface and the cutter may be broken when it becomes severe. Furthermore, the cutter deflection will directly influence the machined surface quality. As an extension to our previous research, the work presented in this thesis focuses on tool path generation considering machining dynamic factors. The target is to improve the existing system in terms of reality, optimality, and versatility.

1.5. Research Objectives and Scope

1.5.1. Research Objectives

Based on the identified technology gaps in the literature review, the author proposes to extend our previous work in 5-axis tool path optimization by considering dynamic factors. The generated tool path will be *interference-free* and *chatter-free* while the deflection cutting force will be minimized to reduce the dimensional error. To this end, the following specific research objectives are proposed:

(1) To develop a cutting force prediction model in 5-axis milling by considering cutter run-out and cutter vibration.

(2) To develop a chatter prediction method for given cutter posture and machining conditions in 5-axis milling.

(3) To develop a new representation form for cutter posture ranges (at a CC point) being both interference-free and chatter-free.

(4) To develop a new tool path generation algorithm that is able to select the optimal cutter posture with minimal deflection cutting force at a CC point.

1.5.2. Research scope

For cutting force prediction, the following research scope is covered:

(1) Efficient cutting force prediction in 5-axis milling under ideal conditions will be proposed.

(2) Modelling of cutter run-out will include the effect of cutter run-out on cutting force prediction by considering the cutter run-out as an extra feed.

(3) Modelling of cutter vibration will include the effect of cutter vibration on cutting force prediction. Based on the assumption that the machining system is

a two degree of freedom (DOF) system, cutter vibration is calculated using a numerical analysis method based on the measured modal parameters.

(4) Cutting force coefficients and cutter run-out calibration methods will be also proposed from the initial experimental results.

For chatter prediction, the following research scope is covered:

(1) Modelling of stability in 5-axis machining system under a given cutter posture and machining conditions will be studied.

(2) Stability determination using FD method for modelled dynamic equation of machining system in 5-axis machining will be studied.

For the new representation scheme of interference-free and chatter-free posture range, the following research scope is covered:

(1) Develop a new representation scheme for chatter-free posture ranges. For a cutter along any given posture (lead and tilt angles) at a point on the machining surface, the stability status of the machining system is clearly specified.

(2) The chatter-free posture representation scheme can be combined with interference-free scheme (A-map) to form a comprehensive feasible posture map.

For the new tool path generation algorithm, the following research scope is covered:

(1) Develop a new overall framework for generating dynamically feasible tool paths for 5-axis milling of sculptured surfaces.

(2) Develop an optimization algorithm for cutter posture assignment aiming at the minimal deflection cutting force.

1.6. Organization of the Thesis

In the remaining of the thesis, each chapter will cover an individual topic of the research scope. Each topic is approached in a self-contained manner containing the following steps: introduction of background and relevant literature, specification of inputs and outputs, illustration of methodology, case studies and discussion. A brief overview is provided as follows.

Chapter 2 presents the newly proposed cutting force prediction method for 5-axis sculptured surfaces machining. As a contribution, cutter run-out and cutter vibrations are considered in order to improve prediction accuracy. In Chapter 3, a new chatter prediction algorithm for 5-axis machining is proposed. Under any given cutter posture and machining condition, the stability criterion for the machining system is established using a discretization method. A chatter-free posture range representation scheme is also proposed. In Chapter 4, construction of the new representation scheme for chatter-free and interference-free posture range is described. In Chapter 5, the newly proposed tool path generation method in 5-axis machining towards minimal deflection cutting force is presented for iso-planar tool path generation. Chapter 6 presents some case study and simulation results for tool path generation in 5-axis machining. Chapter 7 draws the conclusions by discussing achievements and limitations of the research, as well as direction of possible future work.

CHAPTER 2

CUTTING FORCE PREDICTION IN 5-AXIS MACHINING

To generate dynamically feasible tool paths for 5-axis machining, dynamic factors such as cutter deflection and chatter need to be evaluated during tool path generation. In order to predict chatter and determine the deflection cutting force, cutting force must be predicted in the first place. It is therefore considered the first dynamic factor in this study.

In this chapter, the newly proposed cutting force prediction algorithm is presented. Firstly, the cutting force prediction model under ideal machining conditions is presented. This is followed by the introduction of the proposed cutting force prediction algorithm considering the influence of cutter vibrations and cutter run-out. Both two factors affect cutting force through influence on the uncut chip thickness. The effect of cutter run-out is modelled as an extra feed for machining, which produces a cyclic change on the uncut chip thickness. Meanwhile, for cutter vibrations, by solving the differential motion equation with the measured modal parameters, real-time vibrations of the cutter during machining are obtained, which are taken as a feedback of the machining system on the designed feed-per-tooth.

2.1. Background

Cutting force is considered one of the most important dynamic factors influencing the machining performance and accuracy of machined surface (Feng and Menq 1996). Therefore, efficient and exact modelling of cutting force has been the focus of many studies, such as dynamic response of machining systems, prediction of chatter and process planning.

Study on cutting force prediction started on the force prediction in orthogonal cutting in turning operation. The cutting law was firstly studied in orthogonal cutting and then extended into oblique cutting. For simplicity, the cutting law can be simplified as a linear law. This is to say that the cutting force is determined by cutting force coefficients and machining conditions (feed-per-tooth, depth-of-cut and width of cut) (Kaymakci *et al.* 2012). On the other hand, milling is an intermittent cutting process as the cutter has one or more teeth, and only the teeth engaged in cutting generates cutting force. In addition, in order to eliminate the abrupt entry and exit in milling operation, most of the cutter teeth have a helix angle which will make the cutter teeth have a lag. These features increase the complexity of cutting force prediction in milling. To predict cutting force in milling operation, the discrete method is generally adopted to discretize the cutting edge into elemental cutting edge undergoing oblique cutting. By summing all the cutting force generated by these elemental cutting edges, the cutting force can be predicted for milling. When the cutting force is known at each point of time, dynamic equation of the machining system can be established, which can be subsequently used to predict chatter. In addition, the predicted cutting force can also be used to estimate cutter deflection, which is closed related to the dimensional error.

2.2. Related Works

Over the years, much research has been conducted to predict cutting force under given machining conditions (Li *et al.* 2001; Gradišek *et al.* 2004; Lamikiz *et al.* 2004; Wan *et al.* 2007; Gonzalo *et al.* 2010). It has been established that cutting force is codetermined by the cutter-material-specific cutting force coefficients and the process-specific uncut chip thickness. Among the previous research, (Lee and Altintas 1996) had done some notable and influential work on predicting cutting force. With their model, the cutting edge is discretized into infinitesimal elements and an oblique cutting condition is assumed for each element. The uncut chip geometry for each element can be calculated from the cutter geometry and machining conditions. The cutting force coefficients needed for cutting force prediction are calibrated from orthogonal machining experiments (Budak and Altintas 1993). Later, some researchers proposed to directly calibrate the cutting force coefficients from oblique cutting. Some considered the cutting force coefficients as constants (Sun *et al.* 2009; Cao *et al.* 2012) while some considered the coefficients as functions of depth-of-cut (Gradišek *et al.* 2004; Lamikiz *et al.* 2004). When the depth-of-cut is small, the difference of these two prediction methods is trivial.

Meanwhile, cutter run-out is a common source of inaccuracy in machining. It affects the cutting force by changing the effective uncut chip thickness (Fontaine *et al.* 2007). To achieve better prediction accuracy, cutter run-out has been considered in various cutting force prediction models (Li and Li 2004; Diez Cifuentes *et al.* 2010; Yao *et al.* 2013). (Fontaine *et al.* 2007) studied the effect of cutter run-out on cutting force in inclined surface for ball-end cutters. Two kinds of cutter run-out models are presented for accurate cutting force prediction (Rivière-Lorphèvre and Filippi 2009). The run-out of a cutter can be defined by the offset between rotational and geometric centres of cutter and location angle of the offset (Wan *et al.* 2007; Wan *et al.* 2009; Sun and Guo 2011), which can be calibrated from experimental data(Wan *et al.* 2009) or measured from dial gouge (Lee *et al.* 2007).

Moreover, due to the limited rigidity of machining system made up by the cutter, holder, and machine tool, vibrations of the cutter are inevitable, as a result of the cyclically changing cutting force. The relative scale of vibration amplitude to feed-per-tooth is considered as the key factor that affects the prediction accuracy. In our experiments, under finish machining condition when feed-per-tooth was in the range of 0.01mm to 0.1mm, the amplitude of vibrations was in the range of 0.001mm - 0.012mm, which is high enough to produce noticeable effects on the prediction results. Therefore, vibrations of the cutter should also be incorporated in the force prediction model for more accurate prediction. Although the vibrations caused by cutting force have been studied for chatter prediction (Li and Liu 2008), the effect of cutter vibrations on cutting force prediction has not been covered previously. In this study, both cutter run-out and cutter vibrations are considered in the cutting force prediction model in an integrated manner.

In the proposed method, the machining system consisting of the machining tool and cutter is modelled as a vibration system, for which the modal parameters can be obtained with an impact test on the cutter tip. The input to the system is the cutting force that is affected by three factors, i.e., designed feed-per-tooth, variation of feed-per-tooth caused by cutter run-out, and variation of feed-per-tooth caused by cutter vibrations. The output of the system is the displacement of the cutter, which will be imposed on the designed feed-per-tooth and used for making a more accurate prediction of the cutting force. The above method can be applied to both 3-axis and 5-axis machining. For 5-axis machining, the cutter-workpiece engagement information as well as the feed vector of machining will be transformed into the cutter frame for calculation. The effectiveness of such a method has been verified with a series of simulations and corresponding experimental validation.

2.3. Cutting Force Prediction Considering Run-out and Vibration

2.3.1. Influence of cutter run-out and vibration on cutting force prediction

Traditionally, cutting forces are predicted under the ideal condition, i.e., the cutter's shape is strictly centre-symmetric and rotates about its axis; the material removal process will not have any effect on the shape of cutter. In actual machining, however, the cutter will have run-outs and the machining force will cause the cutter to vibrate. The effect of cutter run-out and vibrations on cutting force is illustrated in Figure 2.1. First of all, due to cutter run-out, the axis of rotation is different from the geometrical axis of the cutter. This will cause variations on the effective radius for the cutting edges: effective radius is increased for certain cutting edges and reduced for the others. The machined surface (red line in Figure 2.1b), therefore, would always deviate from the expected shape under ideal machining conditions (black line in Figure 2.1b). Secondly, due to the flexibility of machining systems, cutter vibrations are inevitable during machining. The vibrations will cause the machined surface to be uneven (blue line in Figure 2.1b), contributing to further deviation of the machined surface. Within one revolution of the tool, such deviations left by the previous tooth will serve to change the effective uncut chip thickness for the current in-cut edge. Meanwhile, run-out and real-time vibrations of the cutter will also cause the location of the current cutting edge to deviate from the assumed location under ideal machining conditions. As a result of these two factors, the cutting force predicted under the ideal condition will deviate from the actual value. In our study, the influence of the cutter run-out and vibrations on both machined surface and cutter location is looked into, enabling us to provide more accurate predictions.

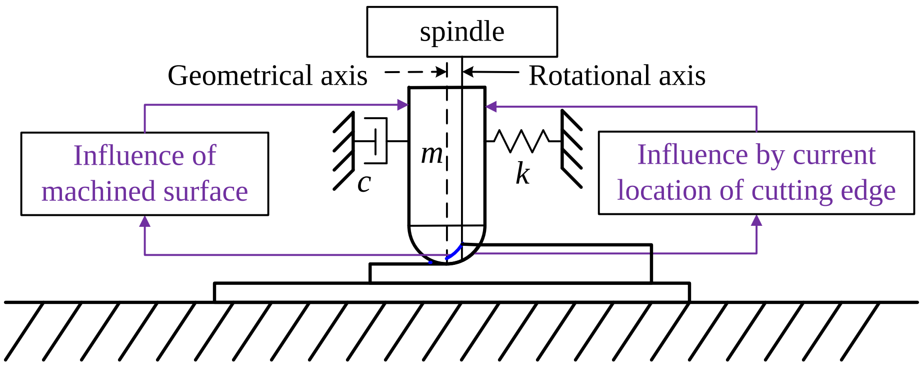

(a) Front view

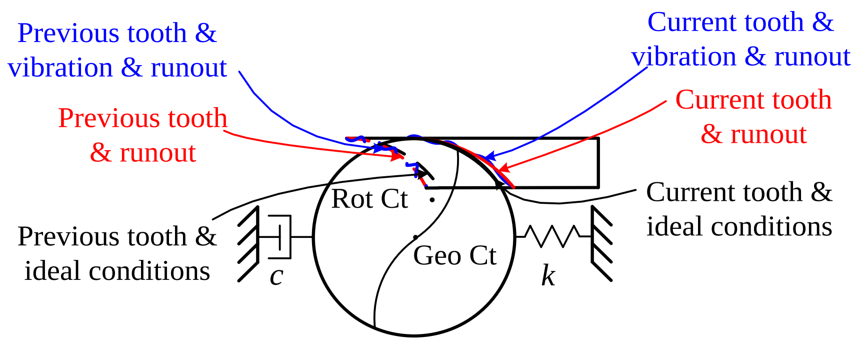

(b) Top view

Figure 2.1 Overview of the influence of cutter run-out and vibrations on cutting force

2.3.2. Cutting force prediction under ideal conditions

The proposed method for cutting force prediction is based on the cutting force model for 3-axis milling (Lee and Altintas 1996). This model can be extended to cover 5-axis machining cases, assuming information on cutter-workpiece engagement is available (Budak *et al.* 2009; Ozturk *et al.* 2009). In this work, we assume that only the ball-end part of the cutter is engaged with the workpiece. This is true for most cases, especially in finish machining stage. In this section, cutting force prediction methods under ideal machining conditions for 5-axis machining, i.e., when cutting force is only affected by the designed feed-per-tooth, will be presented. Cutting force prediction is conducted in the cutter coordinate system (CCS) $\mathbf{O}_T$-$\mathbf{X}_T\mathbf{Y}_T\mathbf{Z}_T$ as opposed to the workpiece coordinate system (WCS) $\mathbf{O}_W$-$\mathbf{X}_W\mathbf{Y}_W\mathbf{Z}_W$ and feed frame $\mathbf{O}_F$-$\mathbf{X}_F\mathbf{Y}_F\mathbf{Z}_F$ (see Figure 2.2a and Figure 2.2b).

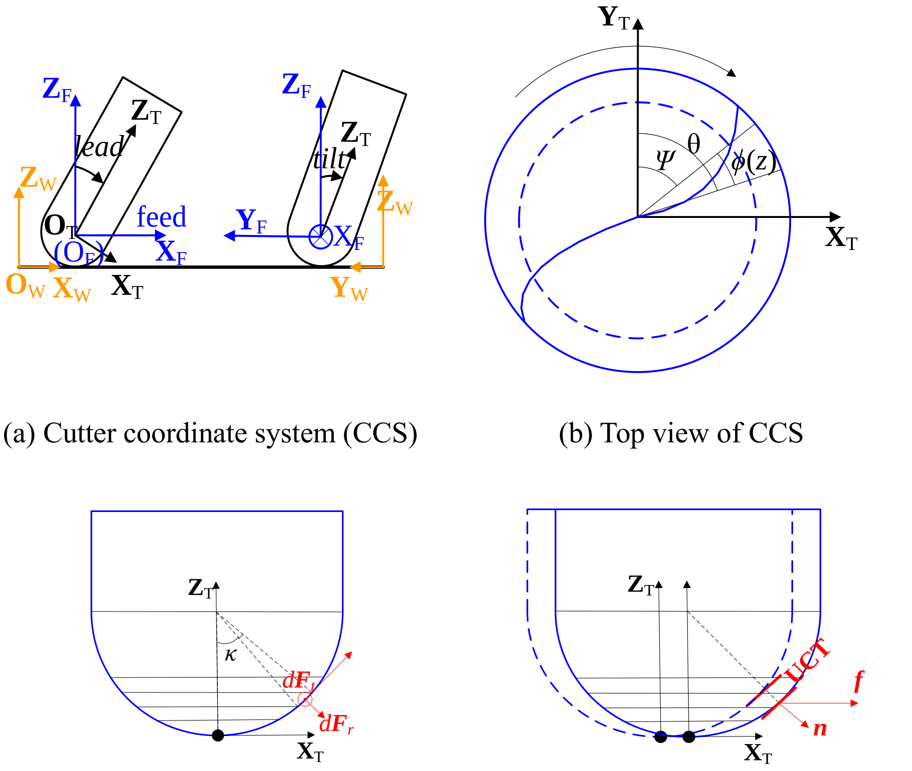

Figure 2.2 Cutting force prediction under ideal machining conditions

To predict cutting force, the cutter is divided along the cutter axis into N_e layers (see Figure 2.2c). Each flute on a layer can be seen as a straight edge undergoing oblique cutting. The cutting force generated by the *i*th elemental oblique cutting edge of *j*th flute is decomposed into *tangential*, *radial*, and *axial* cutting forces, denoted as $dF_t^{i,j}, dF_r^{i,j}, dF_a^{i,j}$, which are given as (Altintas 2000):

$$\begin{cases} dF_t^{i,j}\left(\theta, z_e\right) = K_{te}dS + K_{tc}uct_0\left(\psi, \kappa\right)db \\ dF_r^{i,j}\left(\theta, z_e\right) = K_{re}dS + K_{rc}uct_0\left(\psi, \kappa\right)db \\ dF_a^{i,j}\left(\theta, z_e\right) = K_{ae}dS + K_{ac}uct_0\left(\psi, \kappa\right)db \end{cases} \tag{2-1}$$

where K_{te}, K_{re}, K_{ae} are the edge force coefficients, and K_{tc}, K_{rc}, K_{ac} are the shear coefficients, which can be calibrated for any given combination of cutter, material and machining conditions. dS is the differential element length of the cutting edge; db is the uncut chip width; $uct_0(\psi, \kappa)$ is the uncut chip thickness (UCT) at the elemental cutting edge, which is affected by the angular position (ψ), axial immersion angle (κ) of the cutting edge element and cutter feed. Assuming that the cutter rotates in counter clockwise (CCW) direction, the angular location of any cutting edge element measured from $\mathbf{Y}_\mathrm{T}$ is given by:

$$\psi = \theta + (i - 1)\phi_p - \phi_z \tag{2-2}$$

where θ is the angular position of the first flute measured at the tool tip; ϕ_z is the lag angle caused by the helical shape of the cutting edge and ϕ_p is the pitch angle, and they can be obtained by:

$$\phi_z = z_e \tan(i_0)/R$$

$$\phi_p = 2\pi/N_{fc}$$

where i_0 is the helix angle, z_e is the coordinate value of the elemental cutting edge in $\mathbf{Z}_\mathrm{T}$ direction, N_{fc} is the number of flutes of the cutter, and R is the radius of cutter.

From a kinematic point of view, the UCT can be obtained by projecting the feed vector along the surface normal at a cutting edge element. The normal vector $\boldsymbol{n}_{nv}$ of each cutting edge element can be represented as:

$$\boldsymbol{n}_{nv} = \left(\sin(\kappa)\sin(\psi), \sin(\kappa)\cos(\psi), \cos(\kappa)\right)$$

Suppose that the feed vector is along $\mathbf{X}_\mathrm{T}$, given as $\boldsymbol{f}_{fv}$, the UCT would be given by:

$$uct_0\left(\psi,\kappa\right)=\boldsymbol{n}_{nv}\cdot\boldsymbol{f}_{fv} \tag{2-3}$$

Meanwhile, the length of the cutting edge element dS and the uncut chip width db are given as:

$$dS=\sqrt{\cot^2\left(\kappa\right)+\sin^2\left(\kappa\right)\tan^2\left(i_0\right)+1}dz \tag{2-4}$$

$$db=\frac{dz}{\sin(\kappa)} \tag{2-5}$$

where dz is the thickness of one cutter disk and $\sin(\kappa)$ can be obtained by:

$$\sin(\kappa)=R_z/R$$

where R_z is the circular radius of elemental cutting and can be obtained by:

$$R_z=\sqrt{R^2-(R-z)^2}$$

To obtain the cutting force acting on the cutter, the elemental radial, tangential, and axial cutting forces need to be transformed into the cutter's frame along $\mathbf{X}_T$, $\mathbf{Y}_T$ and $\mathbf{Z}_T$ as:

$$\begin{cases} dF_x^{i,j}=-dF_r^{i,j}\sin(\kappa)\sin(\psi)-dF_t^{i,j}\cos(\psi)-dF_a^{i,j}\cos(\kappa)\sin(\psi) \\ dF_y^{i,j}=-dF_r^{i,j}\sin(\kappa)\cos(\psi)+dF_t^{i,j}\sin(\psi)-dF_a^{i,j}\cos(\kappa)\cos(\psi) \\ dF_z^{i,j}=-dF_r^{i,j}\cos(\kappa)-dF_a^{i,j}\sin(\kappa) \end{cases} \tag{2-6}$$

For a single flute of the cutter, the total cutting force is obtained by integrating the elemental forces produced by the engaged segment at the current time instant. With one revolution of the cutter, one cutting edge element may enter and exit from the engagement region on the cutter. The engagement condition can be obtained through geometrical analysis and represented with entry and exit angles on each cutter disk (e.g., in slotting with a ball-end cutter, the entry and exit angles are 0 to 180 degrees on each cutter disk as shown in Figure 2.3). The total cutting force can be obtained by summing up the contribution of each flute as,

$$\begin{pmatrix} F_x \\ F_y \\ F_z \end{pmatrix} = \sum_{j=1}^{N_{fc}} \sum_{i=1}^{N_e} \begin{pmatrix} dF_x^{i,j} \\ dF_y^{i,j} \\ dF_z^{i,j} \end{pmatrix} \tag{2-7}$$

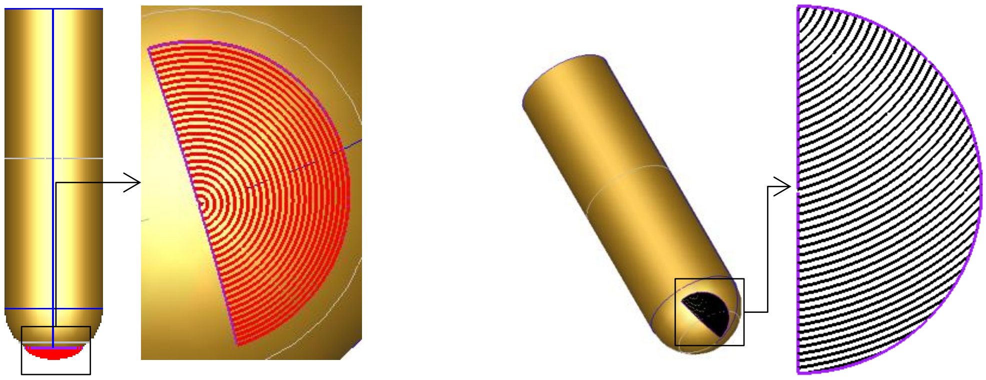

(a) Engagement information of 3-axis posture

(b) Engagement information of 5-axis posture re-constructed from 3-axis posture

Figure 2.3 Construction of engagement information for prediction of cutting force

To predict cutting force in 5-axis milling, the cutter posture (lead and tilt angles) needs to be considered in the calculation of the corresponding cutting engagement. First of all, the cutter-workpiece engagement for the 5-axis posture needs to be obtained, which can be done by extracting the boundary of engagement region from a 3-axis posture, transforming the boundary into the CCS of the new cutter orientation and re-calculating the entry-exit points on each cutter disk as intersections of the cutter disk with the boundary (see Figure 2.3b). The detailed re-construction method can refer to (Geng *et al.* 2015). The UCT can then be calculated using the same principle given in Eq.(2-3) as well. However, the feed vector needs to be transformed into the CCS of the 5-axis cutter orientation. The transformation matrix is given as:

$$T_{cTf}=\begin{bmatrix}1 & 0 & 0\\ 0 & \cos(tilt) & -\sin(tilt)\\ 0 & \sin(tilt) & \cos(tilt)\end{bmatrix}\begin{bmatrix}\cos(lead) & 0 & \sin(lead)\\ 0 & 1 & 0\\ -\sin(lead) & 0 & \cos(lead)\end{bmatrix} \quad (2\text{-}8)$$

where *lead* and *tilt* are angles (see Figure 2.2a) that determines the cutter's posture regarding the feed and cross-feed directions in WCS.

Therefore, to calculate the cutting force at a cutter contact (CC) point for the free-form surface machining under ideal machining conditions, the key task is to obtain the boundary of engagement region, i.e., entry and exit angle $\left(\varphi_{ey}^{i,j},\varphi_{et}^{i,j}\right)$ of the *i*th cutting edge element of *j*th flute, at this CC point for the 3-axis posture. The boundary of engagement region will be determined for each layer and represented with one or several pair(s) of entry angle and exit angle. As shown in Figure 2.4a, when the feed direction at this point is given, the boundary of the workpiece can be divided into left side and right side according to the direction. When the *i*th cutting edge element of the *j*th flute is not intersected with the boundary of the workpiece, such as slotting, the entry and exit angle is (0^o, 180^o). When there is one intersection point, this point will be entry point when the boundary contained the intersection point is a left side compared to the other boundary and the entry and exit angle are obtained by:

$$\varphi_{ey}^{i,j}=\arctan\left(x_{p_{ey}}/y_{p_{ey}}\right);\varphi_{et}^{i,j}=\pi \quad (2\text{-}9)$$

where $x_{p_{ey}},y_{p_{ey}}$ are the $\mathbf{X}_C$, $\mathbf{Y}_C$ coordinate value of the intersection point $\mathbf{P}_{ey}$. Or, this point will be an exit point when the boundary contained the intersection point is a right side compared to the other boundary and the entry and exit angle are obtained by:

$$\varphi_{ey}^{i,j}=0;\varphi_{et}^{i,j}=\arctan\left(x_{p_{et}}/y_{p_{et}}\right) \quad (2\text{-}10)$$

where $x_{p_{et}}, y_{p_{et}}$ are the $\mathbf{X}_C$, $\mathbf{Y}_C$ coordinate value of intersection point $\mathbf{P}_{et}$. When there are two intersection points between the plane with $\mathbf{Z}_T$ and boundary of the workpiece, represented as the points $\mathbf{P}_{ey}$ and $\mathbf{P}_{et}$, the entry and exit angle can be obtained for three situations according to the property of the local workpiece curve in the cutting plane: convex, concave and straight lines. When the local curve is a straight line (shown in Figure 2.4b) or concave curve (shown in Figure 2.4c), the entry and exit angle are obtained by:

$$\varphi_{ey}^{i,j} = \arctan\left(x_{p_{ey}} / y_{p_{ey}}\right); \varphi_{et}^{i,j} = \pi - \arctan\left(-x_{p_{et}} / y_{p_{et}}\right) \tag{2-11}$$

When the local curve is a convex curve (shown in Figure 2.4d), the cutting edge element will first get into the workpiece when its angular position is larger than 0^{o}, and exit when it is $\varphi_{et}^{i,j}$. After a few seconds, the cutting edge element will get into the workpiece again and exit when its angular position is larger than 180^{o}. Therefore, the cutting edge will get into and exit the workpiece twice. The two pairs of entry and exit angle are obtained by:

$$\begin{aligned} &\varphi_{ey,1}^{i,j} = 0; \varphi_{et,1}^{i,j} = \arctan\left(x_{p_{ey}} / y_{p_{ey}}\right) \\ &\varphi_{ey,2}^{i,j} = \pi - \arctan\left(-x_{p_{et}} / y_{p_{et}}\right); \varphi_{et,2}^{i,j} = \pi \end{aligned} \tag{2-12}$$

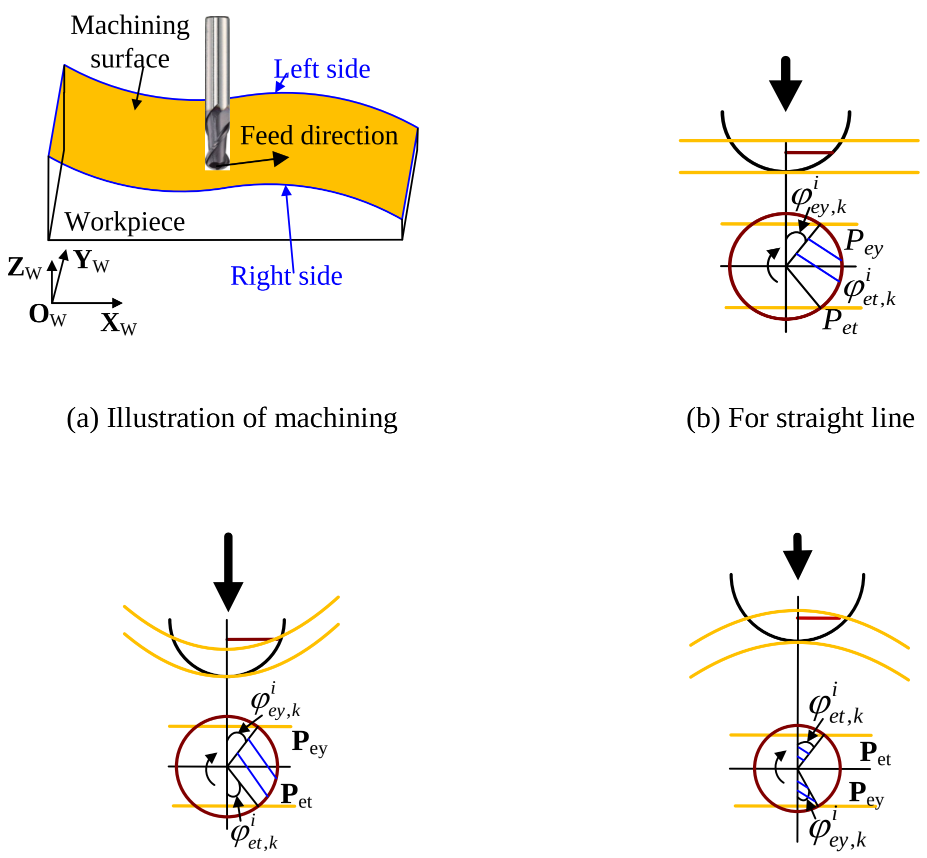

(a) Illustration of machining

(b) For straight line

(c) For concave curve

(d) For convex curve

Figure 2.4 Entry and exit angle calculation

2.3.3. Modelling of cutter run-out for cutting force prediction

To improve the cutting force prediction accuracy, the effect of cutter run-out on cutting force prediction will be presented in this section. As shown in Figure 2.5a and Figure 2.5b, the cutter run-out is defined as cutter axis offset ρ and locating angle for offset ϕ_{ro} . As shown in Figure 2.5c, when cutter run-out is considered, with one revolution of the cutter, the actual amount of feed will include two parts: feed caused by run-out, which is due to the offset of axis of rotation from the geometrical centre $\mathbf{O}_1$ to the actual rotation centre $\mathbf{O}$, and the designed feed-per-tooth. Therefore, the effect of cutter run-out is considered as an extra feed. As shown in Figure 2.5c, this extra feed $\overrightarrow{\mathbf{O}_1\mathbf{O}_2}$ caused by the cutter run-out can be expressed as:

$$\boldsymbol{f}_r = \left(\rho\sin(\phi_{ro}+\theta) - \rho\sin\left(\phi_{ro}+\theta\text{-}\phi_p\right), \rho\cos(\phi_{ro}+\theta) - \rho\cos\left(\phi_{ro}+\theta\text{-}\phi_p\right), 0\right)^T \quad (2\text{-}13)$$

The direction of the feed would be normal to the cutter axis. Then, corresponding extra UCT can be obtained using Eq. (2-3) and expressed as:

$$uct_{ro} = \rho\sin(\kappa)\cos\left(\phi_{ro}+\phi_z\text{-}(i-1)\phi_p\right) - \rho\sin(\kappa)\cos\left(\phi_{ro}+\phi_z\text{-}(i-2)\phi_p\right) \quad (2\text{-}14)$$

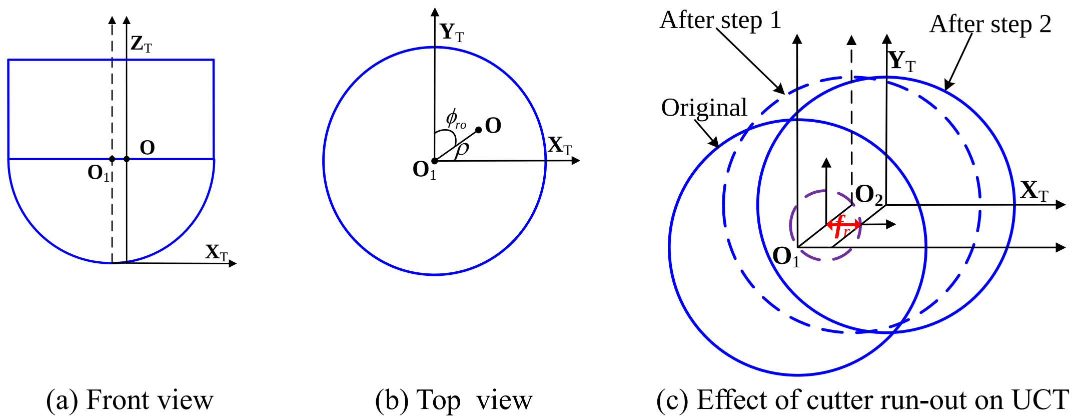

Figure 2.5 Modelling of UCT considering cutter run-out

2.3.4. Modelling of cutter vibration for cutting force prediction

Due to the limited rigidity of the machining system, made up of the cutter, holder and machine tools, vibrations or dynamic displacements of the cutter are inevitable when cutting forces act on the cutter. Although such vibrations happen in all three directions of cutter's frame, vibrations along $\mathbf{Z}_T$ are negligible thanks to the high level of stiffness along the machine spindle. Therefore, as shown in Figure 2.6, the system is simplified as a 2-DOF spring-mass-damper system. For this system, the following differential equation of motion can be obtained:

$$\mathbf{M}\ddot{\boldsymbol{X}}_c(t) + \mathbf{C}\dot{\boldsymbol{X}}_c(t) + \mathbf{K}\boldsymbol{X}_c(t) = \boldsymbol{F}_c(t) \quad (2\text{-}15)$$

where $\mathbf{M} = \begin{bmatrix} m_x & 0 \\ 0 & m_y \end{bmatrix}$, $\mathbf{C} = \begin{bmatrix} c_x & 0 \\ 0 & c_y \end{bmatrix}$, $\mathbf{K} = \begin{bmatrix} k_x & 0 \\ 0 & k_y \end{bmatrix}$ and m_x, m_y, c_x, c_y, k_x, k_y are mass, damping coefficients and stiffness of the system along $\mathbf{X}_T$ and $\mathbf{Y}_T$, respectively.

These are the so-called modal parameters that can be obtained from impact testing. $\boldsymbol{F}_c(t) = \left[f_{x,c}(t) \quad f_{y,c}(t) \right]^T$, where $f_{x,c}(t)$ and $f_{y,c}(t)$ are the continuous cutting forces along $\mathbf{X}_\mathrm{T}$ and $\mathbf{Y}_\mathrm{T}$, which can be obtained with both experimental measurement and theoretical prediction. $\boldsymbol{X}_c(t) = \left[x_c(t) \quad y_c(t) \right]^T$, where $x_c(t)$ and $y_c(t)$ are real time displacements of the cutter in $\mathbf{X}_\mathrm{T}$ and $\mathbf{Y}_\mathrm{T}$ directions.

On the other hand, it should be noted that the displacements of the cutter will affect the dynamic cutting forces by affecting the UCT. As shown in Figure 2.6, in the absence of cutter vibrations, the machined surface is indicated with the black line under ideal conditions and the red line when cutter run-out exists. However, with vibrations of the cutter, the displacements of the cutter will further change the shape of the machined surface by leaving wave-like cutter marks. Meanwhile, on the front surface of the chip (the surface facing the cutter) to be removed, such waves are also left behind by the previous tooth of the cutter (dotted blue line in Figure 2.6). The waves left on both sides of the chip serve to change the UCT together.

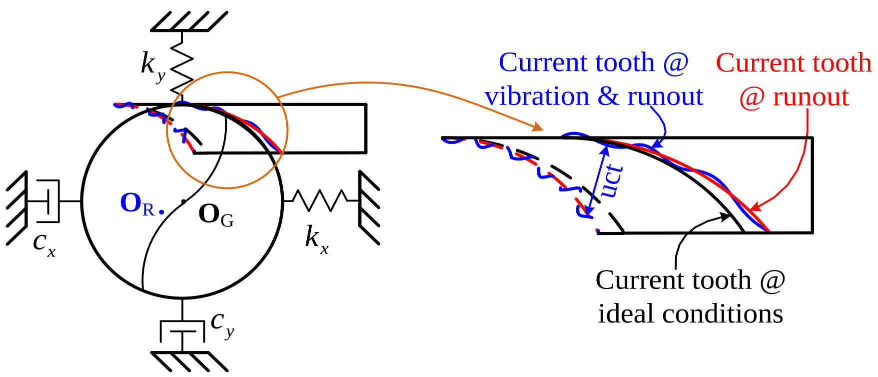

Figure 2.6 Illustration of the effect of vibrations during milling

Similar to the way that cutter run-out is modelled, the influence of cutter vibrations can also be viewed as an extra term on the feed-per-tooth as shown in Figure 2.7. This extra term, denoted as f_v, is given as:

$$\boldsymbol{f}_v = \boldsymbol{X}_c(t) - \boldsymbol{X}_c(t-T) = \begin{bmatrix} x_c(t) - x_c(t-T) \\ y_c(t) - y_c(t-T) \end{bmatrix} \tag{2-16}$$

where T is the tooth-passing period in the time domain.

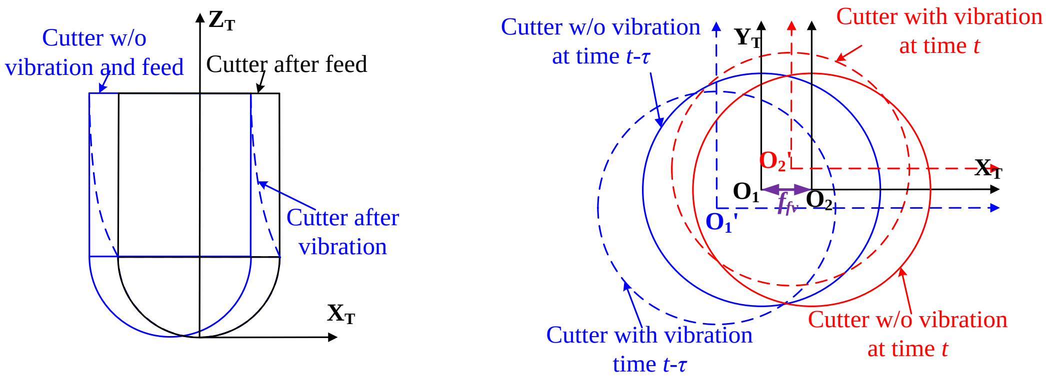

(a) Assumption of feed instead of vibration

(b) Feed considering vibration

Figure 2.7 Effect of cutter vibration on UCT

However, a special condition should be considered when the vibration of the cutter reaches such a magnitude that the cutter jumps out of the cut. In such circumstances, the front surface of the chip would be shaped by the cutter two or more tooth passing periods ago. Taking into consideration this special scenario, $\boldsymbol{f}_v$ is given as:

$$\boldsymbol{f}_v = \boldsymbol{X}_c(t) - \boldsymbol{X}_p = \begin{bmatrix} x_c(t) - x_p \\ y_c(t) - y_p \end{bmatrix} \tag{2-17}$$

where the previous in-cut cutter location $\boldsymbol{X}_p$ is given as:

$$\boldsymbol{X}_p = \begin{bmatrix} x_p \\ y_p \end{bmatrix} = \begin{bmatrix} \min\{x(t-T), x(t-2T) \ldots x(t-NT)\} \\ \min\{y(t-T), y(t-2T) \ldots y(t-NT)\} \end{bmatrix} \tag{2-18}$$

Similarly, the change in the UCT can be obtained from Eq. (2-3) as:

$$uct_v = \sin(\kappa)\sin(\psi)\left[x(t) - x_p\right] + \sin(\kappa)\cos(\psi)\left[y(t) - y_p\right] \tag{2-19}$$

2.3.5. Identification of cutter run-out parameters from experiment data

Although the cutter run-out can be measured by experimental method (Lee *et al.* 2007), it can also be calibrated from the experiment data (Wan *et al.* 2009). As the measurement method needs dial gauge and goniometer to measure the cutter axis offset and locating angle for the offset, which will increase the expense and complexity, the direct calibration method from cutting force experiment data is normally preferred. In this section, a simple calibration method for cutter run-out using measured cutting force data is presented.

With the presence of cutter run-out, the cutting forces generated by the current tooth ($\boldsymbol{F}_{ct}$) and previous tooth ($\boldsymbol{F}_{ps}$) are different, as determined by the run-out parameters ρ and ϕ_{ro}. By investigating the cutting force signals picked-up in 3-axis machining with $2\pi / N_{fc}$ phase difference (the pitch angle of the cutter) in between, the cutter run-out parameters can be identified from the experiment data.

The cutting forces in any direction can be taken for calculating the run-out parameters. As an example, the cutting forces along $\mathbf{X}_\mathrm{T}$ direction are used here. From Eqs. (2-1) and (2-6), at a given angular position τ_0 with one revolution of the cutter, the cutting force is given as:

$$F(\tau_0) = F_0(\tau_0) + \sum_{i,j} uct_{ro}\left(-K_{rc}db\sin\kappa_{ij}\sin\psi_{ij} - K_{tc}db\cos\psi_{ij} - K_{ac}db\cos\kappa_{ij}\sin\psi_{ij}\right) \quad (2\text{-}20)$$

where $F_0(\tau_0)$ is the calculated cutting force in the absence of cutter run-out, which is cyclic with a period of $2\pi / N_{fc}$ (the tooth passing period). Taking Eq. (2-14) into Eq. (2-20) gives us:

$$F(\tau_0) = F_0(\tau_0) + \rho A_1(\tau_0)\cos(\phi_{ro}) + \rho A_2(\tau_0)\sin(\phi_{ro}) \quad (2\text{-}21)$$

where

$$A_1\left(\tau_0\right)=\sin\left(\frac{\phi_p}{2}\right)\sum_{i,j}\left(-2\sin\left(\tau+\frac{\phi_p}{2}-\psi_{ij}\right)\left(-K_{rc}\sin\kappa_{ij}\sin\psi_{ij}-K_{tc}\cos\psi_{ij}-K_{ac}\cos\kappa_{ij}\sin\psi_{ij}\right)dz\right)$$

and

$$A_2\left(\tau_0\right)=\sin\left(\frac{\phi_p}{2}\right)\sum_{i,j}\left(-2\cos\left(\tau_0+\frac{\phi_p}{2}-\psi_{ij}\right)\left(-K_{rc}\sin\kappa_{ij}\sin\psi_{ij}-K_{tc}\cos\psi_{ij}-K_{ac}\cos\kappa_{ij}\sin\psi_{ij}\right)dz\right)$$

The difference in cutting forces at angular positions with a phase angle of $2\pi/N_{fc}$ in-between is thus given as:

$$\Delta F=F\left(\tau_0\right)-F\left(\tau_0-\phi_p\right)=\rho\left(a_1\left(\tau_0\right)\cos\left(\phi_{ro}\right)+a_2\left(\tau_0\right)\sin\left(\phi_{ro}\right)\right) \tag{2-22}$$

where $a_1=A_1\left(\tau_0\right)-A_1\left(\tau_0-\phi_p\right)$ and $a_2=A_2\left(\tau_0\right)-A_2\left(\tau_0-\phi_p\right)$.

From the experimental data, various values of ΔF can be collected, as long as a sufficiently large sampling frequency is used. With each pair of such data, we have:

$$\tan(\phi_{ro})=\frac{\Delta F\left(\tau_2\right)a_1\left(\tau_1\right)-\Delta F\left(\tau_1\right)a_1\left(\tau_2\right)}{\Delta F\left(\tau_1\right)a_2\left(\tau_2\right)-\Delta F\left(\tau_2\right)a_2\left(\tau_1\right)} \tag{2-23}$$

Using Eq. (2-23) and the measured cutting force data, a series of values of $\tan(\phi_{ro})$ can be obtained during one revolution of the cutter. Using the least-square fitting method, the locating angle ϕ_{ro} can then be obtained. Substituting ϕ_{ro} into Eq. (2-22), another series of data for cutter axis offset ρ can be obtained. Similarly, using the least-square fitting method, the cutter axis offset ρ can be obtained. An example is given here to further illustrate this process, in which a Fraisa 2-fulte ball-end cutter (R = 5mm, $i_0=20^{\circ}$) is used and the cutting force coefficients are shown in Table 2.4. Figure 2.8 shows the measured cutting force in $\mathbf{X}_T$ direction which contains 500 sampled positions in one revolution, i.e., 250 positions in one tooth passing period. The $\tan(\phi_{ro})$ in one tooth passing period can be calculated using Eq. (2-27) in the 250 positions and is shown as the blue point in Figure 2.9a. Using the least square fitting method to reduce the effect of noise point during measurement, the fitted $\tan(\phi_{ro})$ is obtained (0.0415) and shown as the red line in Figure 2.9a. Therefore, the locating angle ϕ_{ro} is obtained as 0.0415 rad. By substituting the obtained ϕ_{ro} into Eq. (2-22), the calculated cutter axis offset ρ is obtained in the 250 positions as shown by the blue point in Figure 2.9b. Similarly, the least square fitting method is used and the fitted ρ is shown as the red line in Figure 2.9b and is 9 μm.

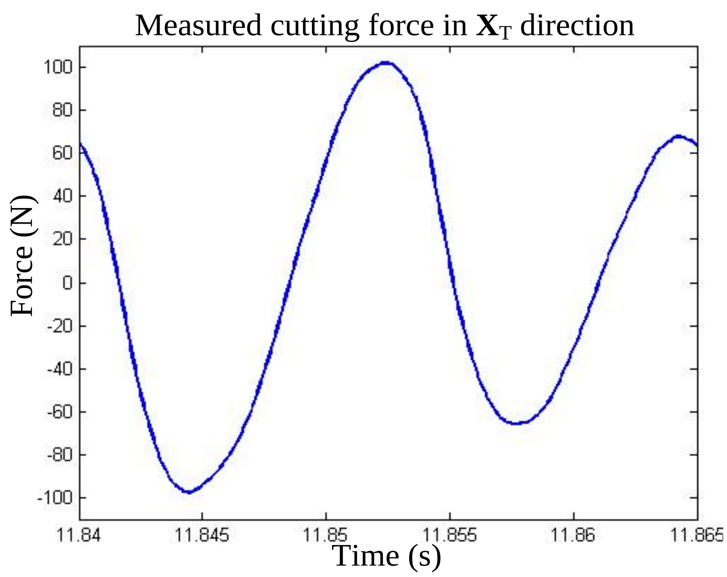

Figure 2.8 Measured cutting force (in $\mathbf{X}_T$) for calibration of cutter runout parameters

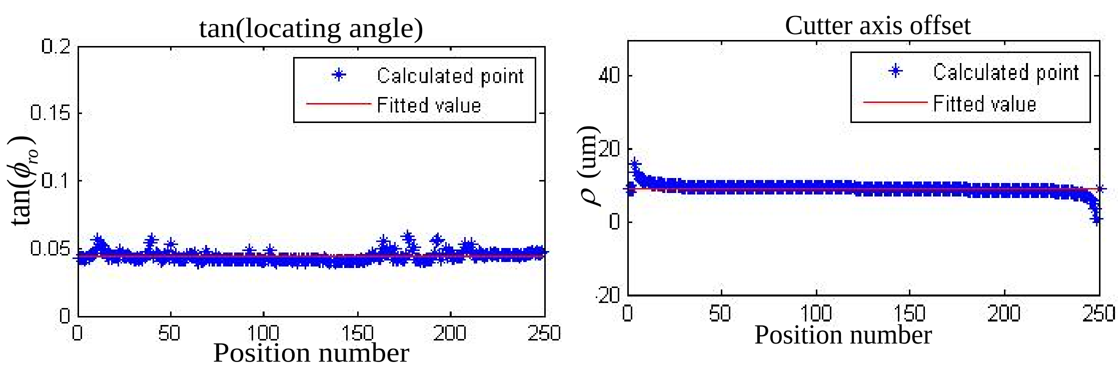

(a) Locating angle for run-out (b) Run-out offset

Figure 2.9 Calibrated cutter run-out parameters

2.3.6. Cutting force coefficients calibration

In order to identify the cutting force coefficients, the following process can be used to identify the cutting force coefficients from orthogonal milling. Eq. (2-1) can be expressed with a different form as:

$$\begin{bmatrix} dF_t \\ dF_r \\ dF_a \end{bmatrix} = \begin{bmatrix} dS & uct_0 db & 0 & 0 & 0 & 0 \\ 0 & 0 & dS & uct_0 db & 0 & 0 \\ 0 & 0 & 0 & 0 & dS & uct_0 db \end{bmatrix} \begin{bmatrix} K_{te} \\ K_{tc} \\ K_{re} \\ K_{rc} \\ K_{ae} \\ K_{ac} \end{bmatrix} \tag{2-24}$$

or in the following compact form:

$$d\mathbf{F}_{ss} = \mathbf{E}_{coe}\boldsymbol{K}_f \tag{2-25}$$

where $d\mathbf{F}_{ss}$ represents dF_t, dF_r, dF_a and $\mathbf{E}_{coe}$ is defined as:

$$\mathbf{E}_{coe} = \begin{bmatrix} dS & uct_0 db & 0 & 0 & 0 & 0 \\ 0 & 0 & dS & uct_0 db & 0 & 0 \\ 0 & 0 & 0 & 0 & dS & uct_0 db \end{bmatrix}$$

and

$$\boldsymbol{K}_f = \begin{bmatrix} K_{te} & K_{tc} & K_{re} & K_{rc} & K_{ae} & K_{ac} \end{bmatrix}^T$$

Similarly, cutting forces are transformed into CCS and expressed as:

$$d\mathbf{F}_c = \mathbf{T}_l\mathbf{E}_{coe}\boldsymbol{K}_f \tag{2-26}$$

where $\mathbf{T}_l$ is the transformation matrix from the local frame to CCS and can be obtained by:

$$\mathbf{T}_l = \begin{bmatrix} -\sin(\kappa)\sin(\psi) & -\cos(\psi) & -\cos(\kappa)\sin(\psi) \\ -\sin(\kappa)c(\psi) & \sin(\psi) & -\cos(\kappa)\cos(\psi) \\ \cos(\psi) & 0 & -\sin(\kappa) \end{bmatrix}$$

$d\mathbf{F}_c$ represents dF_x, dF_y, dF_z. The total cutting forces by integrating each element at each flute are expressed as:

$$\boldsymbol{F}_c = \sum_{j=1}^{N_{fc}} \sum_{i=1}^{N_e} \mathbf{T}_l E_{coe} \boldsymbol{K}_f \tag{2-27}$$

Since the cutting force coefficients are constants, Eq. (2-27) can be represented in a compact form as:

$$\boldsymbol{F}_c = \mathbf{A}_{coe} \boldsymbol{K}_f \tag{2-28}$$

where $\mathbf{A}_{coe}$ is defined as:

$$\mathbf{A}_{coe} = \sum_{j=1}^{N_{fc}} \sum_{i=1}^{N_e} \mathbf{T}_l \mathbf{E}_{coe}$$

and it is determined by *dS*, UCT, and uncut chip width *db*. UCT is calculated by considering cutter run-out and vibration. After $\boldsymbol{F}_c$ is obtained from the measured cutting forces, the cutting force coefficients can be calculated using the least square fitting method and the cutting force coefficients $\boldsymbol{K}_f$ can be obtained by:

$$\boldsymbol{K}_f = (\mathbf{A}_{coe}{}^T \mathbf{A}_{coe})^{-1} \mathbf{A}_{coe}{}^T \boldsymbol{F}_c \tag{2-29}$$

2.3.7. The complete algorithm of cutting force prediction

So far we have modelled the influence of cutter run-out and cutter vibrations on the UCT during machining. The actual cutting force $\boldsymbol{F}_c(t)$ can then be determined by the actual UCT of the machining, given as:

$$\boldsymbol{F}_c(t) = \boldsymbol{F}_c\left(uct_0(t) + uct_{ro}(t) + uct_v(t)\right) \tag{2-30}$$

Substituting Eqs. (2-14), (2-19) and (2-30) into Eq. (2-15), we will have a time-delayed differential equation, which, once solved, would give us the predicted cutting force. However, due to the lack of an explicit representation of the relationship between $\boldsymbol{F}_c\left(t\right)$ and UCT, this second order equation can only be solved using discrete methods under state-space representation. Let $\dot{\boldsymbol{X}}_c(t)=\boldsymbol{Q}(t)$, the state-space representation of the equation can be obtained:

$$\begin{aligned}&\dot{\boldsymbol{X}}_c(t)=\boldsymbol{Q}(t)\\&\dot{\boldsymbol{Q}}(t)=\boldsymbol{F}_c(t)-\boldsymbol{K}\boldsymbol{X}_c(t)-\boldsymbol{C}_c\boldsymbol{Q}(t)\end{aligned} \tag{2-31}$$

In this study, the classical fourth order Runge-Kutta method (Butcher 1987) has been deployed with assumptions of zero initial conditions ($\boldsymbol{X}_c(0)=0,\dot{\boldsymbol{X}}_c(0)=0$) and a carefully chosen time step of 1e-5s. In this way, a prediction of the cutting forces with consideration of cutter run-out and vibrations can be obtained.

The complete cutting force prediction algorithm for 5-axis milling works as follows: at each time instant, the cutter disks that are engaged in machining are first identified. Corresponding to each layer, the UCT contributed by the designed feedrate and cutter run-out is obtained. The previous in-cut cutter position of the cutter corresponding to the current time instant is obtained as well. With such information plus the state of the system at the last time instant, the real-time cutter displacement from vibration can be solved for and the cutting force at the current time instant can be predicted. The real-time cutter displacement would then be saved to be used in predictions at later stage. The complete workflow for the proposed cutting force prediction algorithm is given in Figure 2.10.

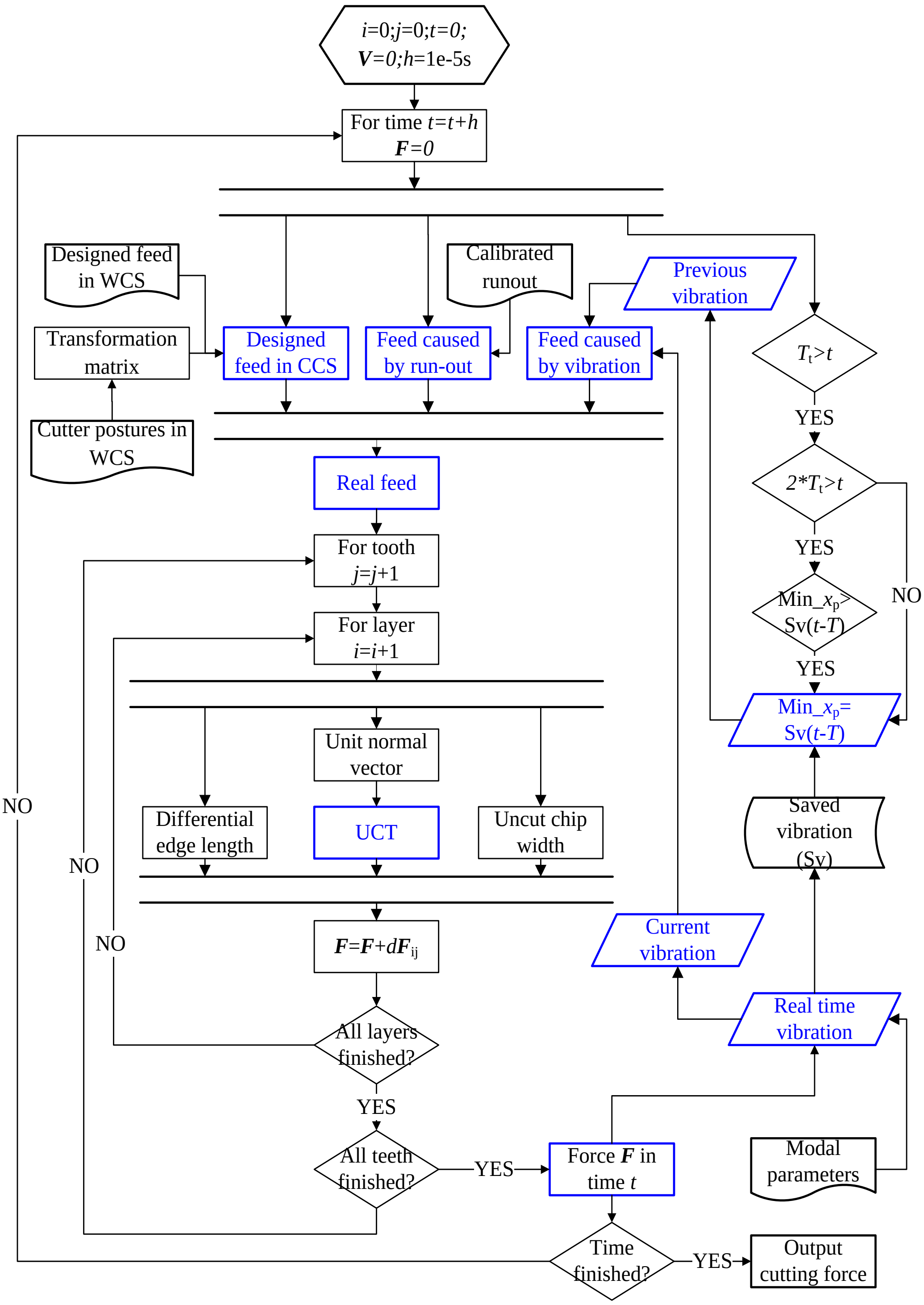

Figure 2.10 Flow chart of the completed algorithm

2.4. Experimental Validation

To validate the proposed cutting force prediction method, a number of experiments have been designed under various machining conditions. The machine tool used is DMG 80P duo Block 5-axis machining centre. The workpiece material used is AL7075. The cutting forces were measured using a stationary Kistler 9443 dynamometer that measures forces in three orthogonal directions. The sampling rate for measurement is 20,000 and the low pass frequency is 300Hz. The setup of the cutting experiments is shown in Figure 2.11a and the setup for impact test is shown in Figure 2.11b. For 5-axis machining, the cutter was pre-oriented with the desired posture at a safety height and then lowered for machining on a pre-formed flat surface. The workpiece is set up in such a way that the WCS is aligned with the three orthogonal measuring directions of the dynamometer. Based on the cutter posture, the transformation matrix between the CCS and the WCS can be obtained. The predicted cutting forces from CCS are then transformed into WCS for a direct comparison.

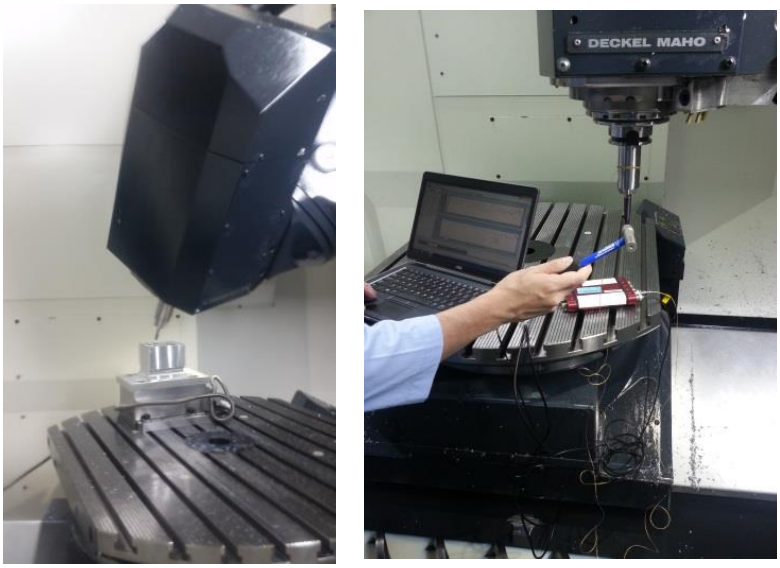

(a) For cutting experiments (b) For modal parameters testing

Figure 2.11 Setup of cutting experiments and modal parameters testing

The experiment conditions for cutting force validation are shown in Table 2.1, in which 9 sets of machining conditions were tested. For each set of machining conditions, different cutter postures are used as shown in Table 2.2. Obviously, any pick from Table 2.1 ("T1" to "T9") and any pick from Table 2.2 ("P1" to "P6") will form a unique condition for an experiment. On the other hand, in the experiments, a Fraisa 2-fulte ball-end cutter (R = 5mm, $i_0 = 20^{\circ}$) is used. The obtained modal parameters are shown in Table 2.3. The calibrated cutting force coefficients are shown in Table 2.4. The identified cutter run-out parameters are: cutter axis offset 9.0 μm, and locating angle of offset 0.0415 rad.

Table 2.1 Machining conditions for experiments

Test	Spindle speed (rpm)	Feed-per-tooth (mm/rev)	Feedrate (mm/min)	Depth-of-cut (mm)	Types
T1	2000	0.05	200	1	Half
T2	3000	0.1	600	1	Slotting
T3	1200	0.1	240	1	Slotting
T4	1200	0.05	120	1	Slotting
T5	5000	0.03	300	1.5	Slotting
T6	5300	0.032	339.2	0.2	Slotting
T7	2000	0.0848	339.2	0.2	Slotting
T8	2400	0.1	480	1	Half
T9	2400	0.1	480	1	Slotting

Table 2.2 Cutter posture combination

Posture	Lead angle (degree)	Tilt angle (degree)
P1	0	0
P2	0	10
P3	0	30
P4	20	0
P5	30	0
P6	30	30

Table 2.3 Modal parameters

Natural frequency (Hz)		Process damping (1%)		Stiffness (N/m^2)	
X_T	Y_T	X_T	Y_T	X_T	Y_T

1412.5	1443.75	0.033112	0.032257	13543571.05	14808892.07

Table 2.4 Calibrated cutting force coefficients

K_{te} (N/mm)	K_{tc} (N/mm^2)	K_{re} (N/mm)	K_{rc} (N/mm^2)	K_{ae} (N/mm)	K_{ac} (N/mm^2)
14.0371	951.751	16.5002	608.561	-1.25118	288.478

As an example, the predicted cutting forces using the proposed method and measured cutting forces under the conditions of “T9 + P6” are shown in Figure 2.12. Figure 2.12a shows the cutting force profiles (both measured and predicted) over a period of 2.5s. Since a complete revolution period is very short (2.5s ≈ 100 revolutions), it is therefore impossible to see how cutting force profiles changed in a clear manner. For a better view on the matching between measured and predicted forces, Figure 2.12b is added to show the cutting force profile for one revolution only, together with Figure 2.12c for one tooth-passing period only. The measured cutting force data are specified with circles, while the predicted values are plotted with dashed lines. The cutting forces in $\mathbf{X}_w$, $\mathbf{Y}_w$, and $\mathbf{Z}_w$ directions are represented with the colours of red, blue, and green, respectively. With each revolution period, it can be seen that the cutting forces generated by each tooth, both measured and predicted, differs in magnitude, which is proof of the effect of cutter run-out on cutting force. Meanwhile, in order to illustrate the effect of cutter vibration on cutting force, predictions of cutting force are made without considering cutter vibration and the results are shown in Figure 2.13. Compared to predictions with consideration of cutter vibrations, the increase in prediction error is obvious.

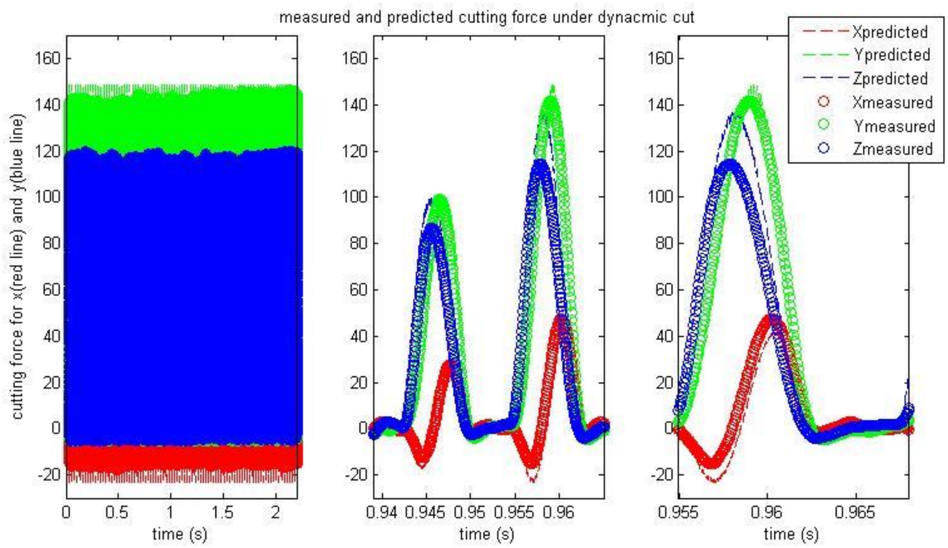

(a) Force in the whole process (b) Force in one cycle (c) Force in specific area

Figure 2.12 Predicted and measured cutting forces (with vibration consideration) for“T9+P6”

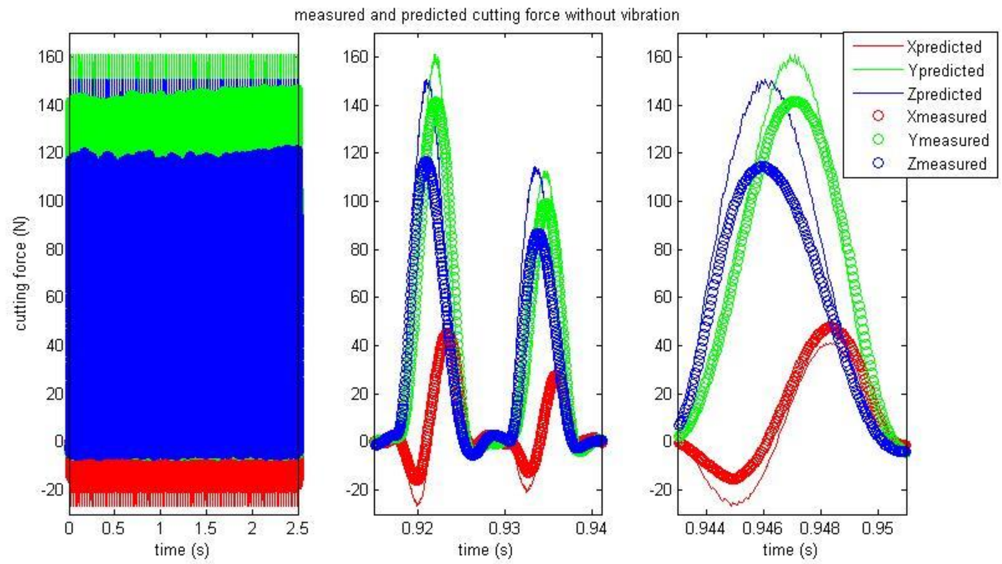

(a) Force in the whole process (b) Force in one cycle (c) Force in specific area

Figure 2.13 Predicted and measured cutting force (without vibration consideration) for “T9+P6”

For direct comparison, the absolute errors between the measured and predicted cutting forces for the models with and without vibration consideration under conditions of “T9+P6” are shown in Figure 2.14. It can be clearly seen that when vibration is considered, the maximum prediction errors along $\mathbf{X}_W$ (from 16.03 N to 14.52 N, 9.42%), $\mathbf{Y}_W$ (from 27.76 N to 17.29 N, 37.72%), and $\mathbf{Z}_W$ (from 41.85 N to 29.46 N, 29.61%) have been reduced significantly. Comparisons of force prediction under other experimental conditions are also listed in Table 2.5. All of them show that certain improvements have been achieved when cutter vibrations are considered.

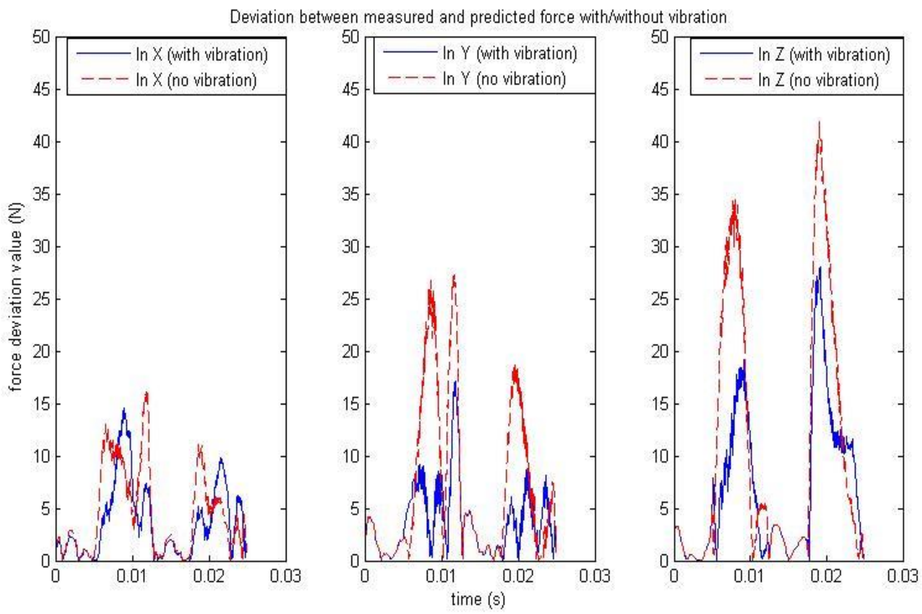

Figure 2.14 Prediction deviation with and without vibration for “T9+P6”

Table 2.5 Comparison of cutting force prediction error when vibration is considered and not considered

	T9+P1	**T9+P2**	**T9+P3**	**T9+P4**	**T9+P5**	**T9+P6**	**T8+P1**	**T8+P2**
X_W w/o vib (N)	73.73	56.36	38.12	34.24	22.26	16.03	56.88	47.12
Y_W w/o vib (N)	34.80	28.21	35.40	42.58	31.29	27.76	69.45	53.48
Z_W w/o vib (N)	18.75	50.15	42.62	39.76	31.73	41.85	51.03	46.88
X_W w vib (N)	50.11	42.38	38.02	22.56	17.53	14.52	43.32	37.18
Y_W w vib (N)	26.91	21.36	22.10	32.81	29.45	17.29	65.48	48.22
Z_W w vib (N)	13.24	40.79	30.18	27.52	27.05	29.46	48.94	40.87

Table 2.5 Comparison of cutting force prediction error when vibration is considered and not considered (Continued)

	T8+P3	**T8+P4**	**T8+P5**	**T8+P6**	**T7+P1**	**T7+P2**	**T7+P3**	**T7+P4**
X_W w/o vib (N)	41.32	31.76	33.18	23.46	10.05	15.41	27.1	7.38
Y_W w/o vib (N)	43.81	35.91	39.57	24.12	18.72	17.43	9.81	20.48
Z_W w/o vib (N)	30.21	32.65	36.42	29.78	14.16	21.39	25.27	17.24
X_W w vib (N)	30.88	28.41	30.26	20.98	8.87	13.28	24.39	6.98
Y_W w vib (N)	26.54	30.62	29.65	19.22	16.28	16.58	8.68	20.41
Z_W w vib (N)	21.34	20.02	32.12	18.92	13.21	17.47	23.65	16.79
	T7+P5	**T7+P6**	**T6+P1**	**T6+P2**	**T6+P3**	**T6+P4**	**T6+P5**	**T6+P6**
X_W w/o vib (N)	7.47	9.89	10.03	13.31	33.43	5.42	5.31	8.52
Y_W w/o vib (N)	22.71	23.93	12.41	17.01	9.84	16.14	18.2	19.12
Z_W w/o vib (N)	19.13	26.17	1077	16.29	35.51	15.12	16.76	22.66
X_W w vib (N)	6.94	9.78	10.00	12.23	31.49	5.01	5.12	8.21
Y_W w vib (N)	22.45	22.12	12.13	15.88	8.77	15.58	17.35	17.11
Z_W w vib (N)	18.77	24.89	10.47	15.98	34.71	14.72	16.23	21.31
	T5+P1	**T5+P2**	**T5+P3**	**T5+P4**	**T5+P5**	**T5+P6**	**T4+P1**	**T4+P2**
X_W w/o vib (N)	50.86	41.74	56.3	28.98	24.47	11.33	47.21	31.39
Y_W w/o vib (N)	67.1	51.35	36.23	57.15	53.45	54.55	56.17	50.01
Z_W w/o vib (N)	36.11	45.43	72.75	35.84	40.39	57.8	36.19	45.7
X_W w vib (N)	50.01	39.96	48.3	28.1	22.74	11.12	45.85	31.39
Y_W w vib (N)	58.75	50.51	28.46	53.41	52.5	49.3	55.15	48.52
Z_W w vib (N)	34.61	43.11	63.25	34.6	38.1	53.1	35.25	44.34
	T4+P3	**T4+P4**	**T4+P5**	**T4+P6**	**T3+P1**	**T3+P2**	**T3+P3**	**T3+P4**
X_W w/o vib (N)	58.55	26.41	27.21	16.47	67.1	46.53	71.6	41.34
Y_W w/o vib (N)	40.72	52.1	54.32	56.05	73.2	75.2	65.41	75.35
Z_W w/o vib (N)	77.31	36.1	41.26	58.45	47.75	59.95	75.5	47.36
X_W w vib (N)	51.05	25.51	25.2	15.73	64.65	45.35	63.35	40.62
Y_W w vib (N)	33.53	50.03	54.31	51.65	70.2	74.13	56.1	72.25
Z_W w vib (N)	67.45	35.85	33.65	53.98	46.33	58.68	64.86	47.05
	T3+P5	**T3+P6**	**T2+P1**	**T2+P2**	**T2+P3**	**T2+P4**	**T2+P5**	**T2+P6**
X_W w/o vib (N)	41.18	20.92	60.21	48.67	56.85	30.24	36.72	16.24
Y_W w/o vib (N)	69.4	56.45	68.5	62.2	52.31	61.32	57.12	42.65
Z_W w/o vib (N)	53.25	57.2	48.33	47.41	59.66	43.69	52.46	45.72
X_W w vib (N)	32.93	20.05	56.87	46.54	52.47	29.65	35.3	16.85

Table 2.5 Comparison of cutting force prediction error when vibration is considered and not considered (Continued)

Y_W w vib (N)	67.31	50.86	68.4	62.1	44.12	59.8	54.37	42.85
Z_W w vib (N)	44.04	51.05	46.78	45.4	50.4	38.41	33.08	39.54
	T1+P1	**T1+P2**	**T1+P3**	**T1+P4**	**T1+P5**	**T1+P6**		
X_W w/o vib (N)	68.38	53.84	33.65	22.28	21.19	16.2		
Y_W w/o vib (N)	69.75	52.69	38.61	39.65	46.45	45.25		
Z_W w/o vib (N)	62.73	46.96	25.74	31.27	37.14	46.79		
X_W w vib (N)	68.38	31.88	30.54	20.06	20.29	16.1		
Y_W w vib (N)	69.03	42.12	29.86	26.54	44.29	42.35		
Z_W w vib (N)	50.69	43.46	16.49	18.98	31.28	39.65		

2.5. Summary

In this chapter, a new cutting force prediction model in 5-axis milling considering cutter run-out and vibrations has been proposed. Based on the observation that the cutter-workpiece engagement in 5-axis milling can be effectively reconstructed from the one in orthogonal milling using a simple transformation, the calculation of UCT in 5-axis milling can be done efficiently and the long computation time can be avoided. The influence of cutter run-out is modelled as extra terms on the designed feed-per-tooth. By assuming the machining system is a 2-DOF spring-mass-damper system, the differential motion equation can be established. By solving this equation for the machining system using the forth order Runge-Kutta method, the real time cutter displacement can be obtained. The influence of the cutter vibrations can also be modelled as an extra feed on the designed feed-per-tooth. Integrating the effect of cutter run-out and cutter vibrations on cutting force prediction, the complete and accurate cutting force prediction method is achieved. Using this prediction method, the cutting force for ball-end cutter in 5-axis milling can be predicted more accurately. Finally, experimental validation using ball-end cutter in 5-axis machining is presented to validate the proposed method. So far, this algorithm is only implemented considering the ball-end cutter, however, the effect of cutter run-out and vibration on cutting force prediction is applicable in any kinds of cutters, including the fillet-end cutter and flat-end cutter.

CHAPTER 3

CHATTER PREDICTION IN 5-AXIS MACHINING AND PSG CONSTRUCTION

Chatter is an important adverse dynamic factor in machining process that will result in poor machined surface quality and may lead to the cutter breakage in extreme situations. Thus, chatter must be avoided during machining process. To this end, chatter prediction is critical for generating chatter-free tool path in 5-axis machining.

In this chapter, the proposed chatter prediction method in 5-axis machining will be presented. Subsequently, at any CC point, a new user-guide map for chatter-free postures will be proposed, which can be used for generating chatter-free tool paths.

As chatter arises when the variation frequency of cutting force approaches the chatter frequency of the machine tool, chatter prediction starts with cutting force prediction. Using the cutting force prediction method presented in the previous chapter, the dynamic cutting force can be predicted. Based on the assumption that 5-axis machining is a 2-DOF vibrational system, the dynamic equation of the 5-axis machining system can be established with the measured modal parameters. The stability of the 5-axis machining system can then be determined using the full-discretization (FD) method. Following this approach, by only changing the cutter posture while keeping other machining conditions unchanged, the stability status under different cutter postures can be generated and chatter-free posture ranges can be identified. This stability-posture map is called the posture stability graph (PSG).

3.1. Background

Chatter is a form of self-excited and regenerative vibration, usually caused by inadequate stiffness of the machining system, made of the cutter, holder, workpiece, and machine tool itself (Altintas 2000; Quintana and Ciurana 2011; Siddhpura and Paurobally 2012). As the cutting force varies periodically and the machining system is not a rigid system, cutter deflection is inevitable and also periodic, which will leave a wavy surface after one teeth machining. This wavy surface will be removed by the next teeth which will also leave a wavy machined surface. The two successive waves will have a phase shift and this phase shift may excite the vibrations. Therefore, the maximum chip thickness may grow exponentially when oscillating at a chatter frequency that is close to but not equal to a dominant structural mode in the machining system (Altintas 2000). The growing vibrations increase the cutting forces and may chip the tool and produce a poor, wavy machined surface.

Possible existence of machining chatter is a key adverse factor that affects the surface finish quality for all machining processes. Therefore, chatter must be avoided during 5-axis machining. At a CC point, the machining conditions that will affect machining stability include: depth-of-cut, spindle speed, and cutter postures. Among these parameters, for 5-axis finish cut of sculptured surfaces, depth-of-cut and spindle speed can be considered approximately constant. This leaves cutter posture as the only variable factor. Therefore, chatter prediction or stability evaluation under a given cutter posture is critical for generating chatter-free tool path in 5-axis machining.

3.2. Related Works

Much research (Merritt 1965; Sridhar *et al.* 1968; Minis *et al.* 1990; Budak and Altintas 1998; Altintas 2001; Bediaga *et al.* 2005; Eynian and Altintas 2010; Peng *et al.* 2014) has been conducted regarding the mechanism of chatter, which shows that a bad combination of spindle speed and depth-of-cut would trigger chatter in 3-axis machining. Stability Lobe Diagram (SLD) has since been developed as a practical tool to guide machinists to select the proper machining condition for chatter avoidance (Rafal 2012; Shamoto *et al.* 2012; Iglesias *et al.* 2014).

Meanwhile, for 5-axis machining, cutter orientation or posture is probably the most important process parameter (Choi and Jerard 1998). A cutter posture is usually described by its lead and tilt angles, defined against the cross-feed and feed directions during machining (see Figure 2.2a). Intuitively, the introduction of cutter posture as an extra variable would make chatter prediction more complicated. An example is provided in Figure 3.1, showing a ball-end cuter machining a straight 'ditch' on a flat surface with two different cutter postures.

The machining parameters are kept exactly the same in both cases (Depth-of-cut: 0.5mm, Spindle speed: 4,800 r/min, Material: AL5075) except the cutter posture (first: lead angle: 60°, tilt angle: 0°; second: lead angle: 40°, tilt angle: 0°). From the microscopic images of the resulted surfaces shown in Figure 3.1b and 3.1c, respectively, completely different surface finish qualities can be observed (chatter marks clearly appear in Figure 3.1c), although the two cutter postures have only 20° difference in the lead angle. The surface quality difference is a result of the difference between stable and unstable machining. Clearly, cutter posture plays a significant role in stability of 5-axis machining.

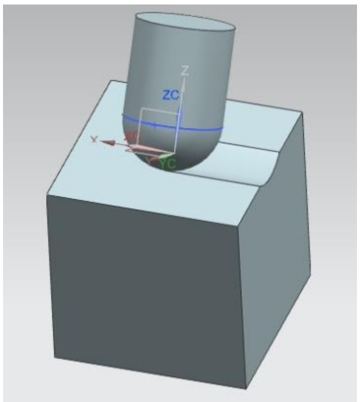

(a) slotting with a ball-nose cutter

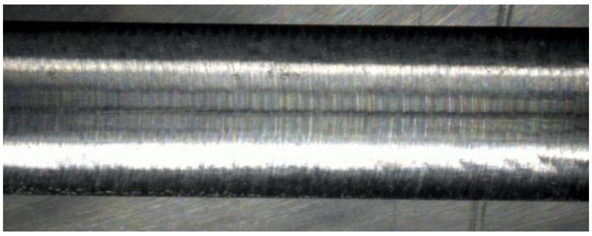

(b) lead angle: 60 °, tilt angle: 0 °

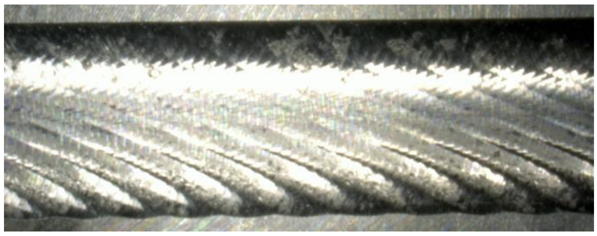

(c) lead angle: 40 °, tilt angle: 0 °

Figure 3.1 Influence of cutter posture on chatter stability and surface finish quality.

During practical machining, spindle speed is usually selected based on the optimal cutting speed for certain materials and the cutter diameter, and thus will be subject to little change. On the other hand, in finish cut, depth-of-cut is also considered approximately constant for the whole surface. Considering this practice, it would be significant to construct a *Posture Stability graph* (PSG), which establishes the relationship between cutter postures and stability of the machining. PSGs can then be used to select chatter-free cutter postures, thus eliminating possibility of chatter at the stage of tool path generation. This would make a significant step towards integrated process planning for 5-axis machining.

Construction of PSG relies on prediction of machining chatter in 5-axis machining. Over the years, much research (Sridhar *et al.* 1968; Minis *et al.* 1990; Budak and Altintas 1998; Ahmadi and Ismail 2012; Cao *et al.* 2012; Wang *et al.* 2014) has been conducted to predict chatter in 3-axis machining, most of which focused on determining maximum chatter-free depth-of-cut for a specified spindle speed by modelling the machining system dynamically. (Sridhar *et al.* 1968) modelled milling operations using linear differential-difference equations with periodic coefficients, the stability of which can be identified analytically. Later, (Minis *et al.* 1990) solved the stability problem for 2D dynamic milling problems with an iterative method, using Nyquist stability criterion to identify the stability limits.(Budak and Altintas 1998) determined chatter stability limit analytically by approximating the time varying directional machining coefficients using their Fourier series components. Meanwhile, limited study has been reported for chatter stability of 5-axis milling. Methods for constructing SLDs under different cutter postures were reported by(Ozturk *et al.* 2007) and (Shamoto and Akazawa 2009). Recently, the influence of cutter lead angle on SLDs was studied by(Mousseigne *et al.* 2012).(Ahmadi and Ismail 2012) even built SLDs for 5-axis peripheral milling of flat surfaces. These methods are still incomprehensive in guiding cutter posture determination during 5-axis tool path generation. With the PSG method proposed in this study, chatter-avoidance can be integrated into the process planning system in a similar manner as the interference-avoidance algorithm (Li *et al.* 2011), to provide the feasible range of cutter postures.

In the remaining of this chapter, the proposed dynamic model of 5-axis machining system is to be presented and the method to solve for the stability of the system using the FD method is to be introduced. Based on the result of stability analysis, PSG can be constructed under any combination of spindle speed and cutter-workpiece engagement condition. Several simulation results under different depths-of-cut, together with corresponding experimental validation results will be presented to show the effectiveness of proposed method.

3.3. Modelling of Chatter in 5-axis Milling

Chatter is predicted based on the stability analysis of the machining system under the excitation of cyclic machining forces. In this section, the dynamic model of the machining system is to be established using the cutting force prediction method presented in the previous chapter, followed by the establishment of dynamic equation of 5-axis machining system. By solving the dynamic equation using the FD method, the stability of the machining system can be determined.

3.3.1. Dynamic cutting force model

Chatter prediction starts with the prediction of dynamic cutting force, which acts as the excitation input for the machining system. The prediction for dynamic cutting force is based on the cutting force prediction method presented in the Chapter 2. Firstly, the cutter is discretized along the cutter axis into N_e layers. As the dynamic cutting force is caused by the dynamic cutter displacement instead of the feed caused by the designed cutter feed, the cutting force generated by a single elemental cutting edge, including tangential dF_t, radial dF_r, and axial dF_a cutting forces is obtained by:

$$\begin{cases} dF_t^{i,j}\left(\theta, z_e\right) = K_{te}dS + K_{tc}t_{uct}db \\ dF_r^{i,j}\left(\theta, z_e\right) = K_{re}dS + K_{rc}t_{uct}db \\ dF_a^{i,j}\left(\theta, z_e\right) = K_{ae}dS + K_{ac}t_{uct}db \end{cases} \tag{3-1}$$

where K_{te} , K_{re} and K_{ae} are the edge force coefficients and K_{tc} , K_{rc} and K_{ac} are the shear coefficients, which can be calibrated for any given combination of cutter and material. dS is the differential element length of the cutting edge; db is the uncut chip width and t_{uct} is the dynamic cutter displacement caused by cutter vibration and it can be calculated as the displacement of the cutter projected along the surface normal at location of the elemental cutting edge, given as:

$$
\begin{aligned}
t_{uct} &= \boldsymbol{n}_{nv} \cdot \boldsymbol{d}_{dv} \\
\boldsymbol{n}_{nv} &= \begin{bmatrix} s(\kappa)s(\psi) \\ s(\kappa)c(\psi) \\ c(\kappa) \end{bmatrix}^{\mathrm{T}} \\
\boldsymbol{d}_{dv} &= \begin{bmatrix} x_c(t) - x_c(t-T) \\ y_c(t) - y_c(t-T) \\ z_c(t) - z_c(t-T) \end{bmatrix}
\end{aligned}
\tag{3-2}
$$

where κ, ψ are height and angular position angles of the cutter element and $\boldsymbol{n}_{nv}$ is the normal vector and $\begin{bmatrix} x_c(t) & y_c(t) & z_c(t) \end{bmatrix}^T$ gives the location of the cutter centre at time t and T is the tooth passing period of the cutter.

Same as the situation in cutting force prediction, a cutting edge will enter and exit from the engagement region. When mapped onto each cutter disk, the engagement region is represented with one or several pairs of entry and exit angles $\left(\varphi_{ey}^{i,j}, \varphi_{et}^{i,j}\right)$. Cutting force will only be generated by certain cutting edge elements whose angular positional angle satisfies $\varphi_{ey}^{i,j} < \psi < \varphi_{et}^{i,j}$. Hence, we propose the following step function $g(\psi)$:

$$
\begin{aligned}
&g(\psi) = 1 \text{ when } \varphi_{ey}^{i,j} < \psi < \varphi_{et}^{i,j} \\
&g(\psi) = 0 \text{ when otherwise}
\end{aligned}
\tag{3-3}
$$

Finally, the elemental cutting force can be transformed to the cutter frame using Eq. (2-6) and rewritten in a matrix form:

$$
\begin{bmatrix} dF_x^{i,j} \\ dF_y^{i,j} \\ dF_z^{i,j} \end{bmatrix}_c = g(\psi)\mathbf{T}_l \begin{bmatrix} dF_r^{i,j} \\ dF_t^{i,j} \\ dF_a^{i,j} \end{bmatrix}
\tag{3-4}
$$

where $\mathbf{T}_l$ is the transformation matrix given as:

$$\mathbf{T}_l = \begin{bmatrix} -\sin(\kappa)\sin(\psi) & -\cos(\psi) & -\cos(\kappa)\sin(\psi) \\ -\sin(\kappa)c(\psi) & \sin(\psi) & -\cos(\kappa)\cos(\psi) \\ \cos(\psi) & 0 & -\sin(\kappa) \end{bmatrix} \tag{3-5}$$

A summation of the elemental cutting forces contributed by each cutter disk will give the total cutting force acting on the cutter. The engagement region can be obtained via geometric analysis. It is worth noting that, when machining with a ball-end cutter, the change in cutter postures will not affect the shape of the engagement region, but only the distribution of the region on the cutter surface. This means engagement information for any posture can be re-constructed from that of a single input posture with reduced computation load (Geng *et al.* 2015).

3.3.2. Dynamic equation of machining system

In the proposed model, the cutter is assumed to have 2-DOF in two orthogonal directions, both normal to the cutter axis. The modal parameters along these two directions can be obtained with two separate impact tests. For the sake of clearer description, a modal frame $\mathbf{O}_\mathrm{M}$-$\mathbf{X}_\mathrm{M}\mathbf{Y}_\mathrm{M}\mathbf{Z}_\mathrm{M}$ is also attached to the cutter (see Figure 3.2), where $\mathbf{X}_\mathrm{M}$ and $\mathbf{Y}_\mathrm{M}$ are along the two impact directions (the directions that impacting test exerted) and $\mathbf{Z}_\mathrm{M}$ is along the cutter axis. It should be noted that although $\mathbf{Z}_\mathrm{M}$ is coincident with $\mathbf{Z}_\mathrm{T}$ of cutter coordinate system (CCS), $\mathbf{X}_\mathrm{T}$ is determined by the feed direction while the $\mathbf{X}_\mathrm{M}$ is determined by the impact direction, which is not influenced by feed direction.

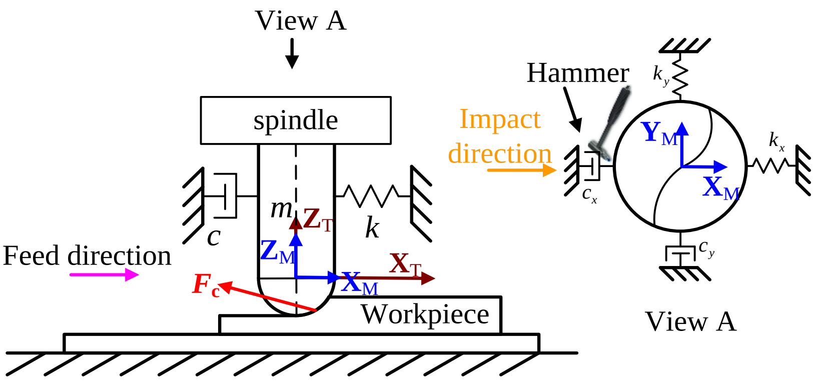

Figure 3.2 Illustration of dynamic machining system

During machining, the static part of the machining force, i.e., the part proportional to dS , which is not affected by the dynamic cutter displacement, will not contribute to the regenerative mechanism (the cause behind chatter) and will thus be dropped. Substituting $db = dz / \sin(\kappa)$, we will have:

$$\begin{bmatrix} dF_x^{i,j} \\ dF_y^{i,j} \\ dF_z^{i,j} \end{bmatrix}_C = \mathbf{T}_l \begin{bmatrix} dF_r^{i,j} \\ dF_t^{i,j} \\ dF_a^{i,j} \end{bmatrix} = g(\psi) \frac{dz}{\sin(\kappa)} \mathbf{T}_l \begin{bmatrix} K_{rc} \\ K_{tc} \\ K_{ac} \end{bmatrix} \boldsymbol{n}_{nv} \left(\begin{bmatrix} x_C(t) \\ y_C(t) \\ z_C(t) \end{bmatrix} - \begin{bmatrix} x_C(t-T) \\ y_C(t-T) \\ z_C(t-T) \end{bmatrix} \right) \tag{3-6}$$

The additional subscript in $x_C(t)$ indicates that the calculation takes place in CCS. Summing up the elemental cutting force from all the involved edges, the total dynamic forces are calculated as:

$$\begin{bmatrix} F_x \\ F_y \\ F_z \end{bmatrix}_C = \sum_{i=1}^{N_{fc}} \sum_{j=1}^{N_e} \begin{bmatrix} dF_x^{i,j} \\ dF_y^{i,j} \\ dF_z^{i,j} \end{bmatrix} \tag{3-7}$$

Defining

$$\mathbf{B}(t) = \sum_{i=1}^{N_{fc}} \sum_{j=1}^{N_e} \left(\frac{g(\psi)}{\sin(\kappa)} \mathbf{T}_l \begin{bmatrix} K_{rc} \\ K_{tc} \\ K_{ac} \end{bmatrix} \boldsymbol{n}_{nv} \right)$$

Eq. (3-7) can be rewritten as:

$$\begin{bmatrix} F_x \\ F_y \\ F_z \end{bmatrix}_C = \Delta z \mathbf{B}(t) \left(\begin{bmatrix} x_C(t) \\ y_C(t) \\ z_C(t) \end{bmatrix} - \begin{bmatrix} x_C(t-T) \\ y_C(t-T) \\ z_C(t-T) \end{bmatrix} \right) \tag{3-8}$$

When the real machining is carried out, we cannot assume that the feed direction is always along with $\mathbf{X}_w$ of the workpiece coordinate system (WCS) shown in Figure 3.3. Here, we assume the feed direction is defined in WCS and expressed as $\boldsymbol{f}_F = [x_w \quad y_w \quad z_w]^T$ as shown in Figure 3.3. Then, the transformation from the feed frame to WCS can be done using the following transformation matrix:

$$\mathbf{T}_{fTw} = \mathbf{T}_{\theta_f} \mathbf{T}_{\gamma_f} \tag{3-9}$$

where

$$\mathbf{T}_{\theta_f} = \begin{bmatrix} \cos(\theta_f) & 0 & \sin(\theta_f) \\ 0 & 1 & 0 \\ -\sin(\theta_f) & 0 & \cos(\theta_f) \end{bmatrix} \mathbf{T}_{\gamma_f} = \begin{bmatrix} \cos(\gamma_f) & -\sin(\gamma_f) & 0 \\ \sin(\gamma_f) & \cos(\gamma_f) & 0 \\ 0 & 0 & 1 \end{bmatrix}$$

$$\theta_f = \arcsin(x_f / \sqrt{z_f^2 + x_f^2})$$

$$\gamma_{fd} = \arctan(-y_f / x_f)$$

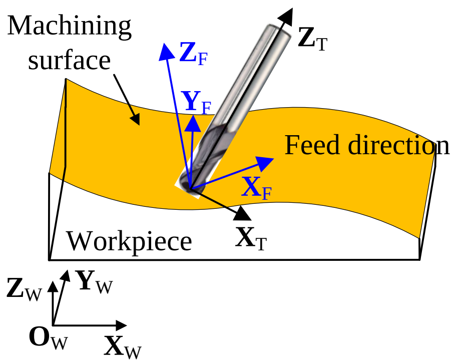

Figure 3.3 Transformation between WCS and feed frame

So far, the cutter displacements and corresponding cutting forces are all calculated in the CCS. However, it should be noted that, in practice, it is impossible to align the modal frame with every CCS corresponding to each cutter posture when impact test is done on the machine. For the sake of convenience, the impacting directions are selected to be along the $\mathbf{X}_{\mathrm{MT}}$ and $\mathbf{Y}_{\mathrm{MT}}$ of machine tool coordinate system (MTCS), when every rotary axis is at zero position on the machine (see Figure 3.4). The modal frame will also rotate with the cutter when a certain posture is taken by the cutter. The transformation matrix between CCS and the modal frame will therefore be determined by the specific structure of the used machine.

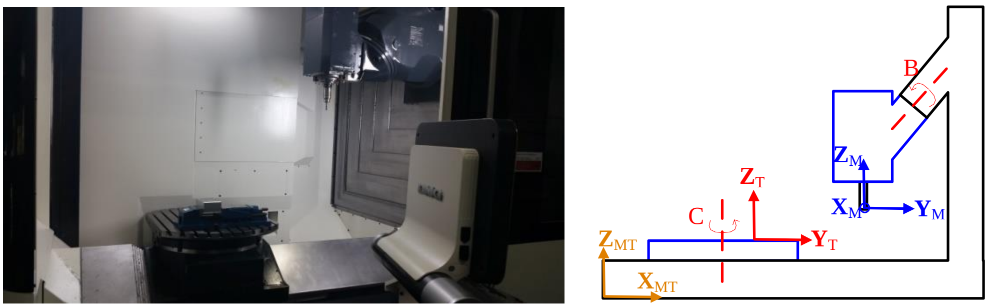

(a) 5-axis machining center (b) illustration of machine structure

Figure 3.4 Determination of impact testing directions.

For instance, in our experiments, the used machine (model: DMG 80P duo Block) has a non-orthogonal swivel head configuration. The transformation between the modal frame and the workpiece frame is given as:

$$\mathbf{T}_{mTf} = \mathbf{T}_{fTw}^{-1}\mathbf{T}_{tTw}\mathbf{T}_{C}\mathbf{T}_{135}\mathbf{T}_{B}\mathbf{T}_{45} \tag{3-10}$$

where $\mathbf{T}_{tTw}$ is the transformation matrix from the machine table to the workpiece, determined by the way the workpiece is set up on the table and the other matrices are given as:

$$\mathbf{T}_{C} = \begin{bmatrix} \cos(C) & -\sin(C) & 0 \\ \sin(C) & \cos(C) & 0 \\ 0 & 0 & 1 \end{bmatrix} \quad \mathbf{T}_{135} = \begin{bmatrix} 1 & 0 & 0 \\ 0 & \cos(135^{\circ}) & -\sin(135^{\circ}) \\ 0 & \sin(135^{\circ}) & \cos(135^{\circ}) \end{bmatrix}$$

$$\mathbf{T}_B = \begin{bmatrix} \cos(B) & \sin(B) & 0 \\ -\sin(B) & \cos(B) & 0 \\ 0 & 0 & 1 \end{bmatrix} \mathbf{T}_{45} = \begin{bmatrix} 1 & 0 & 0 \\ 0 & \cos(45^\circ) & -\sin(45^\circ) \\ 0 & \sin(45^\circ) & \cos(45^\circ) \end{bmatrix} \tag{3-11}$$

Following this, the transformation matrix between the cutter and modal coordinate systems can be obtained as:

$$\mathbf{T}_{cTm} = \left(\mathbf{T}_{mTf}\right)^{-1} \mathbf{T}_{cTf} \tag{3-12}$$

Multiplying $\mathbf{T}_{cTm}$ on both sides of Eq. (3-8) gives us:

$$\begin{bmatrix} F_x \\ F_y \\ F_z \end{bmatrix}_M = \Delta z \mathbf{T}_{cTm} \mathbf{B}(t) \left(\begin{bmatrix} x_C(t) \\ y_C(t) \\ z_C(t) \end{bmatrix} - \begin{bmatrix} x_C(t-T) \\ y_C(t-T) \\ z_C(t-T) \end{bmatrix} \right) \tag{3-13}$$

The dynamic equation for our model of machining system can be written as:

$$\begin{bmatrix} m_x & 0 & 0 \\ 0 & m_y & 0 \\ 0 & 0 & m_z \end{bmatrix} \begin{bmatrix} \ddot{x}_M \\ \ddot{y}_M \\ \ddot{z}_M \end{bmatrix} + \begin{bmatrix} c_x & 0 & 0 \\ 0 & c_y & 0 \\ 0 & 0 & c_z \end{bmatrix} \begin{bmatrix} \dot{x}_M \\ \dot{y}_M \\ \dot{z}_M \end{bmatrix} + \begin{bmatrix} k_x & 0 & 0 \\ 0 & k_y & 0 \\ 0 & 0 & k_z \end{bmatrix} \begin{bmatrix} x_M \\ y_M \\ z_M \end{bmatrix} = \begin{bmatrix} F_x \\ F_y \\ F_z \end{bmatrix}_M$$

which can be re-written as:

$$\mathbf{M}\ddot{\boldsymbol{X}}_M(t) + \mathbf{C}\dot{\boldsymbol{X}}_M(t) + \mathbf{K}\boldsymbol{X}_M(t) = \Delta z \mathbf{T}_{cTm} \mathbf{B}(t) \mathbf{T}_{cTm}^{-1} \left(\boldsymbol{X}_M(t) - \boldsymbol{X}_M(t-T) \right) \tag{3-14}$$

where $\mathbf{M}$, $\mathbf{C}$ and $\mathbf{K}$ represent inertial, stiffness, and damping ratio matrices of the system, obtained through impact testing. $\boldsymbol{X}_M$ is a column vector representing the displacement of the cutter in the modal frame. Eq. (3-14) is the general expression for 5-axis machining. In reality, as the stiffness in the $\mathbf{Z}_M$ direction is very high, the terms in $\mathbf{Z}_M$ direction are usually dropped.

3.4. Chatter Prediction Using FD Method

It is obvious that Eq. (3-14) is a delay differential equation (DDE). At a specified spindle speed, which corresponds to a specific value of the tooth passing period T in

Eq. (3-15), the stability of the equation determines whether chatter exists during machining. Over the years, many attempts have been made by researchers to solve for stability condition. For example, the time domain simulation was proposed by Smith and Tlusty (1993). Although it is the most accurate method to calculate the critical value, it is highly time consuming. Later, Altintaş and Budak (1995) presented the zeroth order approximation (ZOA) method using the zeroth order Fourier term to approximate the time varying cutting force coefficients in milling operation. However, this method cannot accurately predict the critical parameters at low radial immersion milling operations (Insperger and Stépán 2002). Subsequently, by extending the ZOA method, the multi-frequency method was proposed to deal with this problem (Budak *et al.* 2009). However, the order of the Fourier term is still difficult to choose. Semi-discretization (SD) method was thus proposed to convert the DDE into a series of autonomous ordinary differential equations (ODEs), and then the stability of the system is determined by calculating the eigenvalues of the transition matrix, constructed using the coefficients of the series ODEs (Insperger and Stépán 2002; Insperger and Stépán 2004). Temporal finite element analysis (TFEA) was also proposed to deal with highly interrupted milling process (Bayly *et al.* 2003). However, this method is only suitable for very low radial immersion milling process. Recently, (Ding *et al.* 2010) presented a FD method which is similar to the SD method in the sense that both methods approximate the original DDE by a series of ODEs but produces better computational efficiency. In this study, the FD method is adopted to solve the DDE to determine the stability in 5-axis milling. The implementation is described in the following sections.

Firstly, the state variable $\mathbf{u}$ is defined as $\mathbf{u} = \left[\boldsymbol{X}_M(t) \quad \mathbf{M}\dot{\boldsymbol{X}}_M(t) + \mathbf{C}\boldsymbol{X}_M(t)/2 \right]^T$. With the state variables $\mathbf{u}$, Eq. (3-14) can be rewritten as:

$$\mathbf{u}(t)=\mathbf{A}_0^{\mathrm{u}}\mathbf{u}(t)+\mathbf{A}^{\mathrm{u}}(t)\mathbf{u}(t)+\mathbf{B}^{\mathrm{u}}(t)\mathbf{u}(t-T) \tag{3-15}$$

where,

$$\mathbf{A}_0^{\mathrm{u}}=\begin{bmatrix} -\mathbf{M}^{-1}\mathbf{C}/2 & \mathbf{M}^{-1} \\ \mathbf{C}\mathbf{M}^{-1}\mathbf{C}/4-K & -\mathbf{C}\mathbf{M}^{-1}/2 \end{bmatrix}$$

$$\mathbf{A}^{\mathrm{u}}(t)=\begin{bmatrix} 0 \quad 0 & 0 \quad 0 \\ 0 \quad 0 & 0 \quad 0 \\ \multirow{2}{*}{$-\Delta z\mathbf{B}(t)\mathbf{T}_{cTm}$} & 0 \quad 0 \\ & 0 \quad 0 \end{bmatrix}$$

$$\mathbf{B}^{\mathrm{u}}(t)=\begin{bmatrix} 0 \quad 0 & 0 \quad 0 \\ 0 \quad 0 & 0 \quad 0 \\ \multirow{2}{*}{$\Delta z\mathbf{B}(t)\mathbf{T}_{cTm}$} & 0 \quad 0 \\ & 0 \quad 0 \end{bmatrix}$$

The main idea of the FD method is to discrete the time period T into m small time intervals such that $T=m\tau$. Based on the direct integration scheme, on each time interval $k\tau \le t \le (k+1)\tau$, with the initial condition $\mathbf{u}_k = \mathbf{u}(k\tau)$, the response of Eq. (3-15) can be obtained via the direct integration scheme as:

$$\mathbf{u}(t)=e^{\mathbf{A}_0^{\mathrm{u}}(t-k\tau)}\mathbf{u}(k\tau)+\int_{k\tau}^{t}\left\{e^{\mathbf{A}_0^{\mathrm{u}}(t-\xi)}\left[\mathbf{A}^{\mathrm{u}}(\xi)\mathbf{u}(\xi)+\mathbf{B}^{\mathrm{u}}(\xi)\mathbf{u}(\xi-T)\right]\right\}d\xi \tag{3-16}$$

Equivalently, it can be expressed as:

$$\mathbf{u}(k\tau+t)=e^{\mathbf{A}_0^{\mathrm{u}}t}\mathbf{u}(k\tau)+\int_0^t\{[\mathbf{A}^{\mathrm{u}}(k\tau+t-\xi)\mathbf{u}(k\tau+t-\xi)+\mathbf{B}^{\mathrm{u}}(k\tau+t-\xi)\mathbf{u}(k\tau+t-\xi-T)]\}d\xi \tag{3-17}$$

where $0 \le t \le \tau$. Then, u_{k+1}, i.e., $\mathbf{u}(k\tau+\tau)$ can be obtained using:

$$\mathbf{u}_{k+1}=e^{\mathbf{A}_0^{\mathrm{u}}\tau}\mathbf{u}_k+\int_0^\tau\{e^{\mathbf{A}_0^{\mathrm{u}}\xi}[\mathbf{A}^{\mathrm{u}}(k\tau+\tau-\xi)\mathbf{u}(k\tau+\tau-\xi)+\mathbf{B}^{\mathrm{u}}(k\tau+\tau-\xi)\mathbf{u}(k\tau+\tau-\xi-T)]\}d\xi \tag{3-18}$$

Eq. (3-18) can be re-written as:

$$\mathbf{u}_{k+1}=(\mathbf{F}_0+\mathbf{F}_{0,1})\mathbf{u}_k+\mathbf{F}_{k+1}\mathbf{u}_{k+1}+\mathbf{F}_{m\text{-}1}\mathbf{u}_{k+1\text{-}m}+\mathbf{F}_m\mathbf{u}_{k\text{-}m} \tag{3-19}$$

where

$$\mathbf{F}_0 = \mathbf{\Phi}_0$$
$$\mathbf{F}_{0,1} = \left(\mathbf{\Phi}_2 / \tau\right)\left(\mathbf{A}_0^u\right)^{(k)} + \left(\mathbf{\Phi}_3 / \tau\right)\left(\mathbf{A}_1^u\right)^{(k)}$$
$$\mathbf{F}_{k+1} = \left(\mathbf{\Phi}_1 - \mathbf{\Phi}_2 / \tau\right)\left(\mathbf{A}_0^u\right)^{(k)} + \left(\mathbf{\Phi}_2 - \mathbf{\Phi}_3 / \tau\right)\left(\mathbf{A}_1^u\right)^{(k)}$$
$$\mathbf{F}_{m\text{-}1} = \left(\mathbf{\Phi}_1 - \mathbf{\Phi}_2 / \tau\right)\left(\mathbf{B}_0^u\right)^{(k)} + \left(\mathbf{\Phi}_2 - \mathbf{\Phi}_3 / \tau\right)\left(\mathbf{B}_1^u\right)^{(k)}$$
$$\mathbf{F}_m = \left(\mathbf{\Phi}_2 / \tau\right)\left(\mathbf{B}_0^u\right)^{(k)} + \left(\mathbf{\Phi}_3 / \tau\right)\left(\mathbf{B}_1^u\right)^{(k)}$$
$$\mathbf{\Phi}_0 = e^{\mathbf{A}_0^u \tau};\ \mathbf{\Phi}_1 = \left(A_0^u\right)^{-1}\left(\mathbf{\Phi}_0 - I\right)$$
$$\mathbf{\Phi}_2 = \left(\mathbf{A}_0^u\right)^{-1}\left(\tau\mathbf{\Phi}_0 - \mathbf{\Phi}_1\right)$$
$$\mathbf{\Phi}_3 = \left(\mathbf{A}_0^u\right)^{-1}\left(\tau^2\mathbf{\Phi}_0 - 2\mathbf{\Phi}_2\right)$$
$$\left(\mathbf{A}_0^{\mathrm{u}}\right)^{(k)} = \mathbf{A}_{k+1}^u;\ \left(\mathbf{A}_1^u\right)^{(k)} = \left(\mathbf{A}_k^u - \mathbf{A}_{k+1}^u\right)/\tau$$
$$\left(\mathbf{B}_0^{\mathrm{u}}\right)^{(k)} = \mathbf{B}_{k+1}^u;\ \left(\mathbf{B}_1^u\right)^{(k)} = \left(\mathbf{B}_k^u - \mathbf{B}_{k+1}^u\right)/\tau$$

If matrix $\left[\mathbf{I} - \mathbf{F}_{k+1}\right]$ is non-singular, u_{k+1} can be expressed in the following explicit form:

$$\mathbf{u}_{k+1} = \left[\mathbf{I} - \mathbf{F}_{k+1}\right]^{-1}(\mathbf{F}_0 + \mathbf{F}_{0,1})\mathbf{u}_k + \left[\mathbf{I} - \mathbf{F}_{k+1}\right]^{-1}\mathbf{F}_{m\text{-}1}\mathbf{u}_{k+1\text{-}m} + \left[\mathbf{I} - \mathbf{F}_{k+1}\right]^{-1}\mathbf{F}_m\mathbf{u}_{k\text{-}m} \tag{3-20}$$

In case that $\left[\mathbf{I} - \mathbf{F}_{k+1}\right]$ is singular, $\mathbf{u}_{k+1}$can be obtained using:

$$\mathbf{u}_{k+1} = \left(\mathbf{F}_0 + \mathbf{F}_{0,2}\right)\mathbf{u}_k + \mathbf{F}_{m\text{-}1}\mathbf{u}_{k+1\text{-}m} + \mathbf{F}_m\mathbf{u}_{k\text{-}m} \tag{3-21}$$

where

$$\mathbf{F}_{0,2} = \left(\mathbf{\Phi}_1\mathbf{A}_0^u\right)^{(k)} + \left(\mathbf{\Phi}_2\mathbf{A}_1^u\right)^{(k)}.$$

A discrete map can be defined as:

$$\boldsymbol{y}_{k+1} = \mathbf{D}_k \boldsymbol{y}_k \tag{3-22}$$

where vector $\boldsymbol{y}_k$ denotes

$$\boldsymbol{y}_k = col\left(\mathbf{u}_k\mathbf{u}_{k\text{-}1}...\mathbf{u}_{k+1\text{-}m}\mathbf{u}_{k\text{-}m}\right) \tag{3-23}$$

and $\mathbf{D}_k$ is defined as

$$\mathbf{D}_k = \begin{bmatrix} \left[\mathbf{I}-\mathbf{F}_{k+1}\right]^{-1}(\mathbf{F}_0+\mathbf{F}_{0,1}) & 0 & 0 & \dots & 0 & \left[\mathbf{I}-\mathbf{F}_{k+1}\right]^{-1}\mathbf{F}_{m\text{-}1} & \left[\mathbf{I}-\mathbf{F}_{k+1}\right]^{-1}\mathbf{F}_m \\ \mathbf{I} & 0 & 0 & \dots & 0 & 0 & 0 \\ 0 & \mathbf{I} & 0 & \dots & 0 & 0 & 0 \\ \dots & \dots & \dots & \dots & \dots & \dots & \dots \\ 0 & 0 & 0 & \dots & 0 & 0 & 0 \\ 0 & 0 & 0 & \dots & \mathbf{I} & 0 & 0 \\ 0 & 0 & 0 & \dots & 0 & \mathbf{I} & 0 \end{bmatrix} \tag{3-24}$$

Now, the transition matrix $\mathbf{\Phi}$ over one periodic time interval can be constructed using the sequence of discrete maps $\mathbf{D}_k$, (k = 0, …, m-1) , i.e.,

$$\boldsymbol{y}_m = \mathbf{\Phi}\boldsymbol{y}_0 \tag{3-25}$$

where $\mathbf{\Phi}$ is defined by

$$\mathbf{\Phi} = \mathbf{D}_{m-1}\mathbf{D}_{m-2}\dots\mathbf{D}_1\mathbf{D}_0 \tag{3-26}$$

According to the *Floquet* theory, the stability of the system can be determined in the following way: if the modulus of all the eigenvalues λ_Φ of the transition matrix $\mathbf{\Phi}$ is less than 1, the system is stable, otherwise, it is unstable.

3.5. PSG Construction

With the proposed chatter prediction method, given a combination of spindle speed, depth-of-cut, and cutter posture, we are able to determine whether machining will be stable. In practice, since spindle speed is normally fixed by recommended cutting speed, it can be assumed constant. This leaves two important variables during tool path generation, i.e., depth-of-cut and cutter posture. For any depth-of-cut, the feasible range of cutter postures (due to machine axis limits) can be divided into *stable* and *unstable* regions. Postures should only come from stable regions, which is the idea behind PSG.

Construction of PSG at a certain depth-of-cut relies on a sampling algorithm. The boundary between stable and unstable machining will be the set of cutter postures for which the $|\lambda_{\Phi}|$ of the transition matrix $\mathbf{\Phi}$ are equal to 1. For cutter postures with $|\lambda_{\Phi}|$ larger than 1, the postures will be unstable and for those with $|\lambda_{\Phi}|$ smaller than 1, the postures will be stable (Ding *et al.* 2010).

For demonstration, an example of PSG construction is presented for a simple scenario of slotting on a plane (see Figure 3.1a). The machine tool used is a DMG 80P duo Block 5-axis machining centre. The material to be machined is AL7075 and cutter is a Mitsubishi carbide with 10mm diameter (ball-end). The spindle speed is set at 4,800 r/min. The cutting force coefficients and modal parameters are provided in Table 3.1 and Table 3.2, respectively.

Table 3.1 Calibrated cutting force coefficients

K_{te} (N/mm)	K_{tc} (N/mm^2)	K_{re} (N/mm)	K_{rc} (N/mm^2)	K_{ae} (N/mm)	K_{ac} (N/mm^2)
11.4	1079.2	30.2	373.03	-2.3	293.3

Table 3.2 Modal parameters

Natural frequency (Hz)		**Process damping (%)**		**Stiffness (N/m^2)**	
X_M	Y_M	X_M	Y_M	X_M	Y_M
2213.75	1613.75	0.016713	0.013928	6012175.53	6292140.24

Angle sampling was firstly conducted at an interval of 1° for both lead and tilt angles. The range of sampling for both lead and tilt angles are set as 60°, large enough to cover the range of practical machining. For each sampled posture, the maximum modulus of the eigenvalues, $|\lambda_{\Phi}|$, will be obtained. According to the *Floquet* theory, the posture with $|\lambda_{\Phi}|>1$, such as 1.1, will be unstable while the posture with $|\lambda_{\Phi}|<1$, such as 0.9, will be stable. Furthermore, the postures corresponding to $|\lambda_{\Phi}|=1$ will be the boundary of the unstable and stable region. In this example, the obtained points (postures) with $|\lambda_{\Phi}| = 0.9;1.0;1.1$ are plotted with different legends in Figure 3.5a, respectively. A posture contour with the same $|\lambda_{\Phi}|$ can then be constructed through linear interpolation as shown in Figure 3.5b (3 posture contours in total).

The posture contour with $|\lambda_{\Phi}| = 1.0$ is called the *critical contour* in the PSG that basically defines the boundary between the stable postures and unstable postures. For any posture between the contours with $|\lambda_{\Phi}| = 1.0$ and $|\lambda_{\Phi}| = 1.1$, its $|\lambda_{\Phi}|$ will be between 1.0 and 1.1. For example, Poture_1 (see Figure 3.5b) will cause chatter. On the other hand, for any posture beyond of the contours of $|\lambda_{\Phi}| = 1.0$ and $|\lambda_{\Phi}| = 1.1$, e.g., Posture_2 in Figure 3.5b, its $|\lambda_{\Phi}|$ will be smaller than 0.9. Posture_2 is therefore a stable posture. For implementation, the PSG construction algorithm is as follows:

(1) The critical contour(s) is constructed first. Set the posture allowable region as the current region. There may be more than one critical contour in the current region.

(2) If there is no critical contour in current region, output the current region as chatter region when the $|\lambda_{\Phi}|$ inside the range is larger than 1 or as stable area when the $|\lambda_{\Phi}|$ inside the loop is smaller than 1 and exit. Else, number the critical contour(s) and then go to (3).

(3) Each critical contour divides the current allowable region into two areas and each area may be enveloped by critical contour and/or the axes (horizontal and/or vertical). Check the critical contours in ascending order to find a critical contour, which satisfies the requirement that one of the areas divided by it does not contain any other critical contours. The area, which has no

critical contours inside, will be marked as chatter region when the $|\lambda_\Phi|$ inside the loop is larger than 1 and marked as stable region when the $|\lambda_\Phi|$ inside the loop is smaller than 1. The remaining regions will be set as the current region, and then go to (2).

For the example PSG in Figure 3.5a and Figure 3.5b, the chatter regions are marked in green as shown in Figure 3.6. The other regions represent chatter-free postures.

For the same machining case, the depth-of-cut was changed to 0.6 mm and 1 mm. The constructed PSGs are shown in Figure 3.7a and Figure 3.7b, respectively. It can be clearly seen that with the increase of depth-of-cut, the chatter regions become larger in accordance with our expectations.

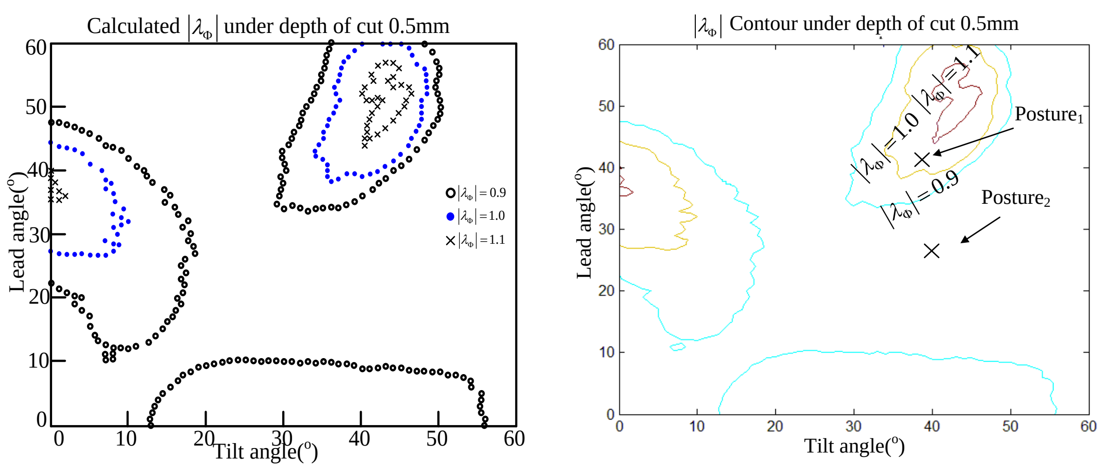

(a) Distribution of $|\lambda_\Phi|$ at sampled points (b) Contour of $|\lambda_\Phi|$

Figure 3.5 Construction of PSG under depth-of-cut = 0.5mm

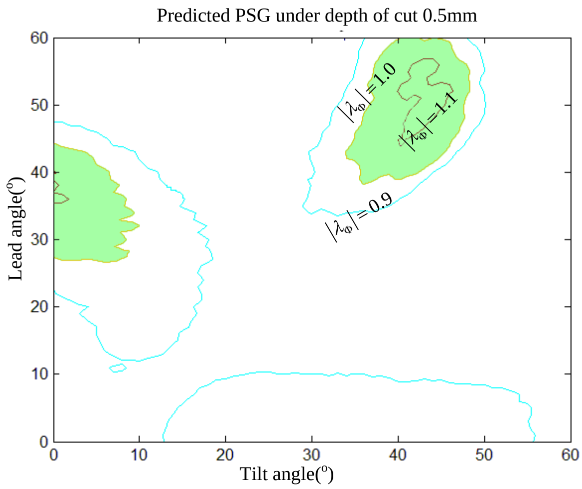

Figure 3.6 PSG under depth-of-cut = 0.5 mm

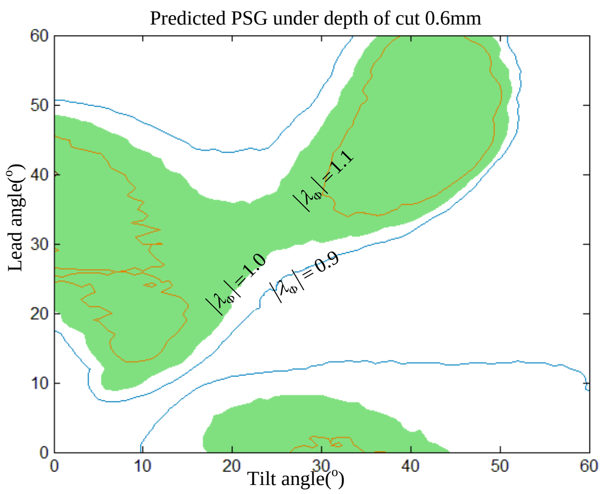

(a) Depth-of-cut = 0.6 mm

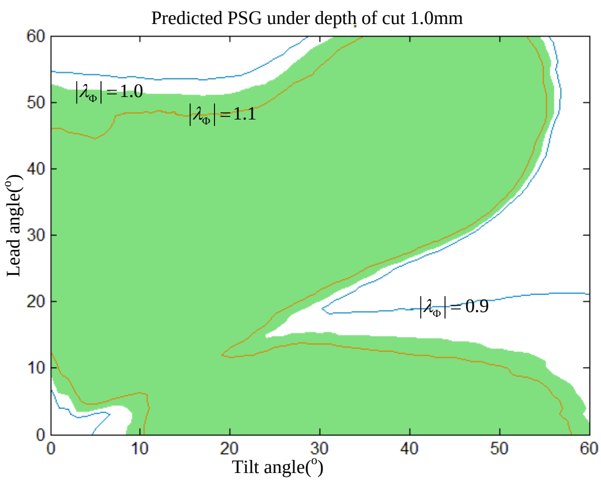

(b) Depth-of-cut = 1.0 mm

Figure 3.7 PSGs under depths-of-cut of 0.6 mm and 1.0 mm.

3.6. Experimental Validation

To test the validity of chatter prediction and generated PSGs in 5-axis machining, a series of machining experiments have been carried out under indexed machining modes. The machine tool, cutter, and spindle speed are exactly the same as those used for the generation of PSGs shown in Figure 3.6 and Figure 3.7, respectively. With the indexed machining mode, the cutter's posture is pre-set and will remain the same during one pass of machining, leaving a consistent machined surface.

Table 3.3 Machining conditions for experiments

Test	Lead angle (^{o})	Tilt angle (^{o})	Depth of cut (mm)	Spindle speed (rpm)
T1	0	0	1	4800
T2	5	0	1	4800
T3	10	0	1	4800
T4	15	0	1	4800
T5	20	0	1	4800
T6	25	0	1	4800
T7	30	0	1	4800
T8	35	0	1	4800
T9	40	0	1	4800
T10	45	0	1	4800
T11	50	0	1	4800
T12	55	0	1	4800
T13	60	0	1	4800
T14	0	5	1	4800
T15	5	5	1	4800
T16	10	5	1	4800
T17	15	5	1	4800
T18	20	5	1	4800
T19	25	5	1	4800
T20	30	5	1	4800
T21	35	5	1	4800

Table 3.3 Machining conditions for experiments (Continued)

T22	0	20	1	4800
T23	5	20	1	4800
T24	10	20	1	4800
T25	15	20	1	4800
T26	20	20	1	4800
T27	25	20	1	4800
T28	30	20	1	4800
T29	35	20	1	4800
T30	40	20	1	4800
T31	45	20	1	4800
T32	50	20	1	4800
T33	55	20	1	4800
T34	60	20	1	4800

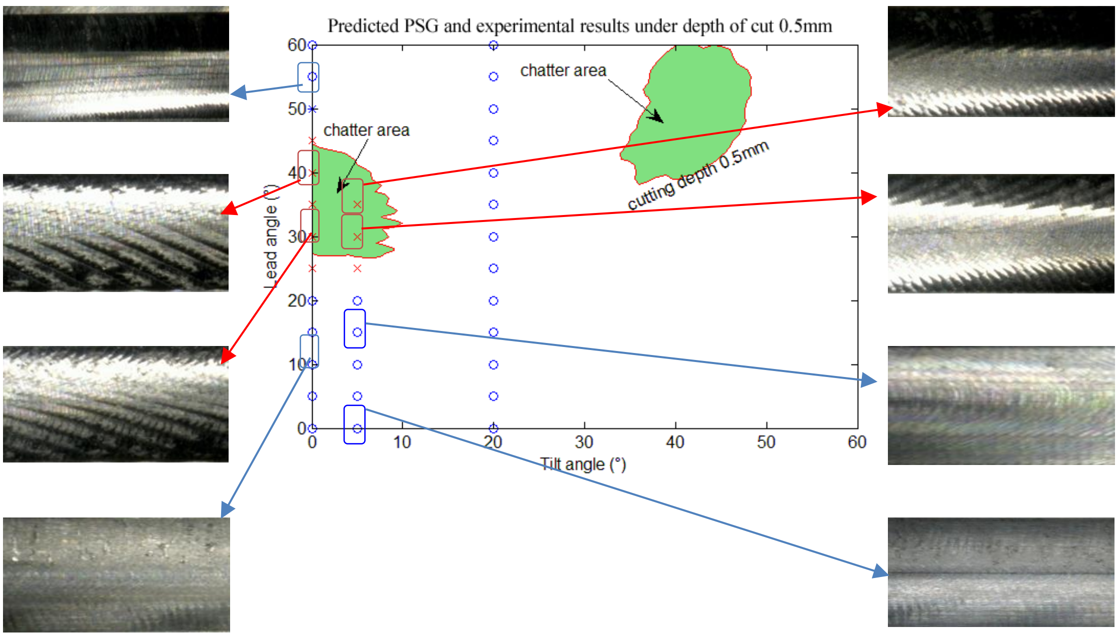

Figure 3.8 Stability comparisons between predicted and experimental measurements.

The first set of the experiments were carried out with depth-of-cut of 0.5 mm. The results are shown in Figure 3.8, where the cutter postures experimented with have been overlaid over the PSG shown in Figure 3.8. Microscopic images of some of the machined surfaces are also provided. It can be seen that the machined surfaces using postures within the chatter area or on the boundary of it (4 in total) show clear chatter marks. On the other hand, those machined surfaces using chatter-free postures (4 in total) look quite smooth. Therefore, it can be said a high level of conformity has been achieved between the prediction and the experimental results.

Another experiment was carried out under the simultaneous machining mode (depth-of-cut = 0.5 mm). The cutter posture was continuously varied from (lead: 0°, tilt: 0°) to (lead: 60°, tilt: 0°) smoothly over 21 cutter locations (CLs) with a fixed interval of 5mm between neighbouring CLs. In other words, the tilt angle was maintained at 0° while the lead angle was changed from 0° to 60° in a linear manner. The interpolation from the starting to the ending cutter posture is conducted by commercial CAM software (UG NX 8.5). At the intermediate CLs, the tilt and lead angles are retrieved as given in Figure 3.9.

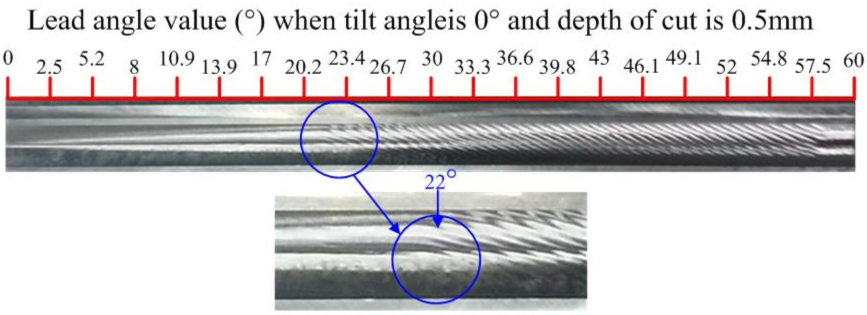

Figure 3.9 Machined surface under varied cutter posture with depth-of-cut 0.5 mm.

According to the PSG (depth-of-cut = 0.5 mm) shown in Figure 3.6, machining would enter chatter zone after the 10th CL with corresponding posture (Tilt: 0°, Lead: 26.7°). This is generally in accordance with the microscopic image of the machined surface, in which chatter mark emerges at around 22° as shown in Figure 3.8. On the other hand, according to the PSG, machining would enter stable area after the 19th CL with corresponding posture (Tilt: 0°, Lead: 54.8°). This is also in accordance with the microscopic image of the machined surface, in which chatter disappear at around 58° as shown in Figure 3.9. This experiment demonstrated the effectiveness of the chatter prediction algorithm. The minor difference between the predicted critical postures and experimental critical postures could be caused by the measurement deviation for modal parameters and ignored influence of cutting force along the cutter spindle.

3.7. Summary

In this chapter, we have proposed the idea of posture stability graph (PSG) to guide the determination of chatter-free cutter postures during 5-axis machining. A procedure to obtain the PSG has also been established. At first, a dynamic model of the machining system under cyclic cutting force is established, in which the influnces of the cutter posture, depth-of-cut, and spindle speed have all been accounted for. The stability of the machining process is then derived from the transition matrix of the system. By identifying cutter postures that will lead to borderline stability under a certain machining condition, the feasible range of cutter orientations will be divided into stable and unstable zones, which forms the PSG. Simulation based tests have been conducted and corresponding machining experiments, inlcuding indexed machining and simultaneous machining, have also been conducted to validate the prediction results. The tests show that a high level of conformity has been achieved between our prediction and the experimental results.

CHAPTER 4

CONSTRUCTION OF CIF-MAP AND ITS APPLICATION IN TOOL PATH GENERATION

In machining practice, both chatter and interference need to be avoided in order to achieve the machined surface with satisfactory quality. Therefore, at the process planning stage for 5-axis machining, the assignment of cutter posture at a generated CC point is probablly the most critical task. In our previous study, for posture assignment at a CC point, an accessibility map (A-map) was proposed to specify the inteference-free posture range for the cutter in use, which can be generated purely based on geometric analysis involving the workpiece (raw and finish states), machine tool, and cutter. It is worth noting that the A-map is generated without any specified feed direction. With the given feed direction at a CC point, the A-map can be further refined to a *posture accessibility graph* (PAG). Based on the current study, for any given posture at a CC point, the machining stability can be evaluated in the form of PSG. Therefore, for the first time, it is possible to select chatter-free and interference-free (CIF) cutter posture at a CC point. With this capability, both chatter and interference can be avoided in the generated tool paths.

In this chapter, the method to construct the CIF cutter posture range at a CC point, called the CIF-map, will be presented. The method to construct the A-map at a CC point is firstly introduced briefly, followed by the transformation from A-map to PAG based on the given feed direction. Finally, the CIF-map is formed by combining the PAG and PSG at a CC point. To construct the CIF-map in the tool path generation stage, some practical issues related to the tool path generation are discussed.

4.1. Background

Process planning for 5-axis milling of sculptured surfaces is complicated, largely due to the process's vulnerability to machining interferences, which may cause irreversible damages to the workpiece, the cutter, and the machine. Therefore, evaluation of a cutter's accessibility to the machining surface is of the highest priority. The important tasks, such as cutter selection and tool-path generation, rely heavily on information obtained in this process. For 5-axis milling process, accessibility of a cutter should be evaluated at an individual surface point. 'Accessible' is synonym for 'interference-free' here, which means at the target surface point, there is at least one cutter posture with which the cutter does not produce any interference with the workpiece and the machine tool.

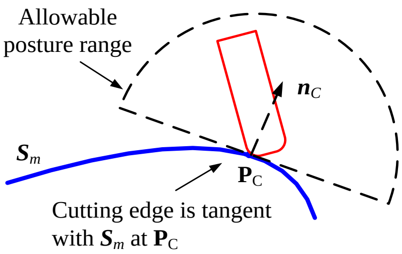

Figure 4.1 Posture range determined by cutter geometries(Geng 2013)

The purpose of accessibility evaluation is to identify the range of postures with which a cutter can access a specific point on surface $\boldsymbol{S}_m$ without causing any interference (see Figure 4.1). In our proposed accessibility evaluation method, the cutter type used is limited to cylindrical cutter with fillet-end. During cutting, the torus portion serves as the cutting edge, which is tangent to $\boldsymbol{S}_m$ at the CC point ($\mathbf{P}_\mathrm{C}$ in

Figure 4.1). Apparently, the allowable posture range is limited to the hemisphere centered at $\mathbf{P}_C$. Besides, an accessible posture must also be within the workspace of the to-be-used 5-axis machine. The remaining constraints are imposed by the requirement for interference avoidance between the cutter and the part.

Generaly speking, there are three kinds of interference in real machining process, i.e., local-gouging (LG), rear-gouging (RG), and global-collision (GC). Still referring to Figure 4.1, when the cutter is placed at $\mathbf{P}_C$, LG occurs when the curvature of the cutter (the torus portion) is smaller than the minimum principal curvature at $\mathbf{P}_C$ such that the cutter cuts off excess material beyond tolerance. RG refers to the situation when the bottom of the cutter (not intended for cutting) protrudes into the machining surface and removes material. GC takes place when the shank or holder of the cutter collides with the machining or non-machining surfaces on the workpiece. A simple illustration of the three kinds of interference is presented in Figure 4.2. To avoid all these types of interference in 5-axis milling, a cutter accessibility evaluation algorithm was developed in our previous study, which generates the A-map for a given cutter placed at a point on a given part surface. The feed direction is unknown during the generation of A-map. In the tool path generation stage, as the feed direction is given, the A-map will be transformed and represented using lead angle and tilt angle, which is named posture accessibility graph (PAG).

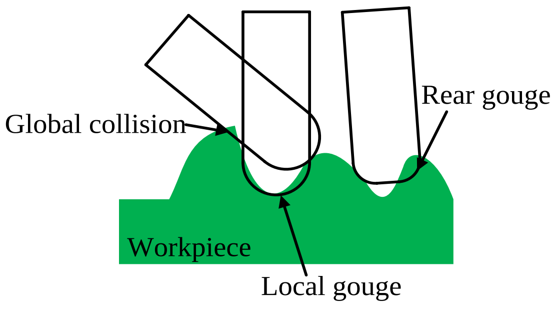

Figure 4.2 Three kinds of machining interference

Meanwhile, chatter prediction in 5-axis machining has been studied in Chapter 3. At each CC point, the posture stability graph (PSG) can be constructed under the given feed direction, measured modal parameters, and machining parameters, such as depth-of-cut and spindle speed. By combining the PAG and PSG at a CC point, the CIF-map can be formed.

4.2. CIF-map Construction

4.2.1. PAG construction

The basic idea behind the A-map construction algorithm is to identify the three interference-free posture ranges corresponding to each type of machining interference (LG, RG, and GC) for a specific cutter at a point on a part surface. The intersection of these 3 ranges plus the range determined by the joint travel limits of 5-axis machines will make up the accessible posture range of the cutter, i.e., A-map. Note that in the original A-map construction algorithm (Li and Zhang 2006), feed direction is assumed unknown. The A-map effectively characterises the accessibility of a cutter to a point, which provides important geometric information for interference-free cutter posture selection. The detailed algorithm for the A-map generation of a fillet-end cutter to a point can be found in (Li and Zhang 2006). Here, a brief illustration is presented.

Firstly, the objects and coordinate systems involved in the A-map construction are introduced. A machining surface is described by a set of NURBS patches with C^2 continuity. A fillet-end cylindrical cutter is described by its major radius, minor radius, and length, as shown in Figure 4.3. There are 3 coordinate frames used in the A-map construction: workpiece coordinate system (WCS) $\mathbf{X}_W\mathbf{Y}_W\mathbf{Z}_W$, local frame $\mathbf{O}_L$-$\mathbf{X}_L\mathbf{Y}_L\mathbf{Z}_L$ and cutter coordinate system (CCS) $\mathbf{O}_T$-$\mathbf{X}_T\mathbf{Y}_T\mathbf{Z}_T$. For the local frame, the origin $\mathbf{O}_L$ is coincident with $\mathbf{P}_C$; $\mathbf{Z}_L$ is coincident with the surface normal at $\mathbf{P}_C$; $\mathbf{Y}_L$ and $\mathbf{X}_L$ are along the maximum and minimum principal directions at $\mathbf{P}_C$, respectively. Meanwhile, for the tool frame, $\mathbf{O}_T$ coincident with the centre of the cutter bottom, $\mathbf{Z}_T$ along the cutter axis, $\mathbf{X}_T$ in the plane determined by $\mathbf{P}_C$ and $\mathbf{Z}_T$, pointing towards $\mathbf{P}_C$. With $\mathbf{O}_L$-$\mathbf{X}_L\mathbf{Y}_L\mathbf{Z}_L$ and $\mathbf{O}_T$-$\mathbf{X}_T\mathbf{Y}_T\mathbf{Z}_T$, a cutter's posture can be defined by an angle pair $(\lambda_{ia}, \theta_{ra})$. λ_{ia}, known as the inclination angle, is defined as the angle between $\mathbf{Z}_L$ and $\mathbf{Z}_T$ (or $\mathbf{Z}_T$', which passes through $\mathbf{P}_C$ and is parallel to $\mathbf{Z}_T$). θ_{ra} is the rotational angle that the cutter rotates about $\mathbf{Z}_L$, which equals the angle between $\mathbf{X}_L$ and the projection of $\mathbf{Z}_T$' on plane $\mathbf{X}_L$-$\mathbf{Y}_L$.

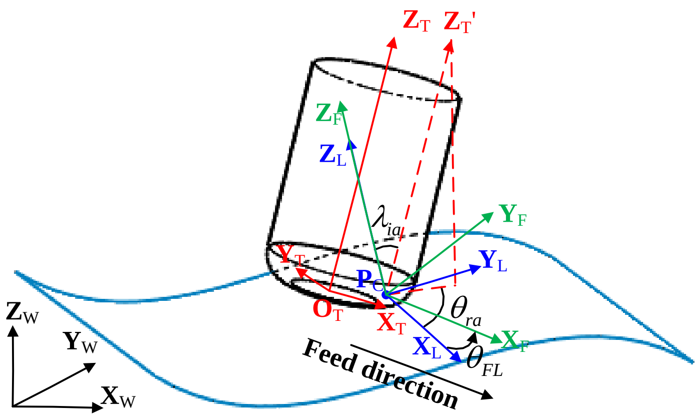

Figure 4.3 The local frame and CCS for accessibility analysis (Geng 2013)

Li and Zhang (2006) developed a set of algorithms for identifying the interference-free range of λ_{ia} with a given θ_{ra} in terms of LG, RG, and GC, respectively. For A-map construction, θ_{ra} is firstly sampled evenly in the range of $\left[\theta_{ra,\min}, \theta_{ra,\max}\right]$ and the feasible range of λ_{ia} at every discrete value of θ_{ra} can then be obtained. In this manner, a numerical approximation of the accessible posture range at $\mathbf{P}_C$, i.e., the A-map of the cutter at $\mathbf{P}_C$, can be obtained. The complete algorithm for obtaining the A-map is given as follows (Geng 2013):

<u>Algorithm: Finding the A-map of a cutter at a CC point $\mathbf{P}_C$</u>

Input: *(a) Sampled point set* $\{P_k,\ k=1,\ 2,\ \ldots,m\}$ *and CC point* $\mathbf{P}_{\mathrm{C}}$

(b) A torus end miller (R, r_f, L)

(c) Titling angle range $\left[\lambda_{ia,\min},\lambda_{ia,\max}\right]$, *rotational angle range* $\left[\theta_{ra,\min},\theta_{ra,\max}\right]$

Output: *A-map and the accessibility of the cutter at* $\mathbf{P}_{\mathrm{C}}$

Begin

(1) Uniformly sample $\left[\theta_{ra,\min},\theta_{ra,\max}\right]$ into k angles, set $i = 0$.

(2) IF $i\le(k-1)$, $\theta_{ra,i}=\theta_{ra,\min}+\left(\theta_{ra,\max}-\theta_{ra,\min}\right)(i/(k-1))$; otherwise, go to (6).

(3) Find the LG-free range $\left[\theta_{ra,\mathrm{i}},\left(\lambda_{ia,\theta-\mathrm{lg}},\lambda_{ia,\max}\right)\right]$. If the accessible range is NULL, $i=i+1$, go to (2).

(4) Find the RG-free range from $\left(\lambda_{ia,\theta-\mathrm{lg}},\lambda_{ia,\max}\right)$. The current accessible range is $\left[\theta_{ra,i},\left(\lambda_{ia,\theta-rg},\lambda_{ia,\max}\right)\right]\left(\lambda_{ia,\theta-rg}\ge\lambda_{ia,\theta-\mathrm{lg}}\right)$. If the accessible range is NULL, $i=i+1$, go to (2).

(5) Find the GC-free ranges from $\left(\lambda_{ia,\theta-r\mathrm{g}},\lambda_{ia,\max}\right)$ at $\{\mathbf{P}_k,k=1,2,\ldots,m\}$. The final accessible range is $\left[\theta_{ra,i},\left(\lambda_{ia,\theta-gc1},\lambda_{ia,\theta-gc2}\right)\right]\left(\lambda_{ia,\theta-gc1}\ge\lambda_{ia,\theta-rg},\lambda_{ia,\theta-gc2}\le\lambda_{ia,\max}\right)$. Return NULL if such a range does not exist. $i=i+1$. Go to (2).

(6) If the A-map is not NULL, output the A-map. Else, $\mathbf{P}_{\mathrm{C}}$ is not accessible.

End

This A-map construction algorithm is further illustrated by the example shown in Figure 4.4, in which the A-map for $\mathbf{P}_{\mathrm{C}}$ (u = 0.2, v = 0.8) on the machining surface of the workpiece (see Figure 4.4a) is obtained. The cutter is of R = 5 mm, r_f = 0.5 mm, and L = 60 mm. The A-map is plotted in Figure 4.4b. The maximum range for θ_{ra} is taken as [0, 2π], which is evenly sampled into 72 discrete values. Accessible ranges regarding the three kinds of interference and the posture range determined by the machine joint limits are also indicated (see Figure 4.4b).

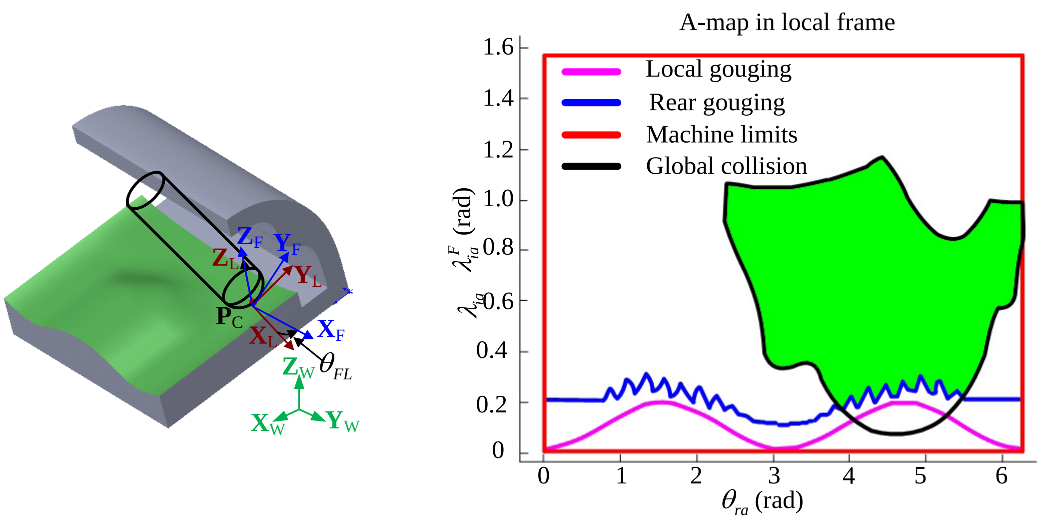

(a) Workpiece and target point $\mathbf{P}_C$ (b) A-map as the intersection of accessible ranges

Figure 4.4 An example of A-map construction (Geng 2013)

Since A-map is generated without the information of feed direction and the cutter posture is normally represented in the local frame. Once the feed direction is specified, the A-map can then be transformed into the feed frame ($\mathbf{O}_F$-$\mathbf{X}_F\mathbf{Y}_F\mathbf{Z}_F$) shown in Figure 4.4a, in which the origin $\mathbf{O}_F$ is coincident with $\mathbf{P}_C$; $\mathbf{Z}_F$ is coincident with the surface normal at $\mathbf{P}_C$; $\mathbf{X}_F$ is along the feed direction at $\mathbf{P}_C$, which is tangent with the machining surface curve in the cutting plane and has θ_{FL} with $\mathbf{X}_L$; $\mathbf{Y}_F$ is subsequently determined using right-hand rule. The cutter orientation can be determined by lead angle and tilt angle, which is defined in Figure 2.2. The sign of the lead and tilt angle is determined by right-hand rule. The interference-free posture range is therefore specified in terms of lead angle and tilt angle.

As $\mathbf{Z}_L$ is same as $\mathbf{Z}_F$, the A-map in the local frame will be transformed into the feed frame and expressed using θ_{ra}^F ($\theta_{ra}^F = \theta_{ra} - \theta_{FL}$) and λ_{ia}^F ($\lambda_{ia}^F = \lambda_{ia}$). This transformation process is like a simple translation of original A-map in the rotational angle direction. Then, the boundary of the A-map, which is represented with many pairs of angle ($\theta_{ra}^F, \lambda_{ia}^F$), will be transformed and represented using tilt and lead angle. The corresponding lead angle (*lead*) and tilt angle (*tilt*) for the given θ_{ra}^F and λ_{ia}^F can be obtained using,

$$\begin{aligned} lead &= \arcsin\left(\cos\left(\lambda_{ia}^F\right)\cos\left(\theta_{ra}^F\right)\right) \\ tilt &= -\arctan\left(\sin\left(\theta_{ra}^F\right)/\tan\left(\lambda_{ia}^F\right)\right) \end{aligned} \tag{4-1}$$

Once an A-map is transformed into the feed frame, a final check will conducted based on machining practice, followed by modification, if necessary. In practical machining, a negative lead angle is usually not allowed. Therefore, the maximum range of lead angle is set as (0^o, 90^o). At the same time, the maximum range of tilt angle is set as (-90^o, 90^o). In practice, the feasible ranges of lead angle and tilt angle are both set (0^o, 60^o). After this final check/modification step, the A-map in the feed frame becomes a *posture accessibility graph* (PAG).

For the example shown in Figure 4.4, the feed direction is given that is 20^o from $\mathbf{X}_L$ (see Figure 4.4a). The A-map is first transformed into the feed frame and represented with lead and tilt angles, shown in Figure 4.5a. Then, the feasible range of (0^o, 60^o) is applied to the lead and tilt angles to modify the A-map. The modified A-map is the PAG represented by lead angle and tilt angles as shown in Figure 4.5b.

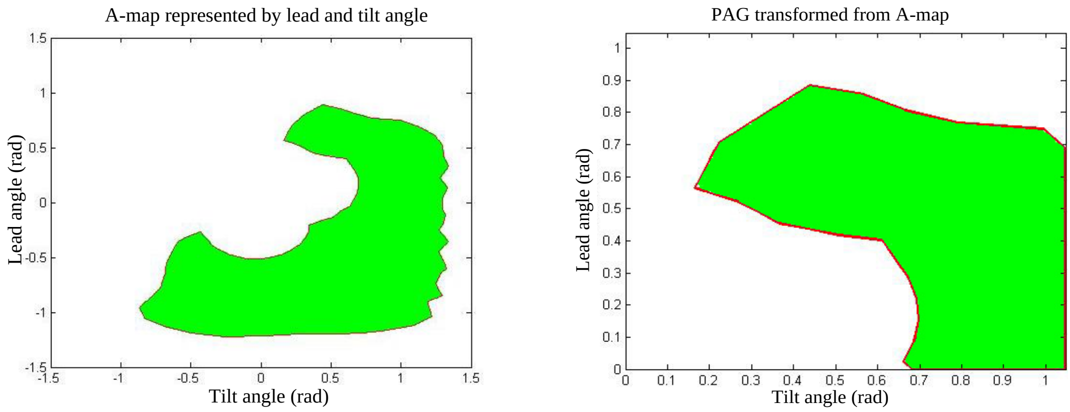

(a) The A-map in feed frame

(b) The obtained PAG

Figure 4.5 PAG transformed from A-map

4.2.2. CIF-map construction

Since both PAG and PSG are represented using lead angle and tilt angles in the feed frame, the corresponding CIF-map can be constructed by simply overlaying PAG over PSG to obtain the intersection. The CIF-map generation is illustrated by the example shown in Figure 4.6, in which the machining surface is a simple plane with a vertical plane as an obstacle and a slotting process is to be carried out (see Figure 4.6a). The depth-of-cut is 1mm and the spindle speed is 4,800r/min. The machine tool used is DMG 80P duo Block 5-axis machining centre. The material to be machined is AL7075 and cutter is a Mitsubishi carbide ball-end cutter with 10 mm diameter. The machining coefficients and modal parameters are provided in Table 4.1 and Table 4.2, respectively. The ranges of lead angle and tilt angles are set to be $(0^\circ, 60^\circ)$ and $(0^\circ, 60^\circ)$, respectively. The corresponding PAG and PSG are generated and shown in Figure 4.6b and Figure 4.6c, respectively. Finally, the CIF-map at this CC point is obtained by intersecting the PAG and PSG as shown in Figure 4.6d, in which the green region specifies the chatter-prone posture range. The region filled by blue hatching represents the chatter-free and interference-free postures.

Table 4.1 Calibrated cutting force coefficients for CIF-map construction

K_{te} (N/mm)	K_{tc} (N/mm^2)	K_{re} (N/mm)	K_{rc} (N/mm^2)	K_{ae} (N/mm)	K_{ac} (N/mm^2)
11.4	1079.2	30.2	373.03	-2.3	293.3

Table 4.2 Modal parameters for CIF-map construction

Natural frequency (Hz)		**Process damping (%)**		**Stiffness (N/m^2)**	
X_M	**Y_M**	**X_M**	**Y_M**	**X_M**	**Y_M**
2213.75	1613.75	0.016713	0.013928	6012175.53	6292140.24

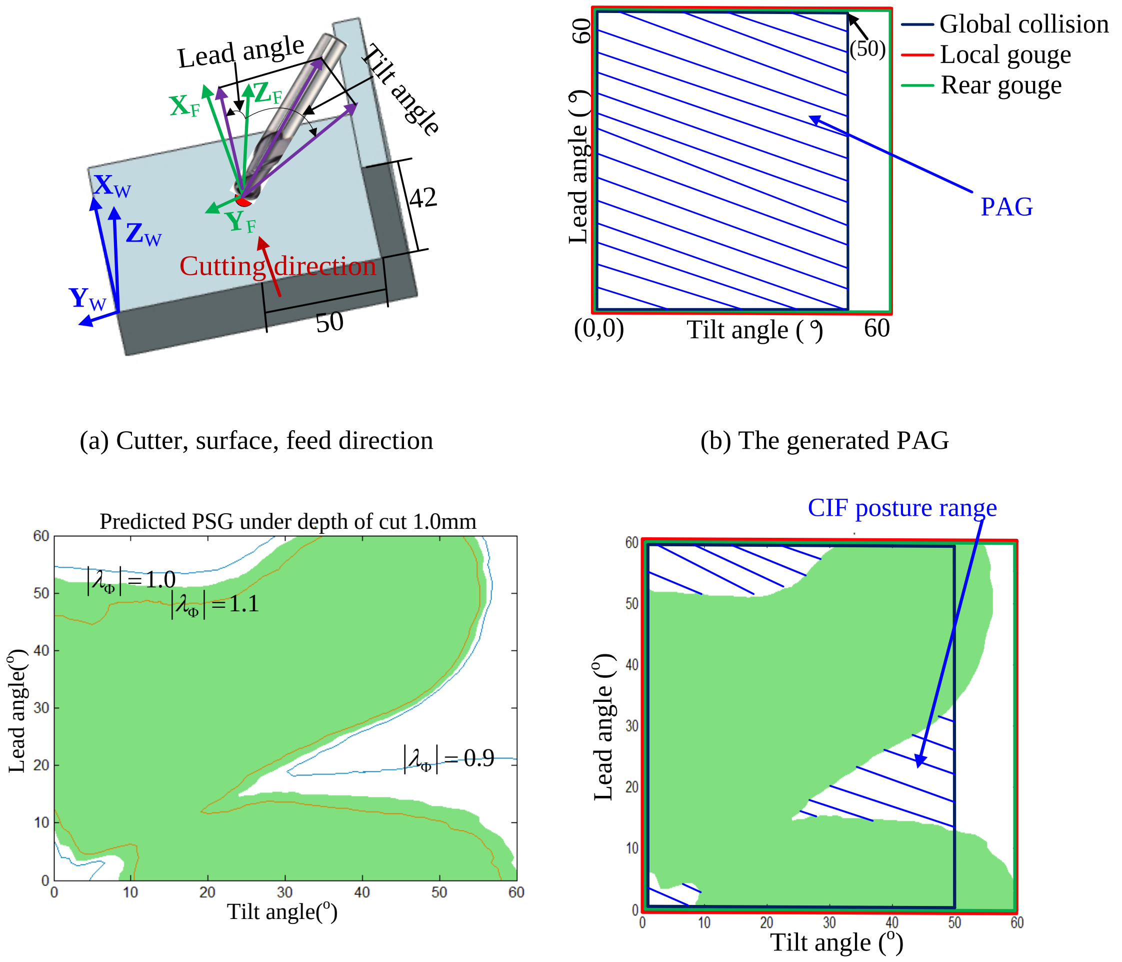

(a) Cutter, surface, feed direction

(b) The generated PAG

(c) The generated PSG

(d) The generated CIF-map

Figure 4.6 An example of CIF-map construction

4.3. Some Practical Issues in CIF-map Construction

In order to generate the CIF-map at each CC point for tool path generation, the PAG and PSG need to be generated first. The construction of PSG needs the information of feed direction and machining paramters, including the depth-of-cut and spindle speed. On the other hand, the feed direction is also necessary to transform the A-map in the local frame into PAG in the feed frame. However, in sculptured surface machining, the feed direction at a CC point is affected by the selected tool path pattern, workpiece geometry and cutting direction. As shown in Figure 4.7, although the cutting direction is fixed, the feed direction changes at different CC points even within the same cutting plane. On the other hand, the adopted tool path pattern could also have effect on feed direction. Therefore, care is required for determining these machining conditions when generating PAG and PSG at a CC point. In the following sections, the determination of feed direction and machining paramters will be studied.

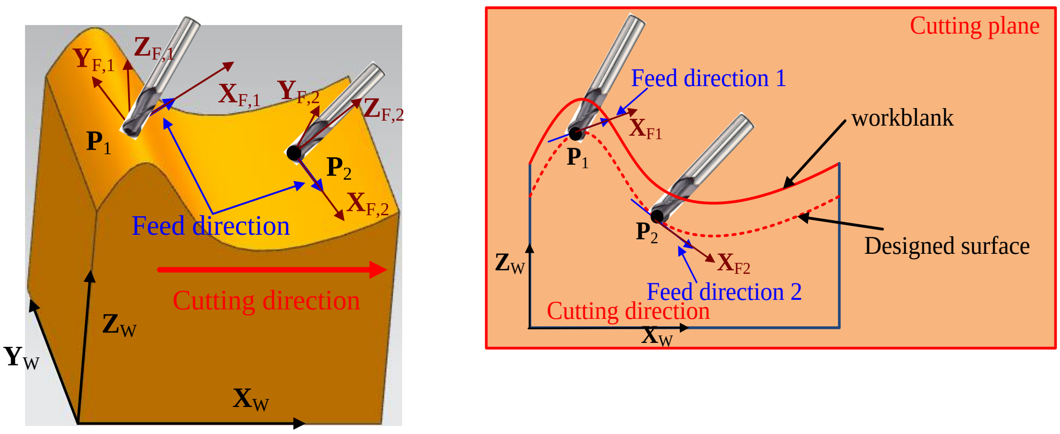

(a) Workpeice geometry (b) Feed direction at different CC point

Figure 4.7 Influence of workpiece surface geometry on feed direction

4.3.1. Determination of feed direction

As the feed direction is influenced by the tool path pattern, workpiece geometry and cutting direction, these three paramters need to be determined first. In this study, only parallel tool path pattern (also known as iso-planar tool path pattern) is used due to its simplicity.

In cutting direction selection for parallel tool path pattern, a heuristic method from our previous work (Li and Zhang 2006) is adopted. The proposed heuristics aim at smooth cutter movement from the selected cutting direction. The possible cutting directions at a point are firstly generated through uniform sampling. For each sampled cutting direction, a special designed parameter called *posture change rate* (PCR) is calculated based on information collected at all the sampled points. The direction with the minimum PCR would be selected as the cutting direction to produce smooth cutter movement.

Once the cutting direction is determined, the intersection curve between the cutting plane and the designed workpiece surface can be obtained and the tangent line at each cutter contact (CC) point at the curve can be determined (see Figure 4.7b). In most of cases, the cutting plane is normal to the $\mathbf{X}_W$-$\mathbf{Y}_W$ plane, this is to say that the cutting plane is passing through the $\mathbf{Z}_W$. Therefore, the cutting direction $\boldsymbol{f}_{cd}$ can be defined in the WCS and expressed as $\left(x_w, y_w, 0\right)$. After normalization, the cutting direction $\boldsymbol{f}_{cd}$ is represented by $\left(x_w / \sqrt{x_w^2 + y_w^2}, y_w / \sqrt{x_w^2 + y_w^2}, 0\right)^T$. The slope of each tangent line at each CC point in the WCS can be calculated and defined as K_s. Then, the feed direction can be obtained using:

$$\boldsymbol{f}_F = \left(x_w / \sqrt{x_w^2 + y_w^2} \quad y_w / \sqrt{x_w^2 + y_w^2} \quad K_s\right)^T \tag{4-2}$$

A simple example is shown in Figure 4.7 to illustrate this method. The cutting direction is along $\mathbf{X}_W$, so the cutting direction can be expressed as (1, 0, 0). At the CC point $\mathbf{P}_1$, the slope of the tangent line is 0.3. Then, the feed direction at $\mathbf{P}_1$ is $(1, 0, 0.3)^T$.

4.3.2. Determination of machining parameters

Usually, with the change of cutter posture, the real depth-of-cut varies from a CC point to the next. As shown in Figure 4.8a, the real depth-of-cut is different under different cutter postures for the flat-end cutter. This will cause cutting force variation and the system dynamic equation will be affected as well. Subsequently, the stability of the machining system will also be affected. Therefore, to construct an accuarate PSG, the real depth-of-cut should be calculated for each cutter posture, which will increase the prediction complexity tremendously.

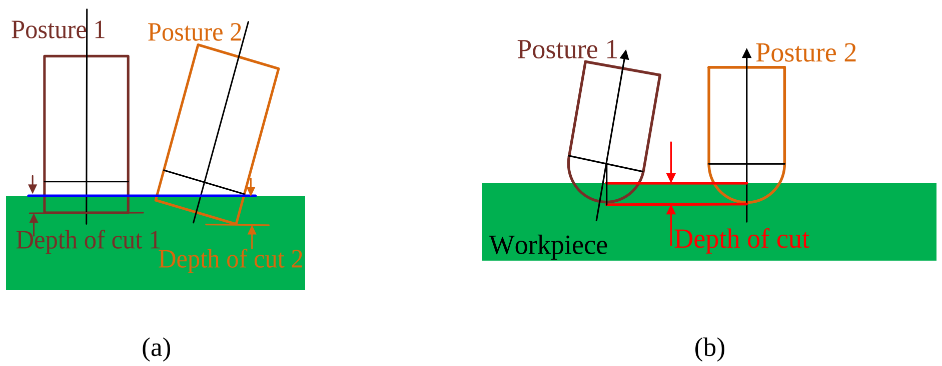

Figure 4.8 The depth-of-cut for flat-end and ball-end cutters

In practice, depth-of-cut is usually defined when the lead angle (*lead*) and tilt angle (*tilt*) are both at 0 and marked as d_{ideal}. For a fillet-end cutter, the real depth-of-cut (d_{real}) can be obtained using:

$$d_{real} = d_{ideal} + (R - r_f)\sin(lead)\sin(tilt) \tag{4-3}$$

where R is the radius of the cutter and r_f is the corner radius of the cutter. In an extrreme case where a ball-end cutter is used, the depth-of-cut is constant as $r_f = R$ for ball-end cutters (see Figure 4.8b) .

4.4. Discussion

In this chapter, the CIF-map construction method is presented and its application in tool path generation is studied in detail. When the PAG and PSG are constructed at each CC point, the CIF-map can be identified easily by intersecting the A-map and PSG together. The PAG is constructed by transforming the A-map conisdering the effect of feed direction. The PSG is constructed using the method in previous chapter. To apply the CIF-map in tool path generation, some practical issues have been considered, including the determination of feed direction and depth of cut. However, as the determination of engagement condition (whethter the elemental cutting edge of a cutter is in-cut or not) is only implemented for ball end cutter in the prediction of chatter and cutting force in this thesis, the engagement condition for other types of cutters should be determined first before the construction of PSG and subsequently construction of CIF-map.

CHAPTER 5

TOOL PATH GENERATION IN 5-AXIS MACHINING BASED ON DYNAMIC ANALYSIS

In the existing version of the proposed process planning system (Geng 2013), there are two approaches for cutter posture assignment at the generated CC points on a single path. The first one is based on a heuristic that targets maximum cutting strip width (CSW) between neighbouring paths. It is computational efficient but does not guarantee the quality of the solution. Moreover, the heuristic lacks consideration for tool-path smoothness. The second approach formulates the posture assignment task as a constrained optimization problem. The optimization objective function cover measures of machining efficiency as well as tool-path smoothness. This approach represents perhaps the most advanced level so far for process planning of 5-axis machining in a static mode. However, due to lack of consideration for dynamic factors, chatter may take place in the generated tool paths, causing poor surface quality on the machined surface. It is, therefore, desirable to incorporate the consideration of dynamic factors into the process planning system.

Since the CIF-map represents the feasible posture space in terms of interference and chatter at a CC point, a simple improvement to the posture assignment algorithm (the second approach) is to replace the A-map with the CIF-map. In this way, the generated tool paths will be chatter-free, and at the same time, possess good quality in terms of overall tool path length and tool path smoothness. On the other hand, during finish cut stage, surface quality is commonly considered the most important factor. To minimize the effect of cutter deflection on the machined surface, the posture assignment task can be treated as an optimization problem towards minimizing maximum deflection cutting force (MDC-F).

In the following sections, the overall framework of the proposed iso-planar tool path generation system for 5-axis machining is firstly introduced, in which the methods for CC point generation, cutter posture assignment, and path interval determination are described for ball-end cutters. Next, the definition of MDC-F will be presented first, followed by the description of a proposed Particle Swarm Optimization (PSO) algorithm for finding the cutter posture with minimal MDC-F under given machining parameters.

5.1. Workflow of Tool Path Generation

The tool path pattern used in this proposed system is iso-planar. The tool paths are generated by intersecting the given machining surface with multiple parallel cutting planes. Although many novel tool path patterns have been proposed in the recent years (Makhanov 2010), the iso-planar pattern is still the most widely used in CAM software and studied by researchers due to its high robustness and simplicity (Apro 2008).

With the iso-planar pattern, a series of cutting planes along the specified cutting direction are taken to intersect the machining surface, producing a series of intersection curves representing the tool paths. As the cutting direction is determined using the algorithm proposed in (Li and Zhang 2006), tool path generation (CL generation from the current path) will start from the first tool path, which is located at a sufficiently small offset from the machining surface boundary, producing the first intersection curve. CC points are then generated on the first intersection curve, which are the points of contact between cutter and target surface. Since the cutter is assumed moving linearly between neighbouring CC points, deviations will be created between the cutter's trajectory and the machining surface. The generated CC points will ensure that the deviation is below the specified surface error tolerance.

Next, posture assignment takes place at each CC point in the current path. Before that, the PAG and PSG at each CC point need to be constructed to form the CIF-map. With the CIF-map for each CC point, posture assignment can be carried out by following any one of established strategies (Li and Zhang 2006; Geng 2013). Up to this point, the current tool path is completely generated. Following that, the position of next path will be determined. This process of "intersection curve generation – CC point generation – posture assignment – path interval determination" continues until the whole surface is completely covered. An illustration of the overall workflow is shown in Figure 5.1. The steps for this process are summarized and presented as follows:

1) Set the first cutting plane to be just off the surface edge with a small distance Δy_0. The location of the current cutting plane is then $y_i = y_{\max} - \Delta y_0$ (i = 1). The intersection curve represents the current path.
2) Generate the CC points on the current path. During this process, the deviation between the cutter trajectory (determined by interpolator) and the intersection curve is kept just below the given surface error tolerance τ_{se}.
3) At each CC point, construct the PAG and PSG, and then form the CIF.
4) Select the optimal cutter posture, at each CC point, from its CIF-map based on one of available optimization strategy.
5) If path^i is the last path, output the CL data and exit. Else, go to (6).

6) Calculate the cutting strip width (CSW) on the current path (Geng 2013). Determine the side-step Δy_i between the current and the next paths. The scallop height tolerance τ_{sh} is imposed as a constraint.

7) Set $i=i+1$ and $y_i = y_{i-1} - \Delta y_{i-1}$. If $y_i - y_{\min} < \mu$, set $y_i = y_{\min} + \mu$ (μ is a small offset from the surface boundary, e.g. 0.1mm) and mark path^i as the last path. Go to (2).

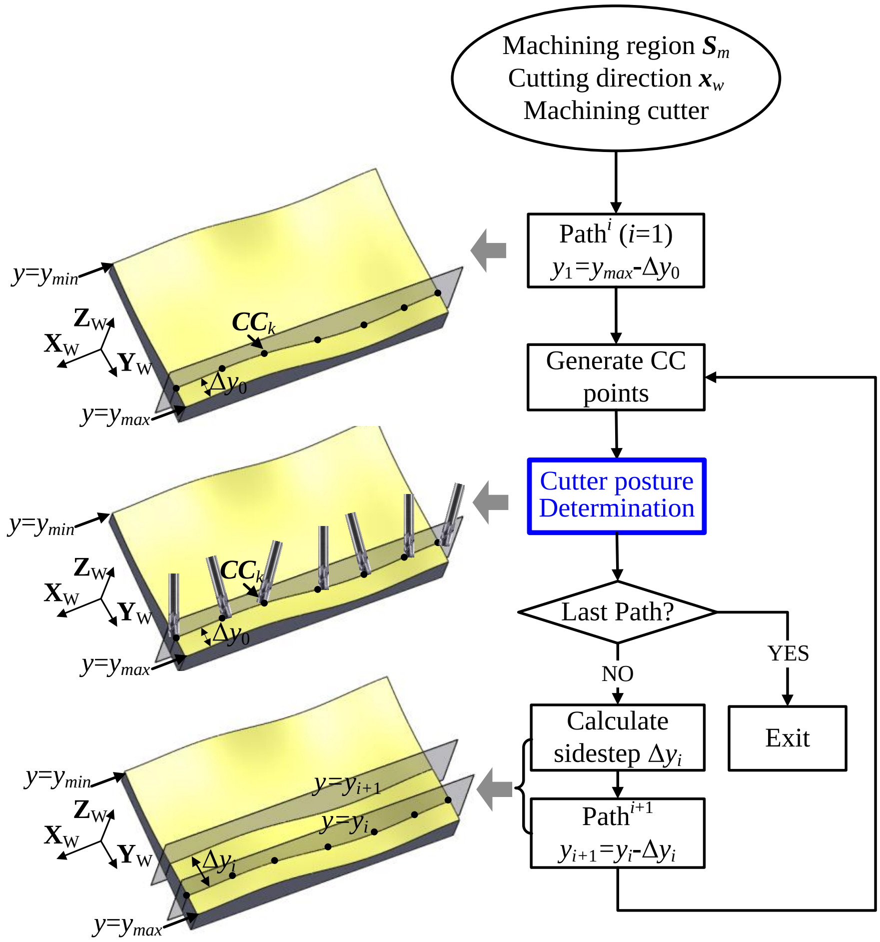

Figure 5.1 The overall approach for generation of iso-planar toolpath

5.1.1 CC point generation

As shown in Figure 5.1, tool path generation starts from the first tool path which is at an offset of Δy_0 from the boundary on the surface $\boldsymbol{S}_m$, i.e., $y_i = y_{\max} - \Delta y_0$. In the current tool path, CC points will be generated on the intersection curve between the cutting plane and $\boldsymbol{S}_m$. During this process, two aspects should be well considered. First, CC points are discrete and the trajectory of the cutter between neighbouring CC points would be a straight line segment when linear interpolators are used in 5-axis machining. As a result, deviations would be inevitable between the cutter trajectory and the intersection curve. According to the requirement of surface quality, this deviation should not exceed the surface error tolerance τ_{se}. This requirement puts a limit on the step-forward distance between neighbouring CC points. Given the current CC point $\mathbf{P}_i$ and next CC point $\mathbf{P}_{i+1}$ in the current cutting plane $y = y_1$, the deviation, $d\left(\mathbf{P}_i\mathbf{P}_{i+1}, \boldsymbol{S}_m\right)$, is shown in the Figure 5.2. Second, during real machining, each trajectory of the cutter between neighbouring CC points will require one time of acceleration and deceleration of the machining joints. For shorter machining time, it is preferable to keep the number of CC point minimal. Regarding a single path, this means that the step-forward distance between CC points should be maximized to increase machining efficiency.

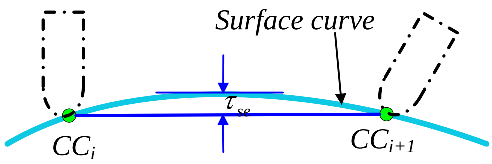

Figure 5.2 Deviation between the adjacent CC points

As the start point on the intersection curve can be used as the first CC point, the next CC point will be generated iteratively to achieve the maximum step-forward distance while keeping the deviation close but smaller than the given surface error tolerance τ_{se}. This condition can be expressed as the following:

$$\left(1-\delta\right)\tau_{se} \le d_{\max}\left(\mathbf{P}_i\mathbf{P}_{i+1}, \boldsymbol{S}_m\right) \le \tau_{se} \tag{5-1}$$

where $d_{\max}\left(\mathbf{P}_i\mathbf{P}_{i+1}, \boldsymbol{S}_m\right)$ represents the maximum deviation and δ is a small value such as 0.01. To carry out the optimization process mentioned above, the following iterative approach is adopted:

1) Set the initial value for step-forward length (denoted as L_i) between $\mathbf{P}_i\mathbf{P}_{i+1}$ regarding local surface geometry at $\mathbf{P}_i$;
2) Search for an estimated point $\mathbf{P}_{i+1}$ from $\mathbf{P}_i$ based on L_i.
3) Check whether the deviation $d_{\max}\left(\mathbf{P}_i\mathbf{P}_{i+1}, \boldsymbol{S}_m\right)$ between the tool trajectory and surface curve meets the condition in Eq. (5-1).
4) If the condition is satisfied, L_i is found and $\mathbf{P}_{i+1}$ can be obtained. Otherwise, L_i is increased or reduced using an updating rule. Go back to steps (2).

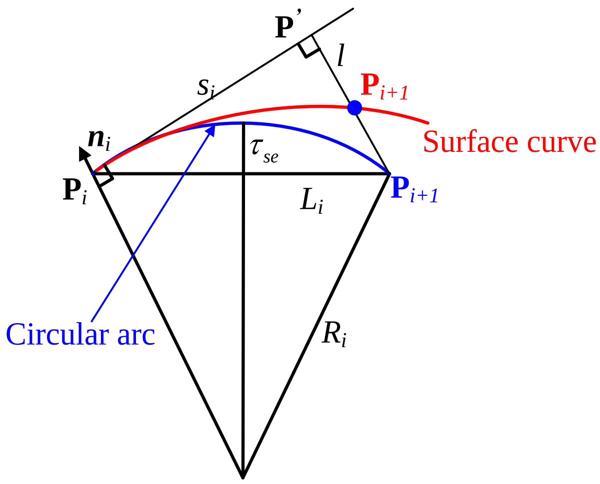

Figure 5.3 Obtain next CC point based on initial estimation of step-forward

To set the initial value for step-forward length at a CC point, the local curvature should be taken into consideration. For simplicity, as shown in Figure 5.3, the surface shape in the vicinity of $\mathbf{P}_i$ is approximated by a circular arc, whose radius is the reciprocal of the curvature κ_c at $\mathbf{P}_i$ on plane $y = y_1$. In this way, the initial estimation of step-forward length at $\mathbf{P}_i$ is given as:

$$L_i = \sqrt{8R_i\tau_{se} - 4\tau_{se}^{\;2}} = 2\sqrt{\frac{\tau_{se}(2-\kappa_c\tau_{se})}{\kappa_c}} \tag{5-2}$$

Based on the estimated value of L_i, the algorithm proceeds to search for the next CC point $\mathbf{P}_{i+1}$ on intersection curve based on $\mathbf{P}_i$. Firstly, based on the approximated circular arc, a tangent distance s is calculated as $s = (R-\tau)L_i / R$ (see Figure 5.3). This gives $\mathbf{P}^{'} = \mathbf{P}_i + s_i \boldsymbol{f}_i$, where $\boldsymbol{f}_i$ is the tangent direction at $\mathbf{P}_i$. $\mathbf{P}_{i+1}$ is then obtained to be the intersection point between the intersection curve and a line through $\mathbf{P}^{'}$ and along the opposite of $\boldsymbol{n}_\mathrm{i}$ (see Figure 5.3), given as $\mathbf{P}_{i+1} = \mathbf{P}^{'} - l\boldsymbol{n}_i$, where l is the distance of $\mathbf{P}_{i+1}$ from $\mathbf{P}^{'}$. The detailed algorithm to generate the next CC point can refer to (Geng 2013).

5.1.2 Cutter posture assignment

After the CC points are generated for the current path, a cutter posture needs to be assigned at each CC point. Before this, the PAG, PSG, and subsequently CIF-map at each CC point need to be constructed identified using the method presented in the Chapter 4.

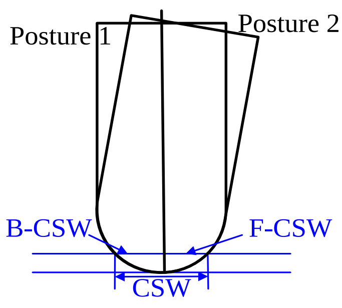

Figure 5.4 Influence of ball-end cutter on CSW

When selecting a posture for a CC point from its CIF-map, the heuristic for maximum CSW will not fit the ball-end cutter situation. As shown in the Figure 5.4, when a ball-end cutter is used, the forward-CSW (F-CSW) and backward-CSW (B-CSW) will remain constant on the same path even when the cutter posture varies between adjacent CC points. Therefore, the total CSW is not affected by the ball-end cutter posture in 5-axis machining. The max-CSW heuristic is thus dropped. Another strategy is to follow the optimization algorithm in (Geng 2013) aiming at short tool path length and good tool path smoothness. The algorithm can easily work for the current situation by simply replacing the A-map with CIF-map.

In this study, we propose another posture assignment strategy aiming at minimizing cutter deflection along the tool path. As cutting force will cause cutter deflection inevitably and subsequently the shape error on the machined surface, the deflection cutting force should be minimized. It should be noted that the optimal cutter posture causing minimal cutter deflection would be selected from CIF-map to assure the machining process chatter-free and interference-free. This cutter posture determination process will be presented in detail in Section 5.2.

5.1.3. Path intervals determination

After the first tool path is generated, the other tool path will be generated using an iterative manner. Procedures for CC point generation and posture determination are the same as that of the first path. The key is to determine the location of the next tool path under the constraint of scallop height tolerance.

Similar to the generation of a single tool path, requirements for side-steps determination are two-fold. First, between two adjacent tool paths, a scallop will be created. The height of such a scallop should stay below the scallop height tolerance (τ_{sh}). Given the cutter postures on neighbouring path, the scallop height is solely determined by the side-step between them: the smaller the side-step, the lower the scallop. On the other hand, it is also preferable to finish the whole surface with the least number of tool paths. For this reason, the side-step between tool-paths should be maximized. Considering these two conflicting requirements, an optimization problem is formulated: to maximize the side-step between two paths without breaching the limit imposed on scallop height.

To keep the scallop height between neighbouring paths below the given tolerance, a certain level of overlap should be kept between the CSWs of neighbouring paths. An illustration of this situation is shown in Figure 5.5. We assume that for a CC point $\mathbf{P}_m$ on ith path, there is a corresponding CC point $\mathbf{P}_n$ on $(i+1)$th path along the feeding direction $\boldsymbol{f}$. On the plane normal to the cutting direction (e.g., plane $x = x_{i+1,m}$ in Figure 5.6), the effective cutting shapes of the cutter at $\mathbf{P}_m$ and $\mathbf{P}_n$ are shown in Figure 5.6, with their CSWs overlapped

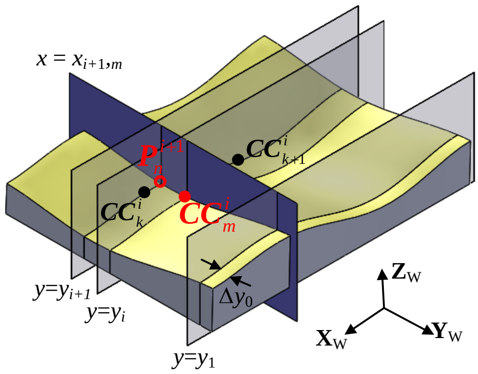

Figure 5.5 Determination of interval between adjacent tool paths

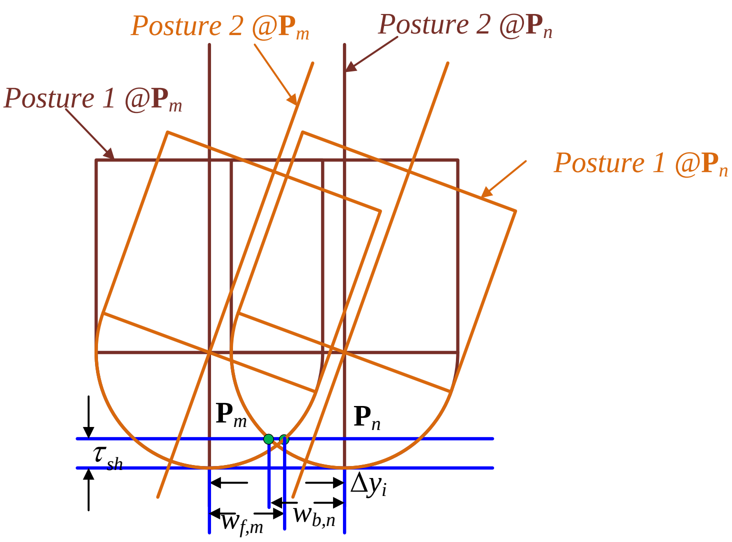

Figure 5.6 Path interval in 5-axis machining for a ball-end cutter

For a ball-end cutter, since cutter posture does not affect F-CSW and B-CSW, the path interval (shown in Figure 5.6) will not vary with the posture change. For simplicity, the calculation of path interval is calculated under the vertical orientation. To make sure the scallop height generated by two adjacent tool paths under the given scallop height tolerance, the path interval must meet the following condition:

$$\Delta y_i < w_{f,m} + w_{b,n} \tag{5-3}$$

At the same time, to maximize the machining efficiency or minimize the total tool path length, it is desirable to increase the path interval to such a level that the resulting scallop height is just below the tolerance. Furthermore, as F-CSW and B-CSW may vary with different CC points in a tool path, the minimum F-CSW of the ith path and B-CSW of the $(i+1)$th path should be used as a safe approximation. Hence, Eq. (5-3) is re-written as:

$$(1-\eta_p)(w^i_{f,\min} + w^{i+1}_{b,\min}) < \Delta y_i < w^i_{f,\min} + w^{i+1}_{b,\min} \tag{5-4}$$

where η_p is a pre-defined value controlling the level of overlapping. For better machining efficiency, a small value, e.g., 0.05, should be used. By iteratively selecting the maximum path interval Δy_i while keeping the scallop height under the given surface scallop height tolerance, the next tool path location can be determined towards maximum machining efficiency. Based the location of the ith path, the location of (i+1)th path can be searched for by following the condition in Expression (5-4) using an iterative approach. The initial side-step Δy_i is estimated to be the minimum CSW on the current path. The procedure is given as follows:

1) Set the initial value of Δy_i as $w_{i,\min}$ on the ith path; $y_{i+1} = y_i - \Delta y_i$.
2) Obtain the CC points on the (i+1)th path and assign the postures using the Max-CSW heuristic. Calculate the CSWs at all the CC points and obtain $w_{b,\min}^{i+1}$.
3) Test the condition in Eq. (5-4). If the condition is not met, adjust Δy_i accordingly (increasing or decreasing) by a small proportion and go to step (2). Otherwise, Δy_i is found.
4) Set $y_{i+1} = y_i - \Delta y_i$. If $y_i - y_{\min} < \mu$, set $y_i = y_{\min} + \mu$. Stop.

The detailed algorithm to calculate the CSW can be found in (Geng 2013). After the next tool path location is determined, the CC points and corresponding cutter posture assignments will be repeated until the last tool path is finished.

5.2. Posture with Minimal MDC-F

In this section, a new optimization strategy for cutter posture assignment at a CC point is proposed. The optimal cutter posture will be selected towards minimal cutter deflection. As the material property of cutter is fixed once the cutter is selected, cutter deflection is only affected by cutting force during machining process. Therefore, it can be said that the cutting force causing minimal cutter deflection should be selected.

Furthermore, the optimal cutter posture should be selected from the CIF-map at the CC point. In the following section, the cutting force caused minimal cutter deflection is determined first and followed by the introduction of optimal cutter posture search algorithm.

5.2.1. Definition of MDC-F

As the stiffness of cutter in $\mathbf{Z}_{\mathrm{T}}$-axis is much higher than those in $\mathbf{X}_{\mathrm{T}}$ and $\mathbf{Y}_{\mathrm{T}}$ axes, the influence of cutting force on machined surface quality is mainly from the cutting force in $\mathbf{X}_{\mathrm{T}}$ and $\mathbf{Y}_{\mathrm{T}}$ direction, i.e., $F_{x,c}$ and $F_{y,c}$ (see Figure 5.7a). Therefore, the cutting force related to the machined surface quality is normal to the cutter axis and named as deflection cutting force, which can be obtained by $\sqrt{F_{x,c}^2 + F_{y,c}^2}$ (Geng *et al.* 2015). To minimize the machined surface error, the deflection cutting force should be minimized. However, in practice, as the cutting force varies with the cutter rotation, the deflection cutting force also varies with cutter rotation. There will be a maximum cutting force in a complete rotation of the cutter, which is called the *maximum deflection cutting force* (MDC-F). Therefore, the first task is to find the MDC-F under a given posture, i.e., the maximum force acting normal to the cutter axis during machining.

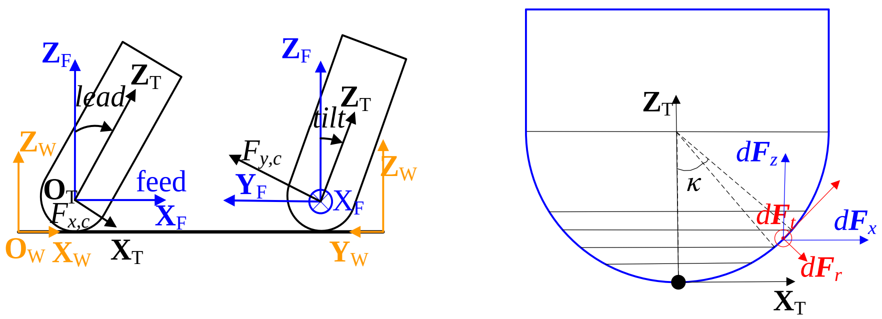

(a) Cutter coordinate system (CCS) (b) Discretization of cutter geometry

Figure 5.7 Cutting force prediction

As introduced in Chapter 2, the elemental cutting force corresponding to a cutter disk can be calculated using Eq. (2-1). At any time instant, the deflection cutting force acting on the cutter is given as:

$$F_{x-y} = \sqrt{\left(\sum_{j}^{N_{fc}}\sum_{i}^{N_e} dF_x^{i,j}\right)^2 + \left(\sum_{j}^{N_{fc}}\sum_{i}^{N_e} dF_y^{i,j}\right)^2} \tag{5-5}$$

As the cutter rotates, a cutting edge will enter and exit from the engagement region, causing the deflection cutting force to change cyclically at the tooth passing frequency. It is therefore necessary to identify the time instance when the MDC-F occurs in one tooth passing period *T*. As the cutting force has no explicit form, a numerical method needs to be employed here. As the *golden section search* (GSS) method have better performance compared to other linear search method in one dimension search (Seiler and Seiler 1989), it will be used to find the MDC-F. GSS is a linear search method like the bi-section search method. The difference between the GSS and bi-section search is the ratio GSS is golden ratio and it is 0.5 in bi-section search.

To find the maximum deflection cutting force, firstly, a series of time instances are sampled evenly from *T*, given as $t_1, t_2, \ldots, t_i, \ldots, t_n$. For t_i that satisfies $F_{x-y}(t_{i-1}) > F_{x-y}(t_i)$ and $F_{x-y}(t_i) > F_{x-y}(t_{i+1})$, the range (t_{i-1}, t_{i+1}) will be searched thoroughly using the GSS method till the stop criterion is meet. As the GSS method is designed to find the minimum value in one dimension search, the fitness F_f of MDC-F search is set as:

$$F_f = 1/F_{x-y} \tag{5-6}$$

Defining the golden ratio *g* = 0.618, the procedure of GSS is given as follows:

1) Set $x_0 = t_{i-1}, x_1 = t_i, x_2 = t_{i+1}$;

2) If the search stop criterion, $x_2 - x_0 < \tau_{tol}$, is met, stop and output x_1 as the solution.

3) When $x_2 - x_1 \geq x_1 - x_0$, $x_2 = x_1 + (1-g)(x_2 - x_1)$; else, $x_0 = x_1 - (1-g)(x_1 - x_0)$;

where τ_{tol} is the pre-defined tolerance and set as 0.1 °in this case.

An example is shown here to illustrate this search process. The workpiece material used is AL7075. The machine tool used is DMG 80P duo Block 5-axis machining centre. The cutter is a Fraisa 2-fulte ball-end cutter (R = 5mm, $i_0 = 20^{\circ}$). The modal parameters and cutting force coefficients are provided in Table 5.1 and Table 5.2. A slotting process (see Figure 3.1a) was carried out. The feed-per-tooth is 0.1 mm/rev and the depth-of-cut is 1 mm. The cutter posture, i.e., lead angle and tilt angle, was set as (30 °, 30 °). The predicted cutting forces calculated at an interval of 0.1 °in cutter frame are shown in Figure 5.8a. Meanwhile, the deflection cutting forces in a whole cutter rotation are shown in Figure 5.8b. The initial sampling density is set as $n_{sd} = 36$. The search process is indicated with red line and shown in Figure 5.8c. It can be seen that the search is completed quite efficiently, with only 9 calculations of the cutting force to achieve the accuracy below 0.1°. For a comparison, the bi-section search method was also tried for this case and the search process is shown in Figure 5.8d. However, 11 calculations were needed to achieve the same result.

Table 5.1 Modal parameters for MDC-F search

Natural frequency (Hz)		**Process damping (1%)**		**Stiffness (N/m^2)**	
X$_T$	**Y$_T$**	**X$_T$**	**Y$_T$**	**X$_T$**	**Y$_T$**
1412.5	1443.75	0.033112	0.032257	13543571.05	14808892.07

Table 5.2 Cutting force coefficients for MDC-F search

Natural frequency (Hz)		**Process damping (1%)**		**Stiffness (N/m^2)**	
X_T	**Y_T**	**X_T**	**Y_T**	**X_T**	**Y_T**
1412.5	1443.75	0.033112	0.032257	13543571.05	14808892.07

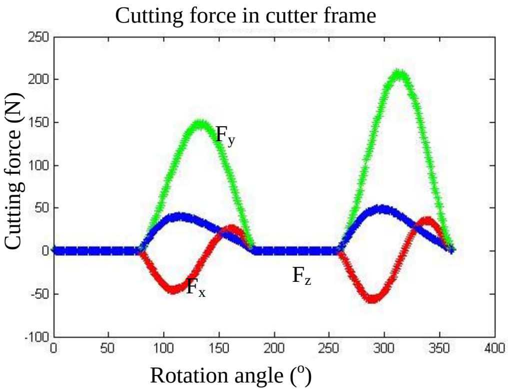

(a) Cutting forces in cutter frame

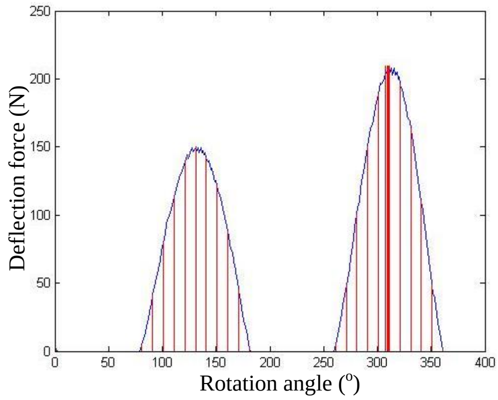

(b) Deflection cutting force

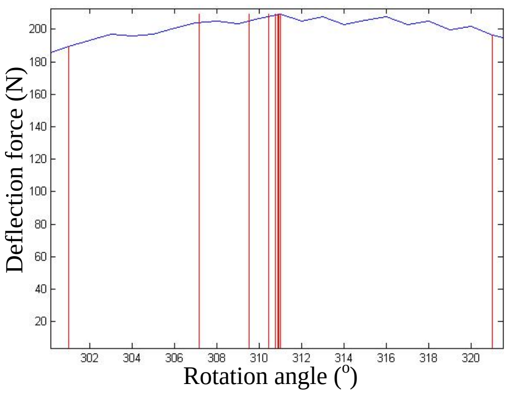

(c) Results from GSS search

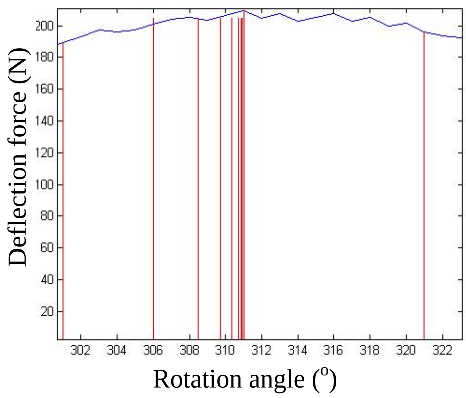

(d) Results from bi-section search

Figure 5.8 Search for maximum deflection cutting force

5.2.2. Search for optimal cutter posture with PSO

For a given posture, the maximum deflection cutting force (MDC-F) can be found by using the method introduced in Section 5.2.1. For posture assignment at a CC point, the goal is to identify a CIF posture that gives the minimum MDC-F. For this task, a search algorithm based on the particle swarm optimization (PSO) is designed and implemented. PSO is a search tool based on swarm intelligence (Engelbrecht 2005). During the search, the locations for a swarm of particles (candidate solutions) in the solution space are continuously updated. At each time instance, a particle's location is updated based on information discovered by the whole swarm and by itself. It is expected that through continuous updating, the particles' locations will converge to the global best location of the solution space.

In the formulation of PSO, $\boldsymbol{W}_i\left(t_{it}\right)$ represents the location of the *i*th particle at iteration t_{it}. In this application, it represents a candidate posture, expressed in the tool frame corresponding to the input posture carrying the engagement information. When $t_{it}=0$, a total of N_s particles are initialized randomly, in which each particle represents a potential solution. The generated particle is represented in an *M*-dimensional solution space depending on the modelled problem solution and *M* is 2 in this application, i.e., lead angle and tilt angle. Each particle *i* in an iteration t_{it} has a position vector and a velocity vector represented as:

$$\boldsymbol{W}_{i,t_{it}}=\left\{w_{i,1}^{t_{it}},w_{i,2}^{t_{it}}\right\} \tag{5-7}$$

$$\boldsymbol{V}_{i,t_{it}}=\left\{v_{i,1}^{t_{it}},v_{i,2}^{t_{it}}\right\} \tag{5-8}$$

A fitness function $\boldsymbol{f}\left(\boldsymbol{W}_{i,t_{it}}\right)$ is defined to determine the quality of the solution. In this application, the fitness function is the MDC-F at the given posture. When $t_{it}=0$, the current particle will be assigned as the personal best solution and global best solution. At iteration $t_{it}>0$, if the fitness value of particle $\boldsymbol{W}_{i,t_{it}}$ is larger than that of its personal best solution $\boldsymbol{P}_i=\left\{p_{i,1},p_{i,2}\right\}$, the personal best solution will be updated with the current particle $\boldsymbol{W}_{i,t_{it}}$. This means that if the deflection cutting force in the current particle is smaller than that in personal best solution, the personal best solution will be updated with the current particle. Similarly, at iteration t_{it}, if the quality of particle $\boldsymbol{W}_{i,t_{it}}$ is better than that of global best solution $\boldsymbol{G}=\{g_1,g_2\}$ for the whole population, this particle will be saved as $\boldsymbol{G}$. The position and velocity of each particle will be updated using the following updated rule:

$$\begin{aligned} &\boldsymbol{V}_{im,t_{it}+1}=\omega_p\times\boldsymbol{v}_{im,t_{it}}+c_{1p}\times r_{1p}\times(\boldsymbol{P}_{i,m}-\boldsymbol{W}_{im,t_{it}})+c_{2p}\times r_{2p}\times(g_m-\boldsymbol{W}_{im,t_{it}}) \\ &\boldsymbol{W}_{im,t_{it}+1}=\boldsymbol{W}_{im,t_{it}}+a_p\boldsymbol{V}_{im,t_{it}+1} \end{aligned} \tag{5-9}$$

where ω_p is called the inertia weight, c_{1p} and c_{2p} are two constants called acceleration factors and usually setting as 2; r_{1p} and r_{2p} are two random numbers in the range of 0.0 and 1.0; a_p is constraints factor and usually set as 1. The updating rules are applied to all the particles in the swarm. During the updating, the global best location and the personal best locations will keep being updated. For the stopping criterion, the search will stop if the global best particle remains unchanged over 30 times. This is to say that the search has converged around the location supposed to be optimal solution. The overall algorithm is summarized as follows:

<u>PSO Algorithm: Search for the cutter posture with minimal MDC-F</u>

Input: Cutting force coefficients, modal parameters and machining conditions

Output: Cutter posture with minimal MDC-F

Set $t_{it}=0$.

Random initializing $\boldsymbol{W}_{i,0}=\{w_{i,1}^0,w_{i,2}^0\}$; $\boldsymbol{V}_{i,0}=\{v_{i,1}^0,v_{i,2}^0\}$ in the solution space. This velocity will be set as the starting search velocity.

Set the global best solution $\boldsymbol{G}$ = 1e8 (an arbitrary large number).

For i = 1:N_s

Obtain the MDC-F of $\boldsymbol{W}_{i,0}$ using GSS as the fitness of the particle $\boldsymbol{f}\left(\boldsymbol{W}_{i,0}\right)$;

Set $\boldsymbol{P}_i = \boldsymbol{W}_{i,0}$.

if ($\boldsymbol{f}\left(\boldsymbol{P}_i\right) < \boldsymbol{f}\left(\boldsymbol{G}\right)$)

$\boldsymbol{G} = \boldsymbol{P}_i$;

end

end

while (true)

if (Stopping criterion is met)

Output $\boldsymbol{G}$ as the optimal posture at the cutter location;

break;

end

for i=1:N_s

Obtain $\boldsymbol{V}_{i,t_{it}+1}$ from $\boldsymbol{V}_{i,t_{it}}$ using the update rule;

Obtain $\boldsymbol{W}_{i,t_{it}+1}$ from $\boldsymbol{W}_{i,t_{it}}$ using the update rule.

Obtain the MDC-F of $\boldsymbol{W}_{i,t_{it}+1}$ using GSS, given as $\boldsymbol{f}\left(\boldsymbol{W}_{i,t_{it}+1}\right)$;

if ($\boldsymbol{f}\left(\boldsymbol{W}_{i,t_{it}+1}\right) < \boldsymbol{f}\left(\boldsymbol{P}_i\right)$)

$\boldsymbol{P}_i = \boldsymbol{W}_{i,t_{it}+1}$;

end

if ($\boldsymbol{f}\left(\boldsymbol{W}_{i,t_{it}+1}\right) < \boldsymbol{f}\left(\boldsymbol{G}\right)$)

$\boldsymbol{G} = \boldsymbol{W}_{i,t_{it}+1}$;

end

end

Set $t = t+1$

End

5.2.3 Case study: optimal cutter posture selection

In order to verify the proposed PSO algorithm to determine the minimal MDC-F, a simple case is presented here. The PSO algorithm was implemented with MATLAB. The lead angle and tilt angle are both set in the range of 0° to 60°, which generally cover the range of practical machining. The workpiece material used is AL7075. The machine tool used is DMG 80P duo Block 5-axis machining centre. The cutter is a Fraisa 2-fulte ball-end cutter (R = 5mm, $i_0 = 20^{\circ}$). The modal parameters and cutting force coefficients are the same as those provided in Table 5.1 and Table 5.2, respectively. The feed-per-tooth is set as 0.1 mm and the depth of cut is 1mm. For the PSO, the swarm size is set as Ns = 20. The feed direction is along the X_W-axis of workpiece coordinate system (WCS) and the workpiece is set up aligning with the machine tool coordinate system (MTCS) as shown in Figure 5.9. To test the effectiveness of the PSO algorithm, a scanning of cutting force (exclusive search) in the feasible search space is conducted with an interval of 1° for both lead and tilt angles. The scanning took about 2,200s on a PC with i5 3.3GHZ CPU and 8GB RAM. The obtained solutions space is shown in Figure 5.10. It can be seen that there is a minima in the solution space and the minimum deflection cutting force is 101.978 N with posture (lead: 60^{o}, tilt: 60^{o}). On the other hand, the PSO algorithm was run and the search record (fitness vs. number of iterations) is shown in Figure 5.11. The search converged very quickly (within 40 iterations) in 1,100 seconds on the same PC. The global best solution matches the minima found earlier. Meanwhile, the traversed locations in the search with PSO are plotted over the search space in Figure 5.12. This clearly shows that, in this case, the PSO algorithm is equally effective in finding the best solution, and much more efficient.

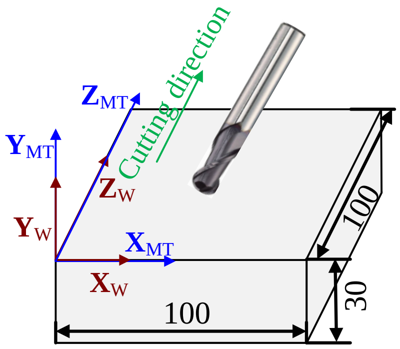

Figure 5.9 Machining set up for the verification of the PSO algorithm

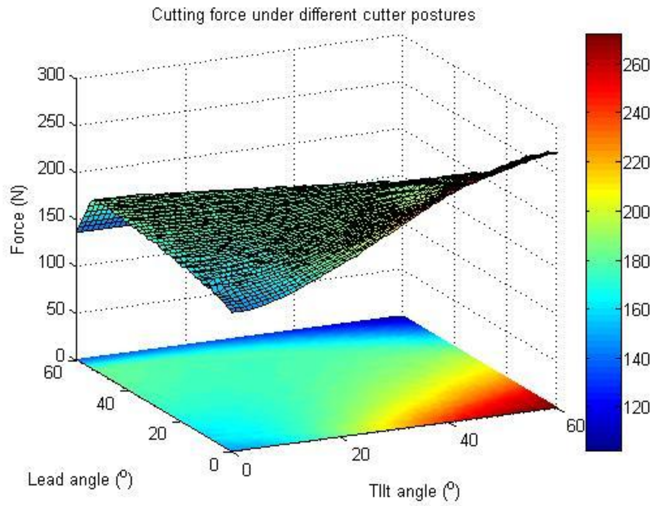

Figure 5.10 Exclusive search results for the minimal MDC-F

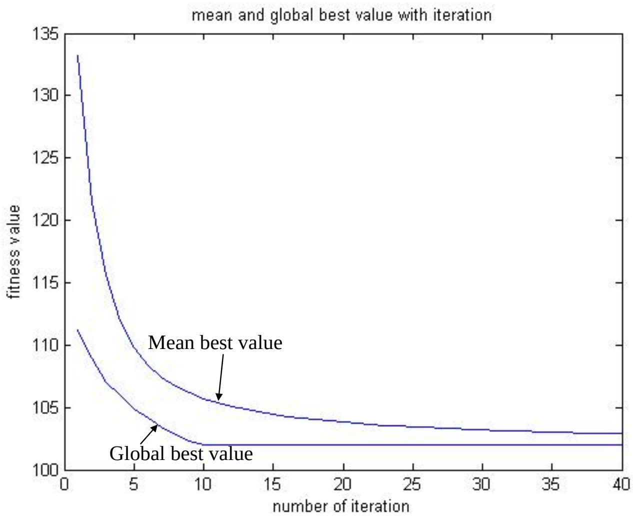

Figure 5.11 Search record from the PSO search

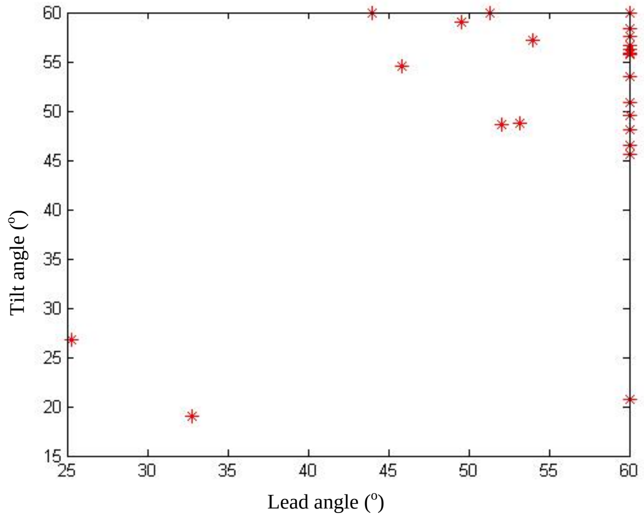

Figure 5.12 Traversed locations by the PSO search

5.3. Summary

In this chapter, a new method is proposed to generate the optimal tool path towards minimal MDC-F while keeping the machining process chatter-free and interference-free. First, the general framework to generate tool path, including CC point generation and cutter posture assignment, is presented. With the introduction of definition of MDC-F under given cutter posture and machining parameters, MDC-F for given cutter posture is obtained by GSS method. Followed this, the PSO method is used to search the cutter posture which generated the minimal MDC-F. Then, this posture will be selected as the optimal cutter posture at this CC point. A simple case study is presented to show the effectiveness of the proposed method to search the optimal cutter posture at a given CC point.

CHAPTER 6

CASE STUDY AND DISCUSSION

In this thesis, cutter posture assignment in 5-axis machining considering machining dynamics is firstly studied, followed by the generation of CIF-map. The application of CIF-map in tool path generation for 5-axis machining has been studied in Chapter 4. The optimal cutter posture assignment from CIF-map at a CC point and subsequently complete tool path generation is studied in Chapter 5. These methods have been implemented using MATLAB. In this chapter, two case studies in CIF-map generation, optimal cutter posture assignment and corresponding optimal tool path generation will be presented. Performance comparison between the proposed method and our previous method is also presented.

6.1. Case Study 1: CIF-map Construction For Different Parameters

In this section, the generation of CIF-maps under different machining conditions is presented. The influence of cutting direction and workpiece geometry on CIF-map construction will also be illustrated. The workpiece material used is AL7075. The machine tool used is DMG 80P duo Block 5-axis machining centre. The cutter is a Fraisa 2-fulte ball-end cutter (R = 5mm, $i_0 = 20^\circ$). The modal parameters and cutting force coefficients and are provided in Table 6.1 and Table 6.2, respectively. The depth-of-cut is 1 mm, feed-per-tooth is 0.1 mm/rev, and spindle speed is 4,800 r/min.

Table 6.1 Modal parameters for case study

Natural frequency (Hz)		**Process damping (1%)**		**Stiffness (N/m^2)**	
X_T	**Y_T**	**X_T**	**Y_T**	**X_T**	**Y_T**
1412.5	1443.75	0.033112	0.032257	13543571.05	14808892.07

Table 6.2 Cutting force coefficients for case study

K_{te} (N/mm)	K_{tc} (N/mm^2)	K_{re} (N/mm)	K_{rc} (N/mm^2)	K_{ae} (N/mm)	K_{ac} (N/mm^2)
14.0371	951.751	16.5002	608.561	-1.25118	288.478

Firstly, the influence of cutting direction on CIF-map will be studied. The workpiece is shown in Figure 6.1, in which two cutting directions, $\mathbf{X}_W$ and $-\mathbf{Y}_W$, are assigned at same cutter contact (CC) point $\mathbf{P}_1$. The PSGs were then generated for these two different cutting directions and shown in Figure 6.2a and Figure 6.2b, respectively. It can be seen that even at the same CC point, when the cutting direction is changed, the PSG also changes. On the other hand, the PAGs for the two different cutting directions are shown in Figure 6.3a and Figure 6.3b, respectively. By intersecting the PAG and PSG under the same feed direction, the CIF-maps represented by hated area under the two cutting directions are shown in Figure 6.4a and Figure 6.4b, respectively. This example is a clear reminder of the significance of the PSG and CIF-map in tool path generation:

(1) Even at the same CC point, the CIF-maps under different feeding directions can be quite different. For example, the machining process with posture (0^o, 0^o) for cutting along $\mathbf{X}_W$ will be stable, while the machining process with same posture for cutting along $-\mathbf{Y}_W$ will be unstable.

(2) While the effect of feed direction on PAG can be intuitively seen, the effect of it on PSG can only be computed through the procedures proposed in this thesis.

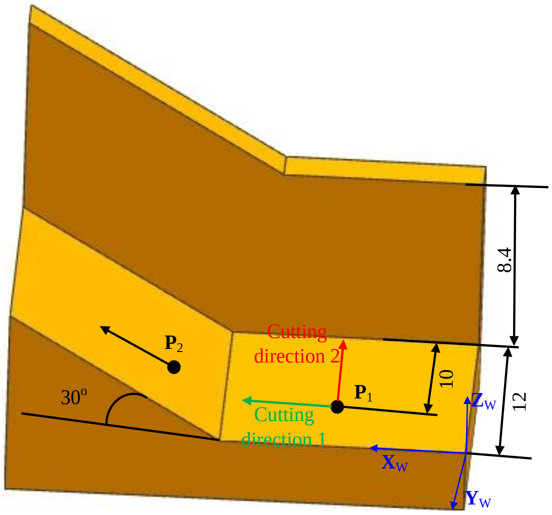

Figure 6.1 Workpiece for case study 1

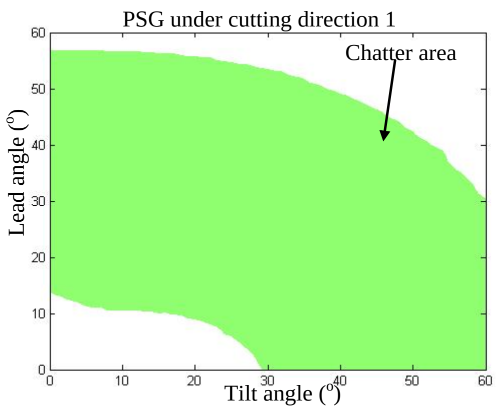

(a) PSG along cutting direction $\mathbf{X}_W$

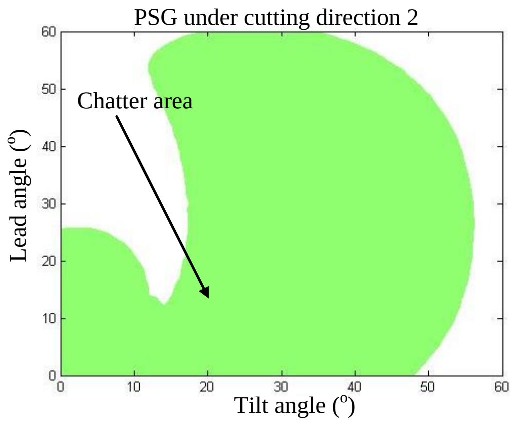

(b) PSG along cutting direction $-\mathbf{Y}_W$

Figure 6.2 PSGs at $\mathbf{P}_1$ for different cutting directions

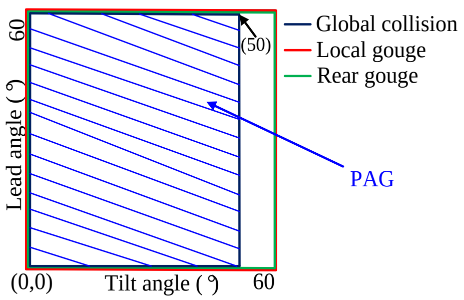

(a) PAG under $\mathbf{X}_W$ direction

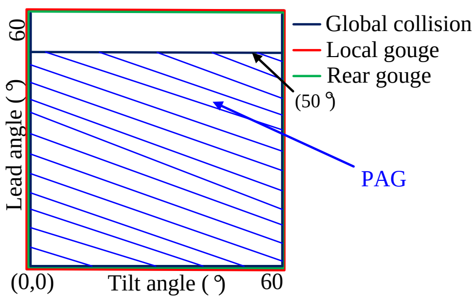

(b) PAG under $\mathbf{Y}_W$ direction

Figure 6.3 PAGs at $\mathbf{P}_1$ for different cutting directions

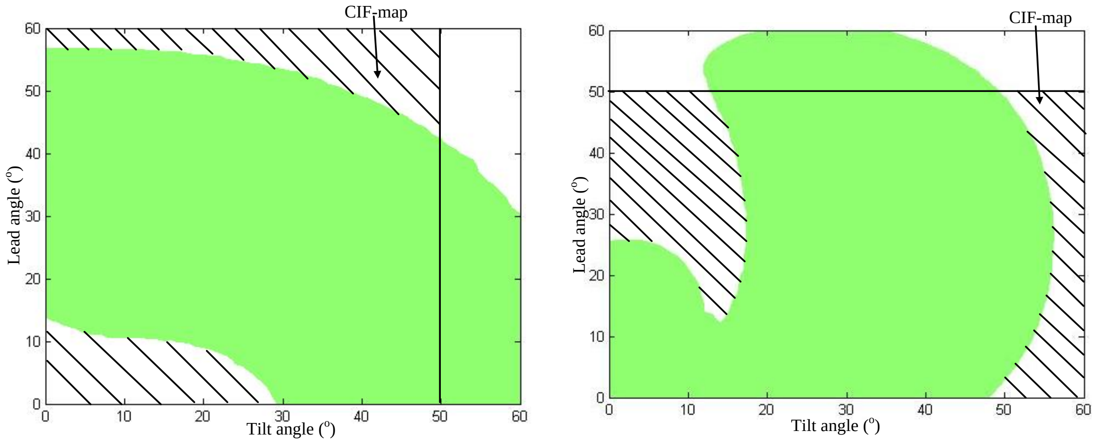

(a) CIF under $\mathbf{X}_W$ direction (b) CIF under - $\mathbf{Y}_W$ direction

Figure 6.4 CIF-maps at $\mathbf{P}_1$ for different cutting directions

Furthermore, for this case, the effect of workpiece surface geometry on CIF-map is also studied. With the cutting direction along $\mathbf{X}_W$, the PSG at CC point $\mathbf{P}_2$ is shown in Figure 6.5. Even along the same cutting direction ($\mathbf{X}_W$), the difference between the PSG at $\mathbf{P}_2$ and the PSG at $\mathbf{P}_1$ (see Figure 6.2a) is very obvious. As a result, the CIF-map at $\mathbf{P}_2$ (see Figure 6.6) is also quite different from the CIF-map at $\mathbf{P}_1$ (see Figure 6.4a).

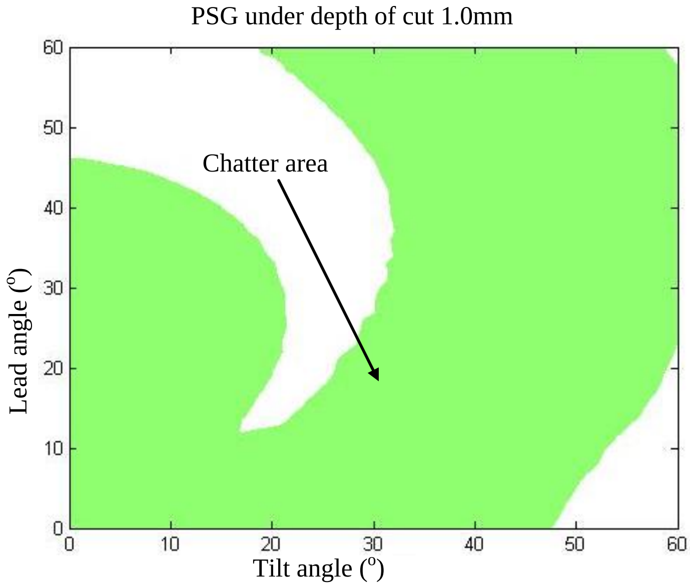

Figure 6.5 The PSG at $\mathbf{P}_2$

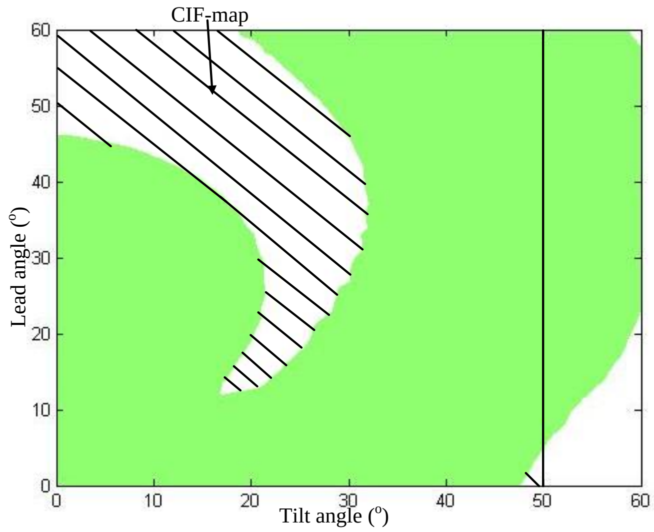

Figure 6.6 The CIF-map at $\mathbf{P}_2$

6.2. Case Study 2: Tool Path Generation

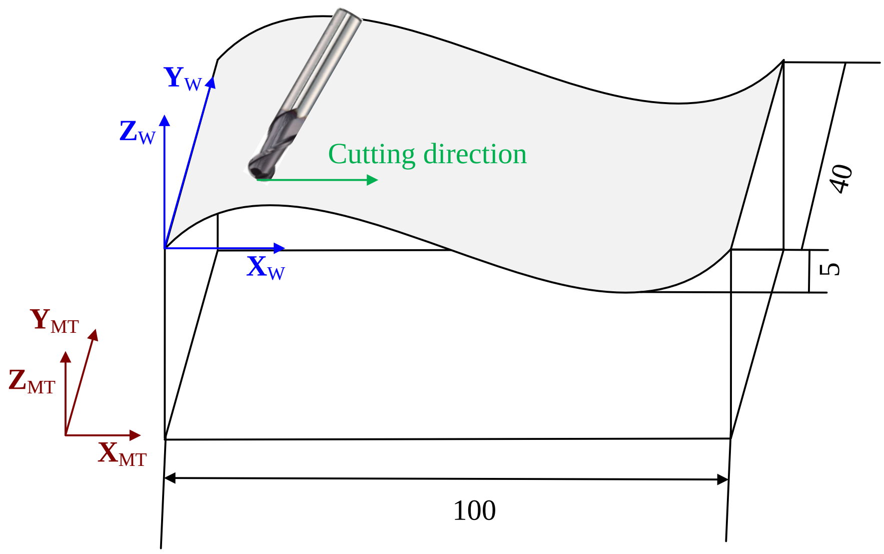

Figure 6.7 Workpiece for tool path generation

In this section, tool path generation using the proposed method will be presented. In addition, the results generated by the proposed method and our previous method will also be compared. The workpiece used for tool path generation is shown in Figure 6.7 with corresponding dimension specified. The machining surface of the workpiece is obtained by extruding the sine curve (in $\mathbf{X}_W$-$\mathbf{Z}_W$ plane) along $\mathbf{Y}_W$, which is expressed as $Z_W = 5\sin((\pi/50)X_W)$. In the tool path generation stage, the surface error tolerance and scallop height tolerance are both set as 0.1 mm. The workpiece material used is AL7075 and the cutter is a Fraisa 2-fulte ball-end cutter (R = 5mm, $i_0 = 20^\circ$). The machine tool used is DMG 80P duo Block 5-axis machining centre. The modal parameters and cutting force coefficients and are provided in Table 6.1 and Table 6.2, respectively. The depth-of-cut is 1 mm, feed-per-tooth is 0.1 mm/rev and spindle speed is 4,800 r/min. The cutting direction is along with $\mathbf{X}_W$. As the generation of CC points in the proposed method is the same with that in our previous method, the generated CC paths using the proposed and previous method will be same as shown in Figure 6.8. A total of 21 tool paths have been generated to finish the whole surface machining. At each tool path, 13 CC point are generated. However, the cutter posture assignment at each CC point will be different and will be discussed later.

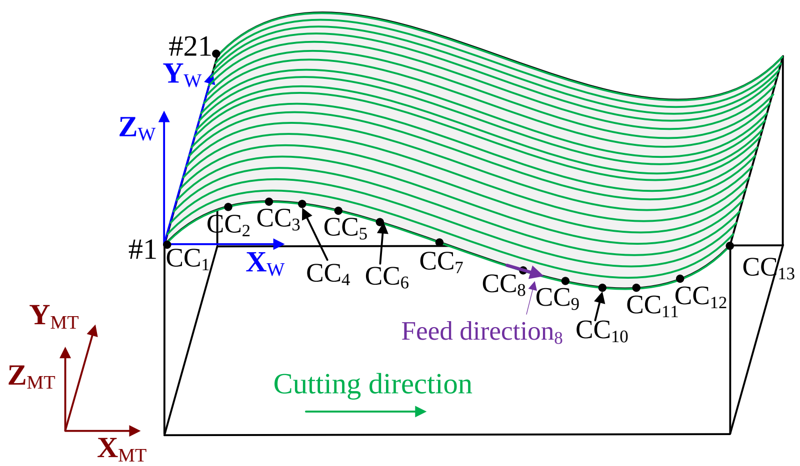

Figure 6.8 Generated tool path for the workpiece

To compare the performance of the proposed method with our previous method, tool path #1 (see Figure 6.8) is used to illustrate the variation, which is just 0.02 mm from the boundary of the workpiece. The resulted postures for all the CC points (total 13) on tool path #1, from the two methods, are shown in Figure 6.9a and Figure 6.9b, respectively. Using our previous method, the vertical cutter posture is assigned to every CC point in order to reduce the joint movement during the machining process (see Figure 6.9b). On the other hand, using the proposed method, the cutter posture (lead: 60°; tilt: 60°) (the definition of lead angle and tilt angle is shown in Figure 2.2a) is assigned to CC_1 to CC_{13} (see Figure 6.9a). To show the comparison in detail, the CIF-maps at CC_4 is shown in Figure 6.10, respectively. Through exclusive search, the MDC-F at CC_4 is shown in Figure 6.11. It can be clearly seen that the MDC-F using the previous method will be 168.67 N while it will be 101.98 N when the proposed method is used at CC_4. Using the proposed method, the MDC-F is significantly reduced by almost 40%.

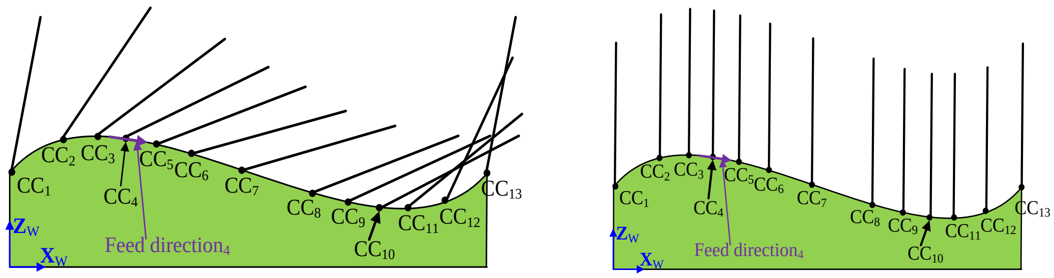

(a) Postures (the proposed method) (b) Postures (the previous method)

Figure 6.9 Tool path #1 using the proposed and previous methods

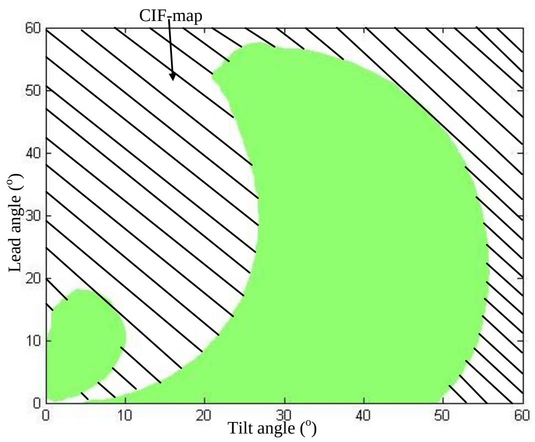

Figure 6.10 CIF-maps for CC_4

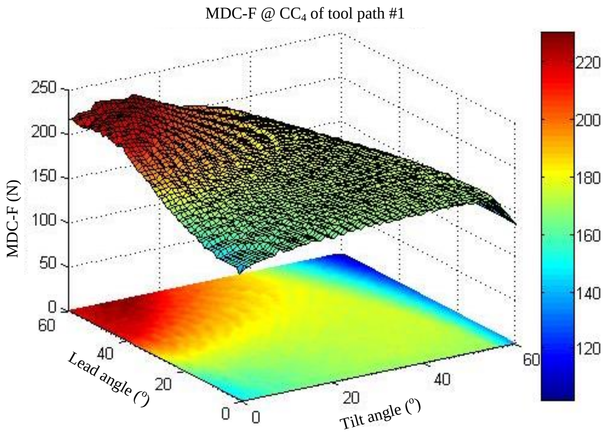

Figure 6.11 Exclusive search results for MDC-F at CC_4 of tool path #1

6.3. Discussion

In this chapter, some simulation results have been presented to show the effectiveness of the proposed methods for CIF-map construction and optimal tool path generation. For CIF-map construction at each CC point, the effect of cutting direction and workpiece geometry has been verified by the simulation results. The results show that the cutting direction has great effect on the CIF-map. With an improper cutting direction, the CIF-map could be very small, which means that the optimization of cutter posture may be limited. Therefore, in the future work, the cutting direction should be determined considering both the effect of posture change rate (PCR) and chatter. For tool path generation, the optimal tool path considering true dynamics have been generated using proposed method. From the comparison between the results generated by the proposed method and the previous method, we can see that the maximum deflection cutting force (MDC-F) is greatly reduced, which means the machined surface quality may be improved. However, currently, the proposed method is only implemented in the machining of simple ruled surfaces and it should be extended to cover truly sculptured surfaces.

CHAPTER 7

CONCLUSIONS AND FUTURE WORK

In this thesis, the main objective is to further investigate techniques for automation of tool path generation in 5-axis sculptured surface machining (finish cut) by considering machining dynamic factors. The specific issues addressed in this thesis are chatter avoidance in cutter posture assignment and optimal tool path generation in minimizing the effect of cutting deflection force. In this chapter, research presented in this thesis will be summarized and possible directions for future research will be pointed out.

7.1. Conclusions

The main achievements of this study are reflected in the following aspects: (1) accurate cutting force prediction in 5-axis machining considering cutter run-out and cutter vibrations; (2) chatter prediction in 5-axis machining and corresponding posture stability graph (PSG) construction. (3) chatter- and interference-free (CIF) cutter posture range construction and its application in tool path generation; (4) optimal cutter posture determination based on dynamics analysis and subsequently optimal tool path generation.

- **Cutting force prediction in 5-axis machining**

An accurate cutting force prediction method in 5-axis machining considering cutter run-out and cutter vibrations is proposed. This is based on the observation that the difference between the cutter-workpiece engagements under different cutter posture for ball-end cutter is the distribution of the cutting engagements in the cutter when only the ball-end part is engaged in cutting. The cutting force for 5-axis machining under ideal machining conditions is predicted using a simple cutting engagement transformation. As the cutter run-out can be seen as an extra feed on designed feed-per-tooth, the effect of cutter run-out on cutting force prediction is easily included. The cutter run-out parameters, including the cutter axis offset ρ and locating angle for offset ϕ_{ro} can be calibrated from the set of experimental data. The cutter vibrations, which can be numerically calculated using the fourth order Runge-Kutta method by assuming that the machining system is a 2-DOF mass-spring-damper system, can also be seen as an extra feed on designed feed-per-tooth. By integrating the effect of cutter run-out and cutter vibrations on designed feed-per-tooth, a more accurate cutting force prediction method in 5-axis machining can be achieved. Furthermore, the cutting force coefficients and cutter run-out also can be calibrated from the experimental data.

- **Chatter prediction and PSG construction**

A machining chatter prediction method in 5-axis machining using the full-discretization (FD) method is proposed. The dynamic cutting force caused by dynamic cutter displacement can be predicted using the proposed cutting force prediction method, and it will be transformed into modal frame considering the effect of lead angle and tilt angle on cutting force transformation. After that, the dynamic equation can be established with the measured modal parameters. Using the FD method, the modulus of the eigenvalue of the transition matrix which is constructed from the dynamic equation can be obtained. The modulus of the eigenvalue indicates the stability of the machining system, i.e., the stability of cutter posture. When the modulus of the eigenvalue is larger than 1, the machining system is unstable.

Otherwise, the machining system is stable. Using a sampling method, the stability of the machining system under different lead angle and tilt angle combination can be determined and the critical boundaries (with modulus of the eigenvalue equal to 1) can be obtained that establish the posture stability graph (PSG). The cutter posture from PSG can assure the machining process chatter-free.

- **CIF-map construction and its application in tool path generation**

Combined with the previously established A-map, a CIF-map construction method in 5-axis machining is proposed. In order to avoid chatter and interference in machining, it is better to select the cutter posture from the CIF-map instead of determination the stability and interference during the cutter posture selection process. In our previous study, accessible-map (A-map) has been proposed to avoid the interference in cutter posture determination. By transforming the A-map in the local frame into the feed frame, the posture accessible graph (PAG) can obtained. By intersecting the PAG with the PSG, the CIF-map can be obtained. The cutter posture from the CIF-map can assure the machining process chatter-free and interference-free. In order to apply the CIF-map in the tool path generation, the feed direction and machining parameters at each CC point have been determined considering the effect of workpiece surface geometry and cutting direction.

- **Optimal cutter posture determination based on dynamics**

Optimal cutter posture determination method in 5-axis tool path generation is proposed based on the true dynamics analysis. At each CC point, the CIF-map considering the effect of cutting direction, machining surface geometry and machining parameters will be generated first. The maximum deflection cutting force for specific cutter posture (combination of lead angle and tilt angle) at each CC point is identified under given machining conditions. By selecting the cutter posture with the minimal maximum deflection cutting force from the CIF-map at each CC point, optimal cutter posture can be determined towards minimal maximum deflection cutting force while keeping the machining process chatter-free and interference-free.

With methods proposed in this thesis, the existing system for process planning of 5-axis machining is significantly enhanced. The consideration of machining dynamic factors in 5-axis tool path generation represents a great leap-forward step towards generating truly machining feasible tool paths, which can be used directly even without any trial cutting. Regarding tool path optimization, minimal cutter deflection has been added as another objective, in addition to the minimal tool path length and path smoothness. This objective is particularly meaningful for finish cut stage as surface quality is probably the more important factor.

7.2. Recommendation for Future Work

Several limitations still exist for the current process planning system, which may indicate possible directions for future research.

Firstly, more experiments in free form surface machining should be conducted to verify the proposed chatter prediction and PSG construction method as the experiments in this thesis are mainly in plane surface and other simple surfaces. Furthermore, the experiments also need to be done to verify the proposed optimal cutter posture determination and corresponding tool path generation method.

Secondly, other types of cutter should be considered during cutting force prediction, chatter prediction, and subsequently PSG and CIF-map construction as the cutter considered in this thesis is mainly ball-end cutter during implementation stage. However, the other types of cutter, such as fillet-end cutter (torus end cutter), are also widely used in 5-axis freeform surface machining. Therefore, the cutting force prediction and chatter prediction should be extended to incorporate other types of cutter. Subsequently, the CIF-map can be constructed considering other types of cutter.

Finally, as cutter vibration can also be obtained during the accurate cutting force prediction stage, the accurate cutter deflection can be obtained and subsequently the machined surface topology can be predicted. Using the predicted surface topology, the machined surface error can be predicted and this can be set as a constraint (predicted surface error should be below user's specific surface roughness) to replace the current optimization objectives, i.e., minimal maximum deflection cutting force.

Reference

Ahmadi, K. and F. Ismail (2011). "Analytical stability lobes including nonlinear process damping effect on machining chatter." International Journal of Machine Tools and Manufacture **51**(4): 296-308.

Ahmadi, K. and F. Ismail (2012). "Modeling chatter in peripheral milling using the Semi Discretization Method." CIRP Journal of Manufacturing Science and Technology **5**(2): 77-86.

Ahmadi, K. and F. Ismail (2012). "Stability lobes in milling including process damping and utilizing Multi-Frequency and Semi-Discretization Methods." International Journal of Machine Tools and Manufacture **54**: 46-54.

Altintas, Y. (2000). Machine tool vibrations. Manufacturing automation : metal cutting mechanics, machine tool vibrations, and CNC design. New York, Cambridge University Press**:** 125.

Altintas, Y. (2001). "Analytical prediction of three dimensional chatter stability in milling." JSME International Journal, Series C: Mechanical Systems, Machine Elements and Manufacturing **44**(3): 717-723.

Altintaş, Y. and E. Budak (1995). "Analytical prediction of stability lobes in milling." CIRP Annals-Manufacturing Technology **44**(1): 357-362.

Apro, K. (2008). Secrets of 5-Axis Machining. New York, Industrial Press, Inc.

Bayly, P., J. Halley, B. P. Mann and M. Davies (2003). "Stability of interrupted cutting by temporal finite element analysis." Journal of Manufacturing Science and Engineering **125**(2): 220-225.

Bediaga, I., I. Egana and J. Munoa (2005). Time and frequency domain models for chatter prediction in milling. DAAM International Scientific Book 2005. Vienna, Austria, DAAM International**:** 33-48.

Budak, E. and Y. Altintas (1993). Prediction of milling force coefficients from orthogonal cutting data. Proceedings of the 1993 ASME Winter Annual Meeting, November 28, 1993 - December 3, 1993, New Orleans, LA, USA, Publ by ASME.

Budak, E. and Y. Altintas (1998). "Analytical prediction of chatter stability in milling. I. General formulation." Transactions of the ASME. Journal of Dynamic Systems, Measurement and Control **120**(1): 22-30.

Budak, E., E. Ozturk and L. T. Tunc (2009). "Modeling and simulation of 5-axis milling processes." CIRP Annals - Manufacturing Technology **58**(1): 347-350.

Budak, E. and A. Tekeli (2005). "Maximizing chatter free material removal rate in milling through optimal selection of axial and radial depth of cut pairs." CIRP Annals-Manufacturing Technology **54**(1): 353-356.

Butcher, J. C. (1987). The numerical analysis of ordinary differential equations: Runge-Kutta and general linear methods, Wiley-Interscience.

Can, A. and A. Unuvar (2010). "A novel iso-scallop tool-path generation for efficient five-axis machining of free-form surfaces." International Journal of Advanced Manufacturing Technology **51**(9-12): 1083-1098.

Cao, H., B. Li and Z. He (2012). "Chatter stability of milling with speed-varying dynamics of spindles." International Journal of Machine Tools and Manufacture **52**(1): 50-58.

Cao, Q., J. Zhao, S. Han and X. Chen (2012). "Force coefficients identification considering inclination angle for ball-end finish milling." Precision Engineering **36**(2): 252-260.

Choi, B. K. and R. B. Jerard (1998). Sculptured surface machining: theory and applications, Kluwer Academic Pub.

Dang, J.-W., W.-H. Zhang, Y. Yang and M. Wan (2010). "Cutting force modeling for flat end milling including bottom edge cutting effect." International Journal of Machine Tools & Manufacture **50**(11): 986-997.

de Lacalle, L. N. L., A. Lamikiz, J. A. Sanchez and M. A. Salgado (2007). "Toolpath selection based on the minimum deflection cutting forces in the programming of complex surfaces milling." International Journal of Machine Tools & Manufacture **47**(2): 388-400.

Diez Cifuentes, E., H. Pérez García, M. Guzmán Villaseñor and A. Vizán Idoipe (2010). "Dynamic analysis of runout correction in milling." International Journal of Machine Tools and Manufacture **50**(8): 709-717.

Ding, Y., L. Zhu, X. Zhang and H. Ding (2010). "A full-discretization method for prediction of milling stability." International Journal of Machine Tools and Manufacture **50**(5): 502-509.

Ding, Y., L. Zhu, X. Zhang and H. Ding (2010). "Second-order full-discretization method for milling stability prediction." International Journal of Machine Tools and Manufacture **50**(10): 926-932.

Engelbrecht, A. P. (2005). Fundamentals of Computational Swarm Intelligence, Wiley.

Eynian, M. and Y. Altintas (2010). "Analytical Chatter Stability of Milling With Rotating Cutter Dynamics at Process Damping Speeds." Journal of Manufacturing Science and Engineering **132**(2): 021012.

Feng, H.-Y. and C.-H. Menq (1994). "Prediction of cutting forces in the ball-end milling process-1. model formulation and model building procedure." International Journal of Machine Tools and Manufacture **34**(5): 697-710.

Feng, H.-Y. and C.-H. Menq (1996). "Flexible ball-end milling system model for cutting force and machining error prediction." Journal of Manufacturing Science and Engineering, Transactions of the ASME **118**(4): 461-469.

Fontaine, M., A. Devillez, A. Moufki and D. Dudzinski (2007). "Modelling of cutting forces in ball-end milling with tool–surface inclination: Part II. Influence of cutting conditions, run-out, ploughing and inclination angle." Journal of Materials Processing Technology **189**(1–3): 85-96.

Fontaine, M., A. Moufki, A. Devillez and D. Dudzinski (2007). "Modelling of cutting forces in ball-end milling with tool–surface inclination: Part I: Predictive force model and experimental validation." Journal of Materials Processing Technology **189**(1–3): 73-84.

Geng, L. (2013). Automated process planning for five-axis point milling of sculptured surfaces, National University of Sinapore.

Geng, L., P. Liu and K. Liu (2015). "Optimization of cutter posture based on cutting force prediction for five-axis machining with ball-end cutters." The International Journal of Advanced Manufacturing Technology: 1-15.

Gong, H. (2010). Tool path generation based on BCELTP for maximizing machining strip width. 3rd International Conference on Intelligent Robotics and Applications, ICIRA 2010, November 10, 2010 - November 12, 2010, Shanghai, China, Springer Verlag.

Gonzalo, O., J. Beristain, H. Jauregi and C. Sanz (2010). "A method for the identification of the specific force coefficients for mechanistic milling simulation." International Journal of Machine Tools and Manufacture **50**(9): 765-774.

Gradišek, J., M. Kalveram and K. Weinert (2004). "Mechanistic identification of specific force coefficients for a general end mill." International Journal of Machine Tools and Manufacture **44**(4): 401-414.

Hyun-Chul, K. (2011). "Tool path generation and modification for constant cutting forces in direction parallel milling." International Journal of Advanced Manufacturing Technology **52**(9-12): 937-947.

Iglesias, A., J. Munoa and J. Ciurana (2014). "Optimisation of face milling operations with structural chatter using a stability model based process planning methodology." The International Journal of Advanced Manufacturing Technology **70**(1-4): 559-571.

Insperger, T. (2010). "Full-discretization and semi-discretization for milling stability prediction: Some comments." International Journal of Machine Tools and Manufacture **50**(7): 658-662.

Insperger, T., B. Mann, B. Edes and G. Stépán (2006). The effect of runout on the chatter frequencies of milling processes. Proceedings of the 9th CIRP International Workshop on Modeling of Machining Operations, Bled, Slovenia.

Insperger, T. and G. Stépán (2002). "Semi‐discretization method for delayed systems." International Journal for numerical methods in engineering **55**(5): 503-518.

Insperger, T. and G. Stépán (2004). "Updated semi‐discretization method for periodic delay‐differential equations with discrete delay." International Journal for Numerical Methods in Engineering **61**(1): 117-141.

Kaymakci, M., Z. Kilic and Y. Altintas (2012). "Unified cutting force model for turning, boring, drilling and milling operations." International Journal of Machine Tools and Manufacture **54**: 34-45.

Kim, G., P. Cho and C. Chu (2000). "Cutting force prediction of sculptured surface ball-end milling using Z-map." International Journal of Machine Tools and Manufacture **40**(2): 277-291.

Kline, W. A. and R. E. DeVor (1983). "The effect of runout on cutting geometry and forces in end milling." International Journal of Machine Tool Design and Research **23**(2–3): 123-140.

Lacerda, H. and V. Lima (2004). "Evaluation of cutting forces and prediction of chatter vibrations in milling." Journal of the Brazilian Society of Mechanical Sciences and Engineering **26**(1): 74-81.

Lamikiz, A., L. N. Lopez de Lacalle, J. A. Sanchez and M. A. Salgado (2004). "Cutting force estimation in sculptured surface milling." International Journal of Machine Tools & Manufacture **44**(14): 1511-1526.

Lasemi, A., D. Xue and P. Gu (2010). "Recent development in CNC machining of freeform surfaces: A state-of-the-art review." Computer-Aided Design **42**(7): 641-654.

Lazoglu, I. (2003). "Sculpture surface machining: A generalized model of ball-end milling force system." International Journal of Machine Tools and Manufacture **43**(5): 453-462.

Lazoglu, I., C. Manav and Y. Murtezaoglu (2009). "Tool path optimization for free form surface machining." CIRP Annals - Manufacturing Technology **58**(1): 101-104.

Lee, K., H. Kim and S. Park (2007). "A run-out measuring method using modeling and simulation in four-fluted end milling." Journal of materials processing technology **187**: 207-211.

Lee, P. and Y. Altintas (1996). "Prediction of ball-end milling forces from orthogonal cutting data." International Journal of Machine Tools and Manufacture **36**(9): 1059-1072.

Li, H. and X. Li (2000). "Modelling and simulation of chatter in milling using a predictive force model." International Journal of Machine Tools and Manufacture **40**(14): 2047-2071.

Li, H. Y. and Y. F. Zhang (2009). Automatic tool-path generation in 5-axis finish cut with multiple cutters. 2009 IEEE International Conference on Virtual Environments, Human-Computer Interfaces and Measurements Systems (VECIMS 2009), 11-13 May 2009, Piscataway, NJ, USA, IEEE.

Li, H. Z. and X. P. Li (2005). "A numerical study of the effects of cutter runout on milling process geometry based on true tooth trajectory." The International Journal of Advanced Manufacturing Technology **25**(5-6): 435-443.

Li, H. Z., W. B. Zhang and X. P. Li (2001). "Modelling of cutting forces in helical end milling using a predictive machining theory." International Journal of Mechanical Sciences **43**(8): 1711-1730.

Li, L. and Y. Zhang (2006). "Cutter selection for 5-axis milling of sculptured surfaces based on accessibility analysis." International Journal of Production Research **44**(16): 3303-3323.

Li, L. L. and Y. F. Zhang (2004). Cutter selection for 5-axis milling based on surface decomposition. 2004 8th International Conference on Control, Automation, Robotics and Vision (ICARCV), 6-9 Dec. 2004, Piscataway, NJ, USA, IEEE.

Li, L. L. and Y. F. Zhang (2006). "An integrated approach towards process planning for 5-axis milling of sculptured surfaces based on cutter accessibility map." Computer-Aided Design and Applications **3**(1-4): 249-258.

Li, L. L., Y. F. Zhang, H. Y. Li and L. Geng (2011). "Generating tool-path with smooth posture change for five-axis sculptured surface machining based on cutter's accessibility map." International Journal of Advanced Manufacturing Technology **53**(5-8): 699-709.

Li, X. P. and H. Z. Li (2004). "Theoretical modelling of cutting forces in helical end milling with cutter runout." International Journal of Mechanical Sciences **46**(9): 1399-1414.

Li, Z. and Q. Liu (2008). "Solution and Analysis of Chatter Stability for End Milling in the Time-domain." Chinese Journal of Aeronautics **21**(2): 169-178.

Lopez de Lacalle, L. N., A. Lamikiz, J. Munoa and J. A. Sanchez (2005). "The CAM as the centre of gravity of the five-axis high speed milling of complex parts." International Journal of Production Research **43**(10): 1983-1999.

Makhanov, S. S. (2010). "Adaptable geometric patterns for five-axis machining: A survey." International Journal of Advanced Manufacturing Technology **47**(9-12): 1167-1208.

Manav, C., H. S. Bank and I. Lazoglu (2011). "Intelligent toolpath selection via multi-criteria optimization in complex sculptured surface milling." Journal of Intelligent Manufacturing **24**(2): 349-355.

Merritt, H. E. (1965). "Theory of self-excited machine-tool chatter: Contribution to machine-tool chatter research—1." Journal of Engineering for Industry-Transactions of the ASME **87**: 447.

Minis, I., R. Yanushevsky, A. Tembo and R. Hocken (1990). "Analysis of Linear and Nonlinear Chatter in Milling." CIRP Annals - Manufacturing Technology **39**(1): 459-462.

Minis, I. E., E. B. Magrab and I. O. Pandelidis (1990). "Improved Methods for the Prediction of Chatter in Turning .3. A Generalized Linear-Theory." Journal of Engineering for Industry-Transactions of the ASME **112**(1): 28-35.

Mousseigne, M., Y. Landon, S. Seguy, G. Dessein and J. Redonnet (2012). "Predicting the dynamic behaviour of torus milling tools when climb milling using the stability lobes theory." International Journal of Machine Tools and Manufacture.

Ozturk, E. and E. Budak (2007). "Modeling of 5-axis milling processes." Machining Science and Technology **11**(3): 287-311.

Ozturk, E., E. Ozlu and E. Budak (2007). Modeling dynamics and stability of 5-axis milling processes. in: Proceedings of the10th CIRP Workshop on Modeling of Machining Operations. Calabria,Italy,**:** 469–476.

Ozturk, E., L. T. Tunc and E. Budak (2009). "Investigation of lead and tilt angle effects in 5-axis ball-end milling processes." International Journal of Machine Tools and Manufacture **49**(14): 1053-1062.

Peng, C., L. Wang, Z. Li and Y. Yang (2014). "Time-domain simulation and experimental verification of dynamic cutting forces and chatter stability for circular corner milling." Proceedings of the Institution of Mechanical Engineers, Part B: Journal of Engineering Manufacture **229**(6): 932-939.

Quintana, G., F. Campa, J. Ciurana and L. L. de Lacalle (2011). "Productivity improvement through chatter-free milling in workshops." Proceedings of the Institution of Mechanical Engineers, Part B: Journal of Engineering Manufacture **225**(7): 1163-1174.

Quintana, G. and J. Ciurana (2011). "Chatter in machining processes: A review." International Journal of Machine Tools and Manufacture **51**(5): 363-376.

Rafal, R. (2012). "Stability criterion for aluminium alloy milling expressed by recurrence plot measures." Proceedings of the Institution of Mechanical Engineers, Part B: Journal of Engineering Manufacture **226**(12): 1976-1985.

Rivière-Lorphèvre, E. and E. Filippi (2009). "Mechanistic cutting force model parameters evaluation in milling taking cutter radial runout into account." The International Journal of Advanced Manufacturing Technology **45**(1-2): 8-15.

Schmitz, T. L., J. Couey, E. Marsh, N. Mauntler and D. Hughes (2007). "Runout effects in milling: Surface finish, surface location error, and stability." International Journal of Machine Tools and Manufacture **47**(5): 841-851.

Seiler, M. C. and F. A. Seiler (1989). "Numerical recipes in C: the art of scientific computing." Risk Analysis **9**(3): 415-416.

Shamoto, E. and K. Akazawa (2009). "Analytical prediction of chatter stability in ball end milling with tool inclination." CIRP Annals - Manufacturing Technology **58**(1): 351-354.

Shamoto, E., S. Fujimaki, B. Sencer, N. Suzuki, T. Kato and R. Hino (2012). "A novel tool path/posture optimization concept to avoid chatter vibration in machining - Proposed concept and its verification in turning." CIRP Annals - Manufacturing Technology **61**(1): 331-334.

Siddhpura, M. and R. Paurobally (2012). "A review of chatter vibration research in turning." International Journal of Machine Tools and Manufacture **61**: 27-47.

Smith, S. and J. Tlusty (1993). "Efficient simulation programs for chatter in milling." CIRP Annals-Manufacturing Technology **42**(1): 463-466.

Sridhar, R., R. E. Hohn and G. W. Long (1968). "A General Formulation of Milling Process Equation - Contribution to Machine Tool Chatter Research .5." Journal of Engineering for Industry-Transactions of the ASME **90**(2): 317.

Sun, Y. and Q. Guo (2011). "Numerical simulation and prediction of cutting forces in five-axis milling processes with cutter run-out." International Journal of Machine Tools and Manufacture **51**(10): 806-815.

Sun, Y., F. Ren, D. Guo and Z. Jia (2009). "Estimation and experimental validation of cutting forces in ball-end milling of sculptured surfaces." International Journal of Machine Tools and Manufacture **49**(15): 1238-1244.

Tournier, C. and E. Duc (2005). "Iso-scallop tool path generation in 5-axis milling." International Journal of Advanced Manufacturing Technology **25**(9-10): 867-875.

Wan, M., W.-H. Zhang, J.-W. Dang and Y. Yang (2009). "New procedures for calibration of instantaneous cutting force coefficients and cutter runout parameters in peripheral milling." International Journal of Machine Tools and Manufacture **49**(14): 1144-1151.

Wan, M., W. H. Zhang, G. H. Qin and G. Tan (2007). "Efficient calibration of instantaneous cutting force coefficients and runout parameters for general end mills." International Journal of Machine Tools and Manufacture **47**(11): 1767-1776.

Wan, M., W. H. Zhang, G. Tan and G. H. Qin (2007). "New algorithm for calibration of instantaneous cutting-force coefficients and radial run-out parameters in flat end milling." Proceedings of the Institution of Mechanical Engineers, Part B (Journal of Engineering Manufacture) **221**(6): 1007-1019.

Wang, M., L. Gao and Y. Zheng (2014). "Prediction of regenerative chatter in the high-speed vertical milling of thin-walled workpiece made of titanium alloy." The International Journal of Advanced Manufacturing Technology **72**(5-8): 707-716.

Wang, N. and K. Tang (2007). "Automatic generation of gouge-free and angular-velocity-compliant five-axis toolpath." Computer-Aided Design **39**(10): 841-852.

Weck, M., Y. Altintas and C. Beer (1994). "CAD assisted chatter-free NC tool path generation in milling." International Journal of Machine Tools & Manufacture **34**(6): 879-891.

Yao, Z.-Q., X.-G. Liang, L. Luo and J. Hu (2013). "A chatter free calibration method for determining cutter runout and cutting force coefficients in ball-end milling." Journal of Materials Processing Technology **213**(9): 1575-1587.

Zeroudi, N., M. Fontaine and K. Necib (2012). "Prediction of cutting forces in 3-axes milling of sculptured surfaces directly from CAM tool path." Journal of Intelligent Manufacturing **23**(5): 1573-1587.

Publication during the research

Wang, S. B., L. Geng, Y. F. Zhang, K. Liu, and T. E. Ng. "Cutting force prediction for five-axis ball-end milling considering cutter vibrations and run-out." International Journal of Mechanical Sciences 96 (2015): 206-215.

Wang, S. B., L. Geng, Y. F. Zhang, K. Liu, and T. E. Ng. " Chatter-free cutter postures in five-axis machining." Proceedings of the Institution of Mechanical Engineers, Part B (Journal of Engineering Manufacture) (under review after second revision)